THERMAL-FLUIDIC ENHANCEMENTS TO IN-LINE IMMERSION CHILLING IN POULTRY PROCESSING

A Thesis
Presented to
The Academic Faculty

By

Saikamal Srinivas

In Partial Fulfillment
of the Requirements for the Degree
Master of Science in Mechanical Engineering in the
George W. Woodruff School of Mechanical Engineering

Georgia Institute of Technology

August, 2021

THERMAL-FLUIDIC ENHANCEMENTS TO IN-LINE IMMERSION CHILLING IN POULTRY PROCESSING

Approved by:

Dr. Comas Haynes, Co-Advisor/Thesis Chair
Georgia Tech Research Institute
Georgia Institute of Technology

Dr. Yogendra Joshi, Co-Advisor
School of Mechanical Engineering
Georgia Institute of Technology

Dr. S. Mostafa Ghiaasiaan
School of Mechanical Engineering
Georgia Institute of Technology

Date Approved: July 28, 2021

To my family: Sreya, Srinivas, and Vani

ACKNOWLEDGEMENTS

I would like to take this opportunity to thank the following individuals and organizations for their constant support and guidance on and off this research project. First off, I would like to thank and appreciate my mom (Vani), dad (Srinivas), and sister (Sreya) for their love and support over my entire life in my academics and life milestones. There is no way I would be able to get to this point without you all. I will miss you all tremendously when I move to Pennsylvania in a short while. I want to thank my, in a way, my second family Billy, Lacey, and Taylor Brackett who have always opened their home and arms to me over the years. I also want to thank my best friends Mackenzie and Gabi Brackett, who are essentially like my brother and sister for so long and have so many fond memories and adventures with them. Thank you to all of my friends and family that I will not list by name because it would take too long to list, and I am afraid I will miss important individuals in my life. Thank you to my advisor, Dr. Comas Haynes, for taking a chance on me and working with me on this research project as well as the IAC program for the past several years. It has truly been a pleasure, and I hope we keep in touch over the years. I would like to thank all of the faculty and staff within the GTRI Food Processing Building for providing such a pleasant atmosphere to work in each and every day. I would like to thank Shartara Rox, Steve Thomas, Gary McMurray, Doug Britton, John Pierson, Stephanie Richter, Daniel Sabo, Wayne Daley, Thomas Gim, Emily Rojewski for their guidance and support on the project. I would like to thank Sean Thomas for his help with prototyping and teaching me how to use different shop instruments and being there to clean up my mess when things go wrong. I would like to also thank and truly appreciate Dr. Aklilu Giorges who I owe much of my technical research and hands-on skill development to. I would not be at this point without the assistance and guidance of Dr. Giorges. I

hope we can stay in touch in the coming years. I would also like to thank the Georgia Agricultural Technology Research Program for providing the funding to pursue this research effort.

TABLE OF CONTENTS

LIST OF TABLES

LIST OF FIGURES

LIST OF SYMBOLS AND ABBREVIATIONS

A	Surface area of object
A_{dim}	Normalized angular displacement
$AgPar$	Agitation parameter
C_p	Specific heat of material
C_1, C_μ	Empirical constants
C_{therm}	Thermal capacitance
$D_{H,ch}$	Hydraulic diameter of flow channel
f_1, f_μ	Functions
h	Convective heat transfer coefficient
k	Turbulent kinetic energy
LCA	Lumped capacitance analysis
LDV	Laser Doppler Velocimetry
m_{water}	Mass of water
p	Pressure
q	Heat transfer rate
Re	Reynolds number
RPM	Revolutions per minute
R_{therm}	Thermal resistance
SR	Spin ratio
T_i	Temperature at time t = 0
$T(t)$	Temperature at time t
T_∞	Chiller medium temperature

t	Time
U	Velocity
U_c	Centerline velocity
$USDA$	United States Department of Agriculture
V_{rel}	Relative velocity
u_i	Velocity components
u_i', u_j'	Reynolds stress
x_i	Coordinate system
Greek Symbols	
ΔT	Temperature difference
Θ	Non-dimensionalized temperature
Θ_{cw}	Non-dimensionalized temperature between carcass and water
δ_{ij}	Kroenecker delta
ε	Rate of dissipation
μ_t	Eddy viscosity
ρ	Density
σ_k	Empirical constant
σ_ε	Empirical constant
τ	Thermal time constant

SUMMARY

Primary poultry chilling utilizes thermal cooling systems to ensure final product quality and safety. Correspondingly, the poultry processing industry is exploring paths to achieve higher energy effectiveness and efficiencies in poultry chilling, without compromising rigid quality/safety standards, by continuously upgrading chiller technologies. Therefore, this thesis addresses these aims in the area of in-line immersion chilling of poultry carcasses by identifying the issues with the incumbent process and proposing a novel approach to enhance the thermal/fluidic dynamics of the chilling process.

An applied research project was completed to make automated in-line immersion chilling a more effective alternative for the poultry chilling process. The objective was to enhance the immersion chilling of "in-line" carcasses through alternate motion patterns and the superimposition of additional kinematics upon the typical translational paths of shackled carcasses. The project had a computational and experimental core that emphasized characterizing and optimizing induced motion effects upon convective heat transfer. The computational flow study reveals secondary flow phenomena such as multiple flow separation points, wake formation, and non-uniform surface pressure/shear distributions suggesting flow "shielding" and non-uniform flow exposure for the traditional in-line immersion chilling line, which further promotes a necessary design alternative that is being proposed. An experimental test rig was configured to test varied shackle rotational superimposition patterns in contrast to the traditional pure translation process through a series of simulated chilling experiments. The experimental results indicate as much as a 34%, 41.7%, and 39.9% reduction in the chilling thermal time constants for the distinct carcass mass categories of 1.4-1.6 kg, 1.6-1.8 kg, and 1.8-2.0 kg, respectively, with further reductions being pursued in the future.

1 INTRODUCTION

Resource conservation in the food processing industry has become an increasingly important concern as energy use in the food industry has been steadily rising over time with the United States Department of Agriculture (USDA) reporting in 2010 that food-related energy use as a share of the nation's energy budget in 2007 was an estimated 15.7 percent [1]. Accordingly, the poultry industry has been exploring methods to achieve higher energy efficiencies in poultry chilling while maintaining product quality by way of continuously upgrading chiller technologies. For these reasons, it is imperative to conduct further research alongside industry partners to explore energy efficient and cost-effective design options within the scope of food process chilling. Specific focus is upon poultry process chilling in the present thesis.

Poultry Processing

To provide context to the poultry chilling step within the scope of poultry processing, the subsequent subsection details the key poultry processing steps. Following this, the poultry chilling process and the various chilling methods will be highlighted.

Poultry Processing Steps

In the primary processing of poultry, there are many steps involved that are critical to assure final product quality as relayed in Figure 1.1 [2]. First, a supply of live birds is brought to the plant and are usually kept in a stable environment for some time to reduce the birds' stress levels that can potentially affect the meat quality. Following this rest time, the birds are unloaded from the crates manually (traditionally) or through automated unloading systems and proceed to a stunning

stage. Stunning is done either through electricity, a mixture of gases, or through mechanical means and

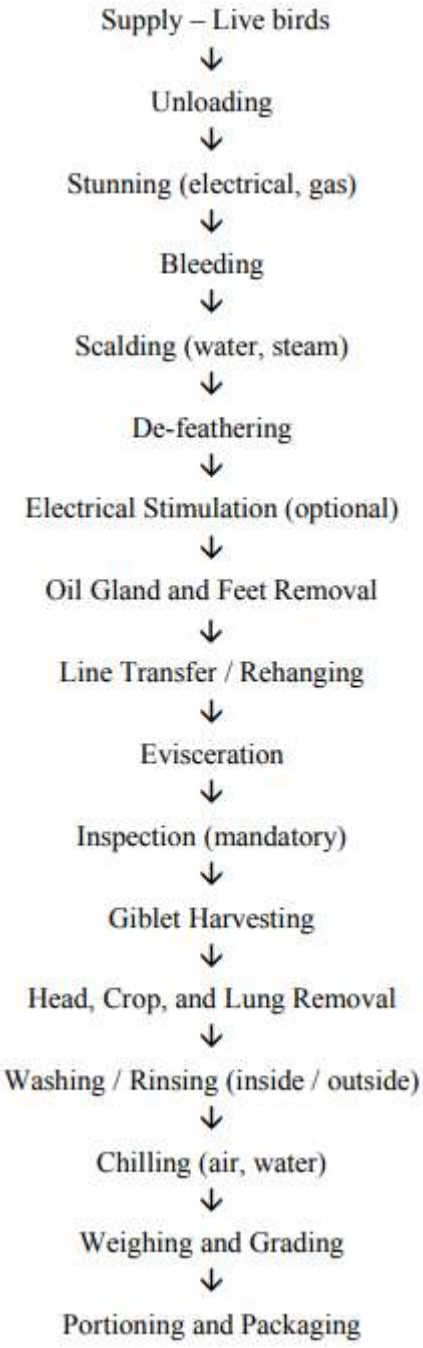

Figure 1.1: Typical process flow of steps in poultry primary processing [2]

is often employed to prevent bruising that can often occur with handling live birds and to promote animal welfare improvement. Next, the stunned birds proceed to the bleed out phase, which can take between 2 to 5 minutes depending on the bird size and type. Following this, the birds proceed to the critical scalding step, in which the birds' feathers are loosened for easier de-feathering by immersing the birds in hot water or steam. In large plants, scalding is done by way of a continuous line where suspended birds are immersed in a long hot water tank through either soft/semi-scalding (50-53 ºC for 1-3 min, used for broilers and young turkeys), sub/medium scalding (54-58 ºC for 1-2 min, used for mature birds), or hard scalding (59-61 ºC for 0.75-1.5 min, used commonly for waterfowl) schemes. The scalding scheme depends on the degree of difficulty in feather removal, the subsequent chilling method, and the matureness of the bird. After hot water scalding, the birds are de-feathered in modern plants via mechanical pickers/pluckers that are tooled with rubber fingers that take the feathers off the carcass. If an optional electrical stimulation stage (used to trigger muscle contraction and speed up post-mortem metabolic changes) is not used in between, the carcass line passes through a stage where the oil glands and feet are removed primarily in an automated process. After shackle transfer and rehang, the carcass line passes through the evisceration stage where the body cavity is opened and the internal viscera is removed. After passing through an inspection stage, the viscera is disconnected and the giblets are harvested and washed in a separate line. The head, crop, neck, and lungs are removed shortly after inspection as well. After the preceding processes, the carcasses are washed to remove any organic and extraneous material to further limit bacterial growth before the chilling process. The carcass line then proceeds to the chilling stage to lower the meat temperature in order to limit bacterial growth. Following the comprehensive chilling stage, the birds are weighed, graded, and either packed or deboned for further processing.

Poultry Chilling

Further detailing the process of chilling poultry, the customary objective in US markets is to reduce the bird core temperature from 37-40 ºC to 4 ºC or lower in 4, 6, or 8 hours from the initial kill for carcasses weighing less than 4 pounds, 4-8 pounds, and greater than 8 pounds, respectively [3]. In European markets, there is a 4 ºC final requirement, but there is no time requirement. Typically, inclusive of all markets, poultry chilling involves one or a combination of air chilling, intermittent water spray chilling, and chilled water immersion chilling. In U.S. markets, immersion chilling via "spin chilling" or auger chilling, as shown in Figure 1.2, has been the traditional chilling method because it is space-efficient, economical, and easy to implement [4] [5]. Immersion chilling is also important to maximizing product yield in US markets as processors prioritize water pickup and retention for the carcasses. However, air chilling or hybrid in-line chilling, which involves a water immersion step preceding air chilling, is gaining traction due to water limitations, wastewater discharge restrictions, cross-contamination concerns, and moisture retention regulations [3]. Additionally, air-chilled poultry meat can be exported to Europe where immersion chilling is not in favor. The main chilling methods will be briefly described as follows.

Figure 1.2: Screw-auger chiller used for water immersion poultry chilling (JBT FATCAT Chilling System)

In air chilling (Figure 1.3), carcasses pass through a cold room or an air tunnel at temperatures between -7 ºC to 2 ºC for approximately 90 to 150 minutes. Primarily used in Europe, the carcasses in this process are typically soft-scalded and sold fresh. The air chilling process is typically multi-staged with a pre-chill stage for one hour at 5 ºC to remove moisture from the carcass and a final chilling stage for up to 1.5 hours at around 0 ºC. To increase the efficiency of the chilling process, cold air may be blown down into the carcass ("downflow" chilling) or across the line of carcasses ("crossflow" chilling) [6].

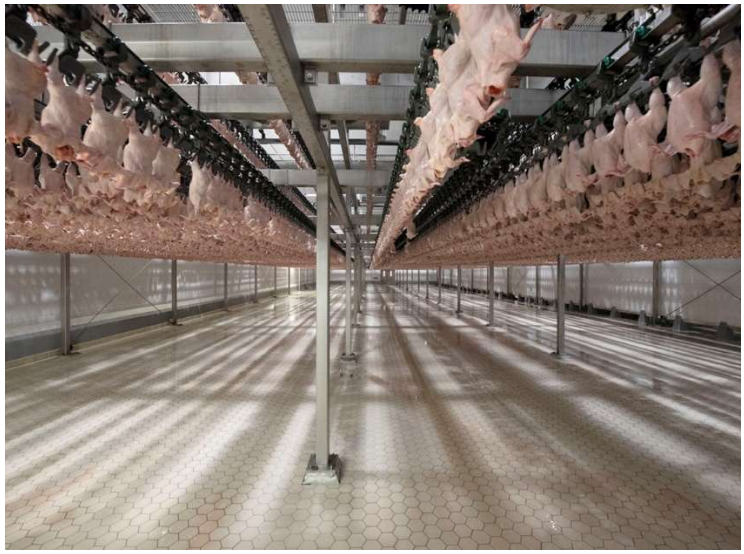

Figure 1.3: Air chilling method for poultry chilling (Meyn)

Intermittent water spray or evaporative chilling is an alternative chilling method often used for hard-scalded carcasses. In this process, the carcass line is periodically sprayed with water as cold air is blown in a "downflow" or "crossflow" manner as specified earlier. Through this method, heat transfer is improved due to the evaporative effect that occurs at the carcass boundary, and there is no noticeable water pickup during the process. The advantages of this method involve less chilling time than air chilling (less than 90 minutes) [5] and less water usage than water immersion chilling (less than 0.1 L per carcass for each series of spray nozzles) [4].

Immersion chilling of poultry carcasses involve batch or continuous-flow immersion operations with chilled water or an ice-water mix. Batch chillers, which have been deemed impractical for high, continuous production rates, involve high labor and handling demands whereas continuous-flow chillers support higher production output and have chilling rates 2-6 times faster than static chillers [7]. In the continuous-flow chillers, there are often two stages: the pre-chiller and the main chiller. In the pre-chiller, the water temperature may be in the range of 7 ºC to 13 ºC, and the dwell time may be approximately 10 to 15 minutes [8]. The carcass core

temperature coming into the pre-chiller is generally about 40 ºC and is reduced to 25 ºC-30 ºC prior to the main chiller. The main chiller primarily utilizes two methods of flow: parallel- and counter-flow. In parallel-flow chilling, the water runs in the same direction as the carcass movement. More widely-implemented, counter-flow immersion chillers involve chilled water flow opposite to the carcass movement through the chiller so that the carcasses are chilled in cleaner and colder water from start to finish. With water immersion chilling, the heat transfer coefficient associated with the chilling is higher than that of the air chilling and spray chilling processes.

In addition to the traditional screw-auger chiller, newer in-line water immersion chilling systems are being developed, as shown in Figure 1.4, and will be the focus of the presented work. In-line immersion chilling, which entails a continuous carcass shackle line passing through channels of chilled water, is a newer technology being introduced into poultry chilling, primarily in a method of "hybrid" chilling where a combination of immersive water chilling and air chilling is used. This method of in-line immersion chilling has many strategic advantages as it has the thermal chilling benefits of water immersion, but it also has the added benefits of product traceability (carcasses are ordered/aligned on individual shackles as opposed to randomized batches in screw-auger chiller), uniform chilling pathway compared to screw-auger chilling, and labor minimization (there is no need for rehanging of carcasses on shackles after chilling as is done in screw-auger chilling). With the benefits, however, there are some deficiencies in in-line immersion chilling that need to be addressed to be make it more viable. The biggest shortcoming to this approach is the extra spatial footprint required as compared to the more compact thermal heat exchange occurring in the screw-auger chiller. However, with the notable benefits of in-line immersion chilling, if there was a novel approach to enhance the chilling rate, then the dwell time

could be reduced, which can lead to corresponding reduction in necessary space required for the chilling operation.

Figure 1.4: In-line water immersion chilling of poultry carcasses (Marel)

Project Overview and Organization

With the closing statement of the preceding section as a preface, the presented work is a detailed exploration of the thermal-fluidic enhancements that can be had with imposing additional shackle line kinematics (i.e., rotation) to the traditional in-line immersion chilling process. With realized improvements gleaned from the work done in terms of the chilling rate, this has significant impact on advancing the viability of in-line immersion chilling in the poultry processing industry. The presented work is divided into two project divisions. Each sub-project details an independent study. However, the combination of the studies as well as the conclusions made from both are complementary and serve to glean insights into the efforts to enhance the thermal-fluidics of the in-line immersion chilling process for poultry.

Computational Study

Chapter 2 includes the methodology and results of the computational study. As will be later discussed, multiple fluid flow simulations were executed using COMSOL® Multiphysics to study complex-shaped bluff body flow, indicative of flow dynamics occurring during in-line immersive poultry chilling. Studies were conducted for a single carcass and a series of carcasses to study the complex flow phenomena. The results of these computational studies speak to the apparent flow dynamics occurring in traditional methods of in-line immersion chilling and improvements that can be made to this current baseline.

Thermal Experimental Study

Chapter 3 includes the methodology and results of the thermal experimental study. The configuration of the experimental test rig as well as the rationale for characterizing chilling performance were detailed in a comprehensive manner. Experimental poultry chilling tests were conducted, and the results from a series of experimental conditions are reported. This section emphasizes the advantages of additional kinematics via shackle rotation to the poultry chilling process.

Conclusion

Chapter 4 provides a summary of the key conclusions made from the computational and thermal experimental studies. A combination of the takeaways from the studies results in a holistic discussion of the thermal-fluidic enhancements to be made to the baseline industrial poultry chilling process. Additionally, future computational studies and experimental trials for the purpose of furthering the conclusions made will be discussed.

2 COMPLEX BLUFF BODY FLOW COMPUTATIONAL STUDY

2.1 INTRODUCTION/MOTIVATION OF STUDY

Particularly for the poultry processing industry, fluid flow around complex geometries is of great importance as the raw product is involved in multi-faceted activities such as transport through heating, cooling, shearing, and other processes to yield a satisfactory final product. Although there are many previous works in studying the flow dynamics around a single or series of simple shapes, there have been limited studies in examining the flow dynamics across complex-shaped bluff bodies, which is highly relevant to the poultry processing industry. In the poultry processing industry, where processing is impacted by spatial limitations, the flow dynamics in the aforementioned processes is not only affected by the shape of the product but also the relative placement of the complex-shaped product in relation/proximity to one another.

Over previous decades, bluff body flow has been investigated with high regard due to its relevance to various engineering and industrial applications such as heat exchanger, aircraft, and wind turbine design. In-line bluff body series flow dynamics has also been studied for insights into the aerodynamics, wake formation, and vortex shedding nuances from single body configurations. Prior research has focused on flow around cylinder bluff bodies with the majority of publications studying circular or rectangular cross-section cylinders in cross flow. Ong and Wallace [9] published an early, fundamental work on flow past a circular cylinder, in which they experimentally characterized stream-wise and lateral velocity statistics such as average and fluctuating velocity components at varied downstream locations in the turbulent wake structure at a Re_d of 3900. In this study, they were able to validate fairly two-dimensional flow in the very near-wake region (x/d = 3 to 10) and experimental velocity fluctuations and Reynolds shear

stresses agreed well with comparable studies. In the near and intermediate wake structures of circular cylinders, Zhou et al. [10] and Scarano and Poelma [11] experimentally studied vortex shedding organization and vorticity field properties in the turbulent flow regime. While square cylinder bluff body flow studies are not as prevalent, Lyn et al. [12] published a comprehensive, experimental Laser Doppler Velocimetry (LDV) study involving a square cylinder placed within a closed water channel with a flow Re of 21,400 to measure and ensemble-average mean and fluctuating flow velocity components.

As mentioned prior, bluff body flow studies extend to configurations involving multiple or series of cylindrical bluff bodies to examine the flow variations resulting from interactions amongst the series. There has been limited experimental study in configurations involving two or more cylinders in series with a few published of numerical simulation studies from Bao et al. [13], Islam et al. [14], and Liang et al. [15]. One experimental work reported by Hetz et al. [16] investigated the implications of varied gap spacing and Reynolds numbers on velocity fluctuations and vortex shedding patterns for a series of five in-line circular cylinders. Gap vortex shedding occurs between consecutive cylinders and is a key phenomenon observed in their study. Similarly, Sewatkar et al. [17] numerically and experimentally studied the flow around an in-line series of six square cylinders for a sweep of gap spacing and Reynolds numbers and proposed a flow regime map (as a function of gap spacing and Reynolds number) comprising of synchronous, quasi-periodic-I, quasi-periodic-II, and chaotic flow regimes.

From the preceding literature review of bluff body flow, it is apparent that there is very limited breadth in the area of complex-shaped bluff body flow so there needs to be more investigation into this area. The motivation behind the subsequent computational flow study is to study the three-dimensional flow dynamics around a single, complex-shaped bluff body and a

series configuration of complex-shaped bluff bodies, representative of product in the poultry processing industry. The numerical results will detail the wake phenomena and resultant velocity and pressure fields in the single and in-line series configuration. The results and conclusions from the numerical flow study provide insight into the resultant flow dynamics experienced by the poultry food product on the processing line.

2.2 FLOW SYSTEM MODEL SETUP

In the poultry processing industry, water and air are the primary media used in the transport, scrubbing, disinfecting, cooling, and heating processes to satisfy final product requirements. Cold chain processing is a major safety intervention that is implemented to limit bacterial growth via low temperatures. As mentioned before, there are many methods for poultry carcass chilling such as batch/screw-auger immersion water chilling, in-line water immersion chilling, air chilling, or a combination of these methods. In this computational study, a single poultry carcass and an in-line series of poultry carcasses with complex geometry are suspended in water channel flow to simulate the three-dimensional flow field encountered during the industrial in-line immersion chilling process.

Using industry operating parameters (i.e. channel dimensions, channel flow velocity) and a complex-shaped bluff body (carcass geometry), the three-dimensional computational domain was constructed as shown in Figure 2.1 using COMSOL® Multiphysics software. For the initial mesh validation study, the bluff body geometry was a simple cylinder configuration, but the key numerical studies involve the complex carcass geometry. The flow channel width and height were defined to be 60.96 cm (24 in) and 46.99 cm (18.5 in), respectively, which are based on standard industry parameters. The total flow domain length is 6.68 m (263 in), which includes the single

bluff body test region length of 31.56 cm (12.4 in), an inlet region of 2.12 m (83.5 in) (4 $D_{H,Ch}$) before the bluff body test section, and 4.25 m (167.3 in) (8 $D_{H,Ch}$) trailing outlet region after the bluff body test section. $D_{H,Ch}$ is defined as the hydraulic diameter of the flow channel. The inlet region was sized accordingly to create a sufficient upstream length for the flow to develop before encountering the bluff body, while the trailing outlet region was sized to sufficiently capture wake formations and vortex shedding from the bluff body(s) in the test section. Within the test section, the bluff body of interest is encapsulated with a cylindrical domain that can be prescribed with transient rotational motion. This feature was not used in the present numerical studies, but it was implemented for future transient studies involving studying the flow dynamics for a single or inline series of rotating carcasses as will be mentioned in Chapter 4 regarding future work. Figure 2.2 shows the overall mesh distribution for the computational domain with Figure 2.3 showing a zoomed view of the test section. As can be seen within the test section, there is a bluff body (cylinder) encapsulated by a cylindrical domain.

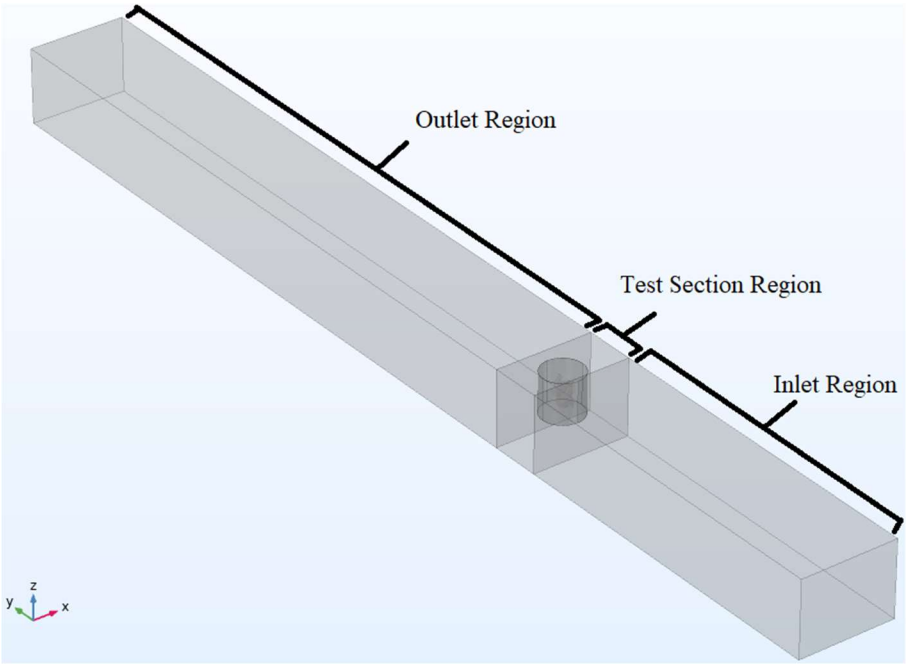

Figure 2.1: Computational domain design of bluff body channel flow

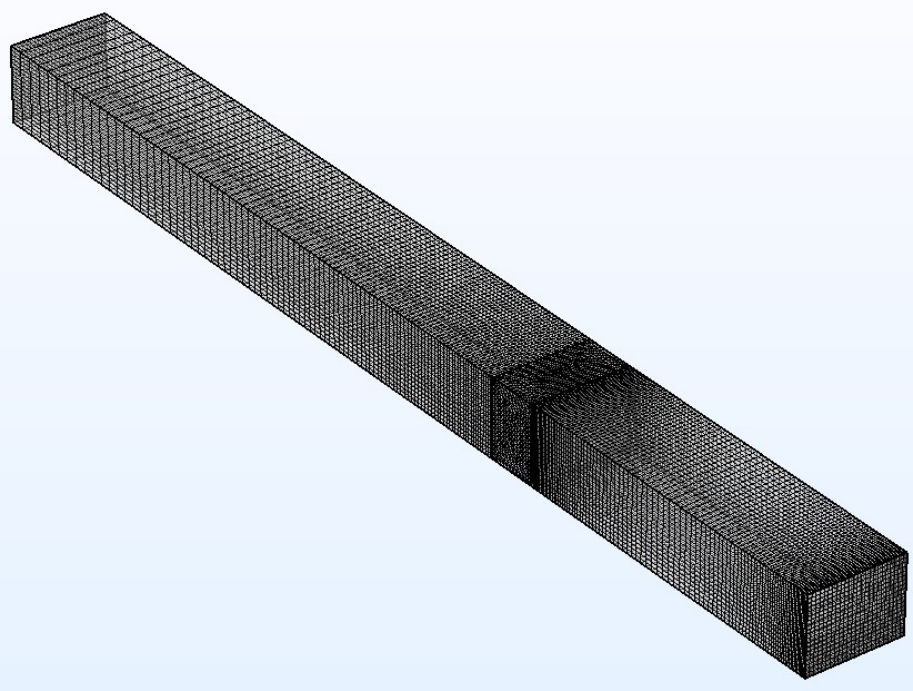

Figure 2.2: Computational domain mesh distribution

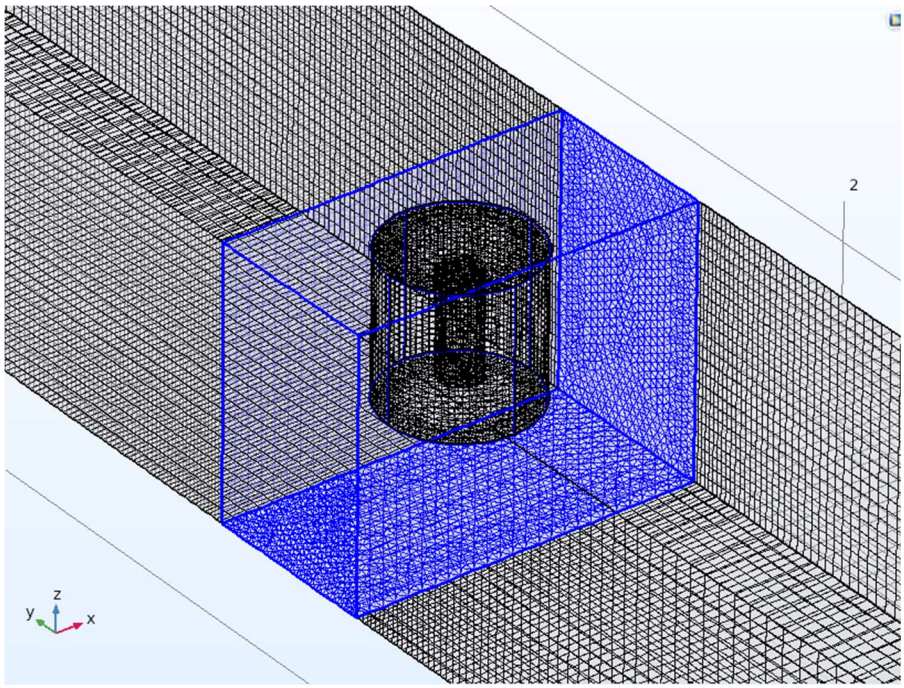

Figure 2.3: Close-up view of test section mesh

2.2.1 Governing Mass, Momentum, and Turbulent Model Theory

For the COMSOL® Multiphysics computational simulations, the incompressible, steady viscous flow involving a Newtonian fluid around a bluff body is simulated by solving the mass continuity, momentum conservation, and low-Re k-ε turbulent model equations. The mass and momentum conservation governing equations for incompressible, steady-state fluid flow are expressed as:

$$\frac{\partial u_i}{\partial x_i} = 0 \tag{2.1}$$

$$\rho u_j \frac{\partial u_i}{\partial x_j} = -\frac{\partial p}{\partial x_i} + \frac{\partial}{\partial x_j}\left\{\mu\left(\frac{\partial u_i}{\partial x_j} + \frac{\partial u_j}{\partial x_i}\right)\right\} + \frac{\partial}{\partial x_j}(-\rho u_i' u_i') \tag{2.2}$$

Where ρ is density, p is pressure, μ is dynamic viscosity, u_i are the velocity components, and x_i is the coordinate system. The Reynolds stress term in Equation 2.2 is modeled using the eddy-viscosity model and Boussinesq assumption as:

$$-\rho u_i' u_i' = \mu_t\left(\frac{\partial u_i}{\partial x_j} + \frac{\partial u_j}{\partial x_i}\right) - \frac{2}{3}\rho k \delta_{ij} \tag{2.3}$$

Where μ_t it the eddy viscosity, k is the turbulent energy and δ_{ij} is the Kroenecker delta, defined as 1 at i=j or 0 otherwise.

Generally, the standard k-ε model is practical and robust for turbulent flow simulation and has been shown to model free shear flow with reasonable confidence [18]. Additionally, it has also proven successful to develop models to capture near wall flow [19] [20] [21]. One turbulent model

that allows for wall calculations without log-boundary layer assumptions is the low-Re k-ε model [22]. The low-Re k-ε model, the kinetic energy (k), and the rate of dissipation (ε) are defined as follows:

$$\rho U_j \frac{\partial k}{\partial x_j} = \frac{\partial}{\partial x_j}\left\{\left(\mu + \frac{\mu_t}{\sigma_k}\right)\frac{\partial k}{\partial x_j}\right\} + \mu_t \left(\frac{\partial u_i}{\partial x_j}\right)^2 - \rho\varepsilon - 2\mu\left(\frac{\partial k^{1/2}}{\partial x_j}\right)^2 \tag{2.4}$$

$$\rho U_j \frac{\partial \varepsilon}{\partial x_j} = \frac{\partial}{\partial x_j}\left\{\left(\mu + \frac{\mu_t}{\sigma_\varepsilon}\right)\frac{\partial \varepsilon}{\partial x_j}\right\} + C_1 f_1 \frac{\epsilon}{k}\mu_t \left(\frac{\partial u_i}{\partial x_j}\right)^2 - 2.0\mu\mu_t\left(\frac{\partial^2 u_i}{\partial x_j^2}\right) \tag{2.5}$$

Where C_1, σ_ε, and σ_k are empirical constants, and f_1 is a function.

Using dimensional analysis for characterizing eddy viscosity ($\mu_t \propto k^a\varepsilon^b$), the turbulent eddy term is expressed as:

$$\mu_t = \rho C_\mu f_\mu \frac{k^2}{\varepsilon} \tag{2.6}$$

Where C_μ is an empirical constant, and f_μ is a function that reduces eddy viscosity near the wall [22]. The previous formulations are solved numerically to simulate the bluff body flow in the completed computational studies.

2.2.2 Simple Cylinder Geometry Configuration

As mentioned prior, the main objective of the computational study was to study the flow around a complex-shaped bluff body indicative of the poultry carcass geometry. The results from this study have relevance to certain processes in the poultry processing industry such as chilling, heating, disinfecting, etc. To setup a domain to reasonably simulate these processes, a modeled flow region, as shown previously in Figure 2.1, was constructed with three distinct regions: inlet,

test section (as shown in Figure 2.4), and outlet. The inlet region is extended to allow for the channel flow to develop before the test section, and the outlet region is elongated to a larger extent to capture the wake profiles and vortex shedding phenomena as well as to provide numerical stability and avoid potential backflow at the outlet.

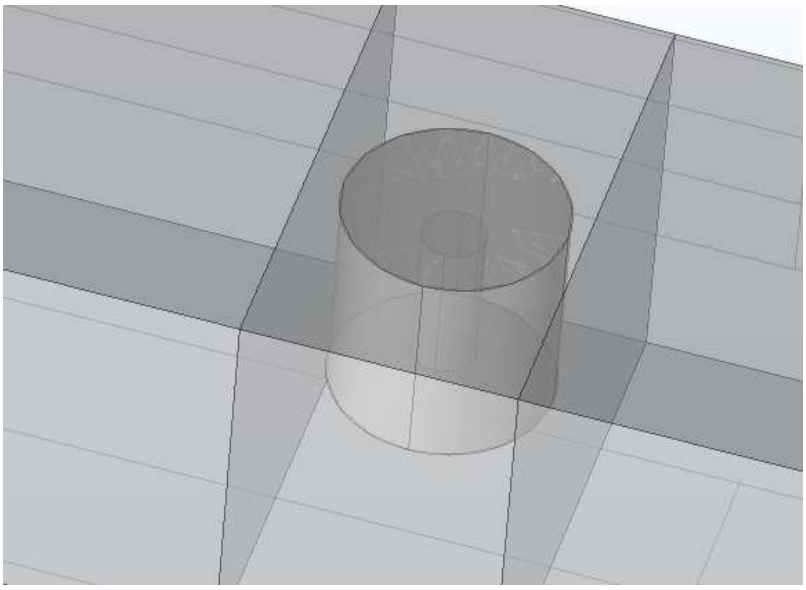

Figure 2.4: Close-up view of computational domain test section

The initial progression step in developing the numerical simulation involving the complex carcass geometry was to place a bluff body with simple geometry within the test section and perform a mesh study to validate mesh independence. The mesh study was conducted using the simple cylinder geometry to reduce the computational cost and time to verify the flow field. Once the mesh study was successfully conducted, the mesh distribution properties for the simple cylinder configuration were extended to the complex carcass geometry configuration, and numerical simulations were performed.

2.2.2.1 Simple Cylinder Geometry Mesh Study

For the mesh study, a single cylinder with a radius of 48.5 mm (1.9 in) and a height of 23.38 cm (9.2 in) (representative of a simplified carcass torso) is placed within the test section

region. The top of the cylinder is justified 8.08 cm from the top of the flow channel to simulate the suspension of the carcass in an industrial channel, and the cylinder's vertical z-axis passing through the center length is 2.28 m (89.8 in) from the channel inlet and centered across the channel width. The computational flow domain was constructed with the versatility to easily substitute bluff bodies of interest within the test section without losing the desired mesh distribution properties. Additionally, although the inlet and outlet sections are extensive, by using a variable grid distribution incorporating a quad-structured, relatively coarse mesh in the inlet and outlet regions, most of the mesh density is prescribed in the test section.

The mesh study was conducted for the simple cylinder bluff body placed within a water channel flow with inlet fluid flow speed of 0.4 m/s (1.31 ft/s), which is typical of the industrial flow condition. Since this is an open channel flow, the top surface of the computational flow domain was prescribed with a slip boundary condition unlike the other three walls of the flow channel that were set to be no-slip. The bluff body surface is also prescribed with a no-slip boundary condition. With the boundary conditions defined, COMSOL® Multiphysics software was used for the fluid flow simulation to solve the governing mass, momentum, and turbulent model equations (Equations 2.1-2.6).

Table 2.1 details the four mesh distributions examined in the mesh study. Varied mesh sizes from 283,694 to 2,073,343 elements are used to solve for the velocity and pressure fields. Preceding Figure 2.2 displays one of the meshes examined in the mesh study (Mesh 1), and preceding Figure 2.3 displays a clearer, zoomed view of the test section with the cylinder bluff body for this particular mesh. Compared to Mesh 1, the total mesh element count for the Meshes 2, 3, and 4 increases by nearly two, four, and seven-fold while the mesh count in the core test section region for these meshes changes three, six, and twelve-fold, respectively. The simulations

were run on 2x Intel®Xeon® CPU ES-2680 V3 at 2.50 Ghz using 2 sockets with 24 cores with computational times to solve for a steady state solution of 28 minutes, 31 minutes, 43 minutes, and 2 hours 4 minutes for Meshes 1, 2, 3, and 4, respectively.

Table 2.1: Mesh distribution study for the flow domain with variable mesh distribution

Mesh		1	2	3	4
Region	inlet	45,600	60,060	77,208	93,600
	test	146,894 (1)	407,912 (3)	934,632 (6)	1,792,543 (12)
	outlet	91,200	120,120	154,560	187,200
Total		283,694 (1)	588,092 (2)	1,165,827 (4)	2,073,343 (7)
U (m/s)		0.4061	0.4047	0.4049	0.4056
$\frac{U_3 - U}{U_3}$		-0.30%	-0.04%	0	0.17%
Computati-onal time		28 minutes	31 minutes	43 minutes	2 hours 4 minutes

In Table 2.1, the mesh element count in each region, relative velocity difference at a defined upstream location, and the computational time are reported. The mesh count ratios (presented in parentheses) in relation to Mesh 1 are reported in the table as well. The flow velocity results for all four mesh cases are compared at the intersection of cylinder mid-section xy- and yz-planes as is displayed in Table 2.1. The upstream velocity comparison amongst the four meshes was taken 2D (cylinder diameter) at the specified xy- and yz-plane intersection. Figure 2.5 displays the flow field contour plot around the cylinder bluff body for Mesh 3 and includes the xy- and yz-plane

data overlaid together in an isometric, three-dimensional view. As can be seen from Table 2.1, it is apparent that the flow profiles for the four meshes agree well with each other with very slight differences. The mesh accuracy was examined further by calculating the grid convergence index (GCI) using the upstream velocity as the parameter of interest and ensuring the accuracy satisfies the asymptotic range of convergence. Conducting GCI analysis for the test section region mesh distribution for Meshes 2 (Coarse), 3 (Medium), and 4 (Fine) with methodology established by Roache [23] [24], the GCI2,3 (GCI between Mesh 2 and 3 refinement) and GCI3,4 (GCI between Mesh 3 and 4 refinement) were determined to be -0.09% and -0.30%, respectively. These low GCI values establish strong mesh grid convergence for the set of meshes. The asymptotic range of convergence for the set of meshes was calculated to be 1.0017, which generally should be approximately equal to 1 to ensure an asymptotic approach to a converged answer and grid independence.

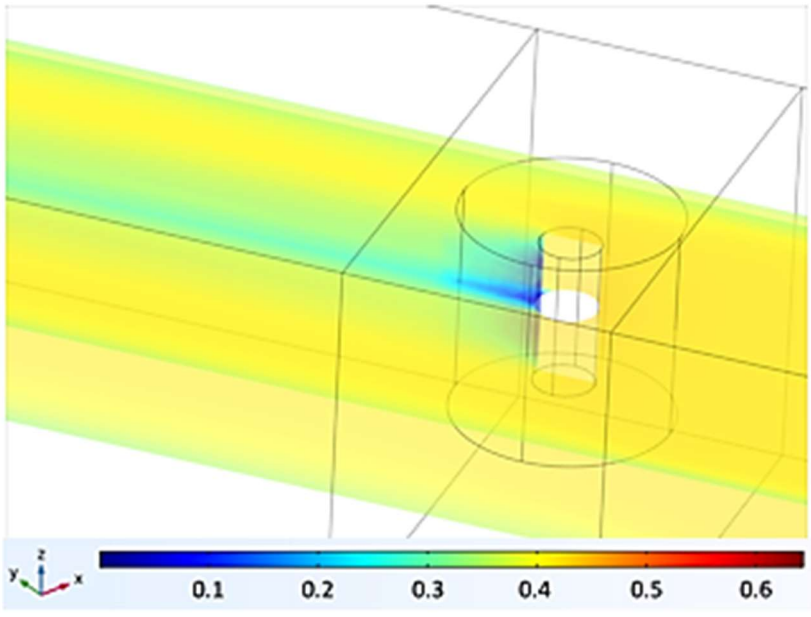

Figure 2.5: Flow velocity (m/s) contour plot for overlaid mid-section xy- and yz-planes for Mesh 3

In conclusion, the change in mesh density does not result in significant flow field variations even with substantial changes in mesh element count with a maximum percent variation of 0.30%. Based on the mesh study results, Mesh 3 was selected for its reasonable mesh fidelity and computational time. For the complex carcass geometry configuration, the mesh distribution is identical for the inlet and outlet regions. However, for the test section region, the mesh element count is varied, but the mesh distribution properties (i.e. max/min element size, tetrahedral shape) are the same.

2.2.3 Carcass Geometry Configuration

With the mesh study completed and the mesh distribution properties set, the simple cylinder was replaced with the complex carcass geometry within the test section. To create the geometry representative of a chicken carcass, a number of constructing and refining steps were taken to create a chicken carcass that was marginally simplified yet still captured the major body features of the chicken. Initially, a geometric mesh file was constructed by way of a 3D scanner, and this geometry was imported into SolidWorks® as a part file as seen in Figure 2.6. This was a key step in the process for capturing the varied, irregular features such as the wings, legs, and tail. However, the imported geometry had no detectable features so it could not be modified in any manner. To solve this issue, the geometric mesh was sliced with intersecting planes across the height of the carcass, and contour curve sketches of the different parts of the carcass were constructed. This allowed each body feature to be independently modified if necessary. Figure 2.7 displays the carcass geometry represented by the contour curve sketches. To construct the solid geometry from this, the ‘Loft’ feature is used to fill out the structure specified by the contour curves.

Figure 2.6: SolidWorks imported 3D scanned carcass geometry

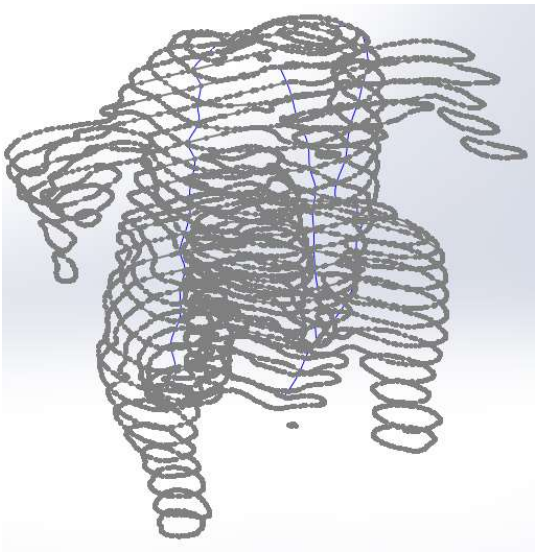

Figure 2.7: Contour curve representation of carcass geometry

With this geometry constructed, the carcass wings and legs were slightly modified by using fillet features to smooth the surfaces and connections to the main torso. This was a critical step in the geometry refinement as sharp edges or surface features would lead to meshing issues when setting up the mesh in COMSOL®. The final, processed carcass geometry can be seen in Figure 2.8.

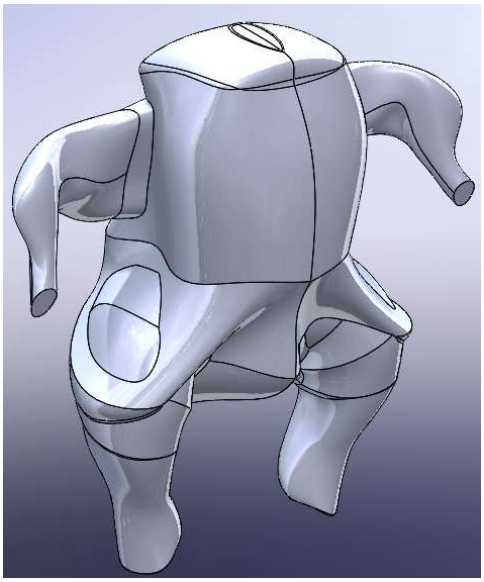

Figure 2.8: Processed carcass geometry

Once imported into COMSOL®, the carcass geometry can be and was scaled to desired size based upon what is relevant to industry or experimentation. Figure 2.9 displays the key geometric parameters for the chicken carcass such as wing-span (WS), torso width (TW), and height (H) as well as the reference planes and coordinate system to which the numerical flow studies refer. For the completed numerical studies, the carcass height (H), torso width (TW), and wing-span (WS) are 180 mm (7.1 in), 70 mm (2.8 in), and 181 mm (7.1 in), respectively. This is typical of a smaller carcass, but this geometry was chosen so that it would fit within the test section without having to make any overall size and mesh adjustments to the region and encapsulating domain. The motivation behind configuring the carcass geometry and studying the complex bluff body flow phenomena via COMSOL® was to give credence to experimental efforts to study and improve the heat transfer/fluid dynamics of in-line immersion poultry chilling by way of a finite series configuration shown in Figure 2.10.

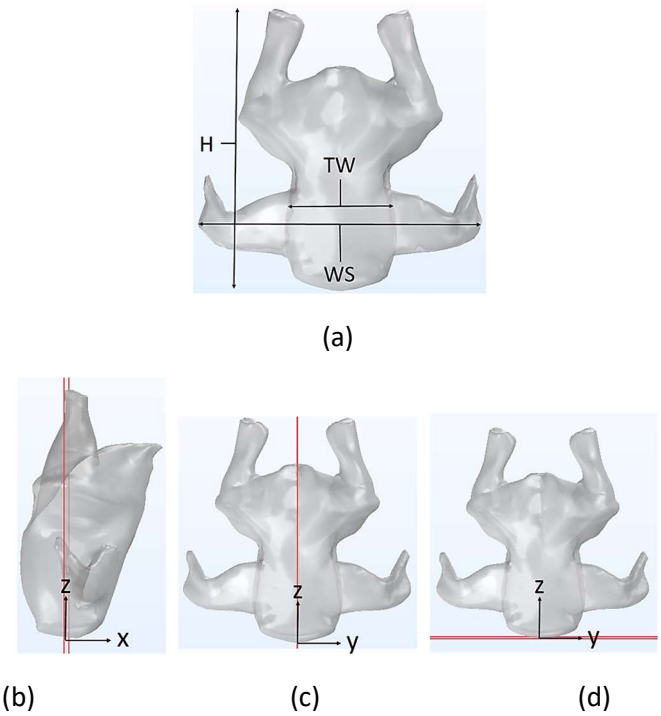

Figure 2.9: (a) Dimensioned features of carcass geometry (b) Reference yz-plane for carcass x-axis (c) Reference xz-plane for carcass y-axis (d) Reference xy-plane for carcass z-axis

Figure 2.10: Finite experimental poultry chilling segment

As mentioned prior, similar mesh distribution properties that were used for the simple cylinder configuration were used to construct the meshes for a single carcass or multiple carcasses in series. Figure 2.11 displays zoomed views of the mesh distribution of the test section region for single and multiple carcasses in series. For the inlet and outlet regions, the mesh distributions are

identical to Mesh 3 in the cylinder configuration with 77,206 and 154,560 elements in the inlet and outlet regions, respectively. Using similar mesh specifications and distribution as used for the simple cylinder for the carcass geometry and test section region, 2,239,536, 5,092,125, and 7,658,981 element meshes were generated in the test section, for one, three, and five chickens, respectively.

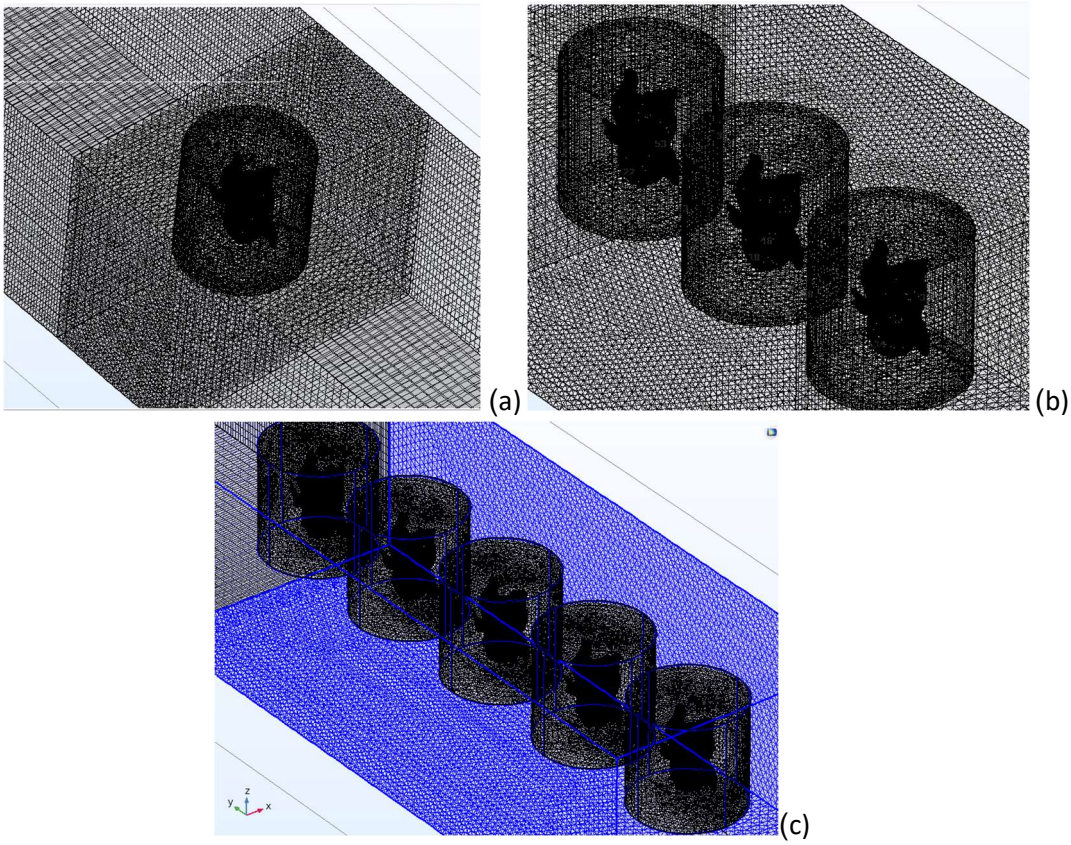

Figure 2.11: (a) Test section mesh view for single carcass study (b) Test section mesh view for series of 3 carcass study (c) Test section mesh view for series of 5 carcass study

2.3 RESULTS AND DISCUSSION

The main objective of the numerical flow studies is to establish a simulation of realistic, industrial flow conditions that are prevalent in poultry processing. In poultry processing applications, the fluid medium (most commonly water or air) is used to deliver thermal transfer (heating/cooling) and mass transfer (disinfection, water/salt uptake, fortification, etc.), and these

processes are generally desired to be uniform for the product. However, the flow dynamics around these irregularly-shaped objects is complex with intertwined boundary layer growth and flow separation, laminar-to-turbulent transition, and recirculation regions. These phenomena lead to the carcass being subject to varied exposure rates in the heating, cooling, disinfection, and other relevant heat/mass transport processes. Therefore, the industrial processes are not designed in an optimal manner as they have to be constructed based on required maximum or minimum requirements for best case scenarios. The over/under exposure due to flow variations can lead to undesired losses and inefficiencies.

Within COMSOL®, by defining representative boundary conditions and assembling the computational domain geometry, the model was designed to reasonably reduce the large poultry processing line to a simplified channel with a test section containing a single or in-line series of chicken carcasses. The presented computational domain comprising of a carcass or series of carcasses was deliberately configured to simulate a finite segment of the in-line immersion chilling line translating through a channel of chilled water. Single and multiple carcasses placed in the flow channel test section were simulated to study the fluid velocity and pressure data. The subsequent section will focus on the complex flow dynamics around one carcass placed within the test section as a way to examine the key nuances of the flow characteristics as it relates to single bluff body configuration without interference from multiple flow disturbances, as would be evident in a series configuration. The section following the single carcass flow study details the flow dynamics of an in-line carcass series configuration with identical industrial inlet flow conditions except the test section length is adaptive to the number of carcasses contained within the region. In both of these configurations, the carcasses are encapsulated within a rotating domain; however, there is no rotation induced so that the flow can be indicative of the industrial baseline of pure carcass

translation through the chilled water channels. The rotating domain feature was implemented for future studies to study the flow dynamics surrounding the carcass line with superimposed shackle rotation.

2.3.1 Numerical Simulation of Single Carcass in Channel Flow

Figures 2.12, 2.13, and 2.14 display a set of zoomed views of the flow field around a single carcass for the front (xz), horizontal (xy), and vertical (yz) planes. The fluid flow fields around a single carcass in the channel flow are visualized at various angles from these contour plane views with the red arrows displaying the flow direction. As fluid flow proceeds from the inlet, it

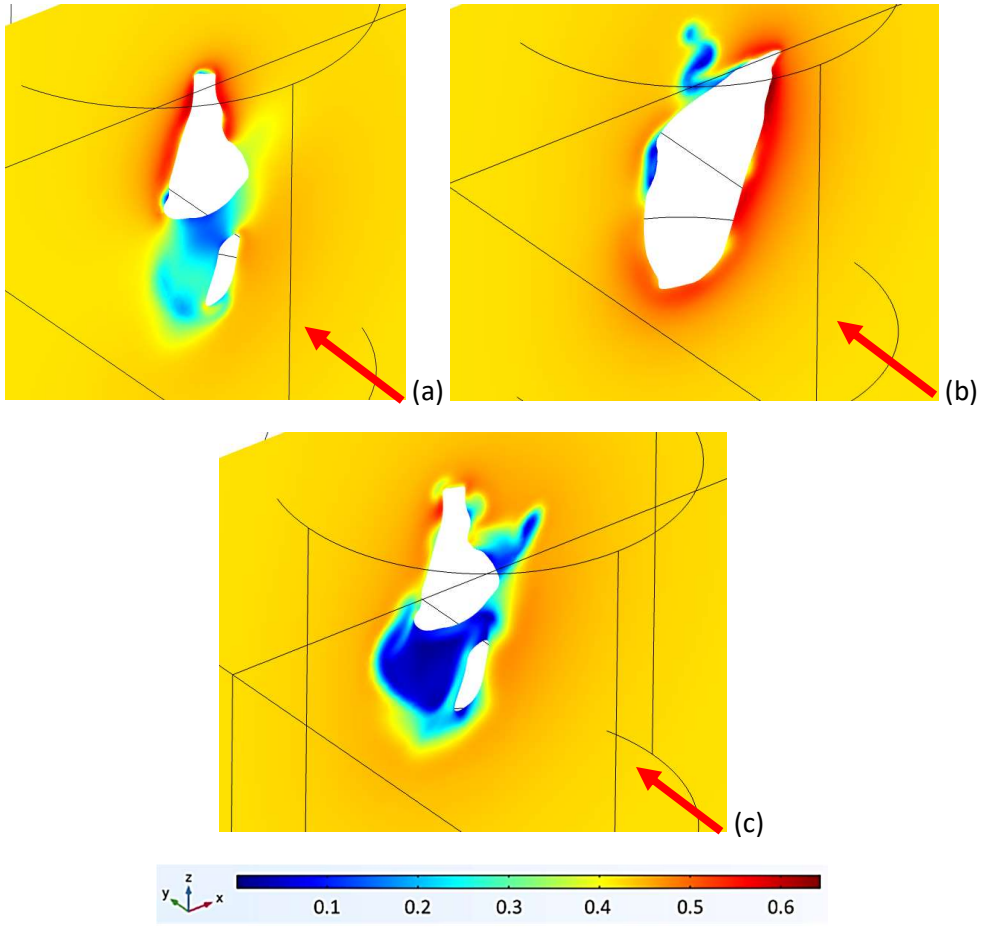

Figure 2.12: Flow field velocity (m/s) in xz-plane (front plane) around chicken. (a) chicken front-half section view (y = -3.75 cm), (b) chicken mid-plane center (y = 0 cm), and (c) chicken back-half section view (y = 3.75 cm)

encounters the carcass body from one side (right leg and wing) first, flows around the front and back of the torso, and then encounters the other back wing and leg. The results indicate a complex flow field with intertwining flow characteristics that must be examined with great caution due to the unavailability of published data for this configuration. Although there is some flow similarities with published works, the highly three-dimensional nature of the flow field is not easy to glean from a two-dimensional plane view. Figure 2.12(a) to (c) detail a series of frontal views (cross-section views) of the fluid flow field as the channel flow progresses downstream across the carcass body. The velocity contour data shows frontal stagnation and low-velocity wake regions that are

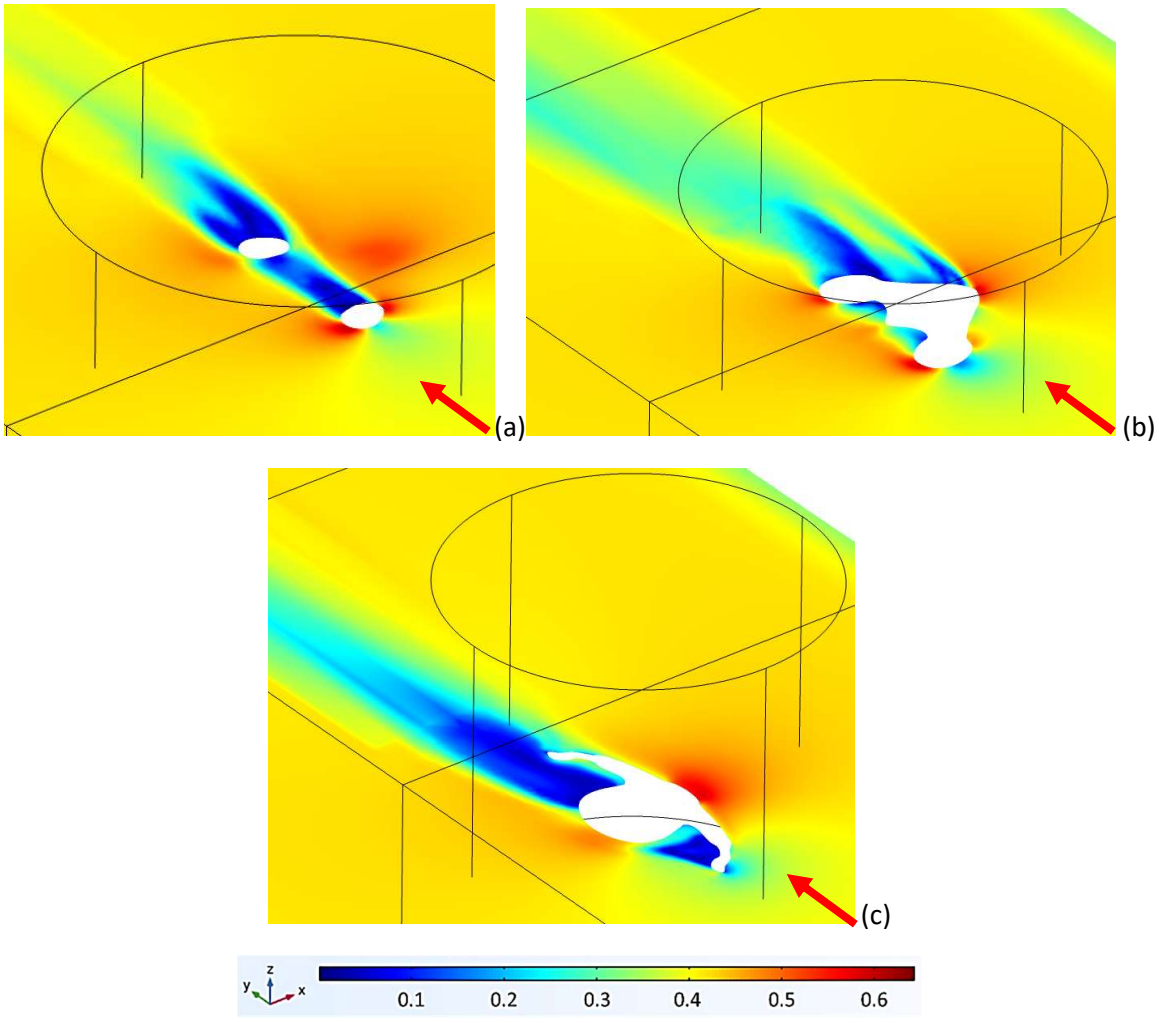

Figure 2.13: Flow field velocity (m/s) in xy-plane (horizontal plane) around chicken. (a) chicken upper leg section (z = 145 cm), (b) chicken bottom/thigh section view (z = 125 cm), (c) chicken chest/wing section view (z = 50 cm)

apparent due to the no-slip carcass surface. The views also capture low flow regions below the leg, where the stagnant region exists at the intersection of the leg and torso.

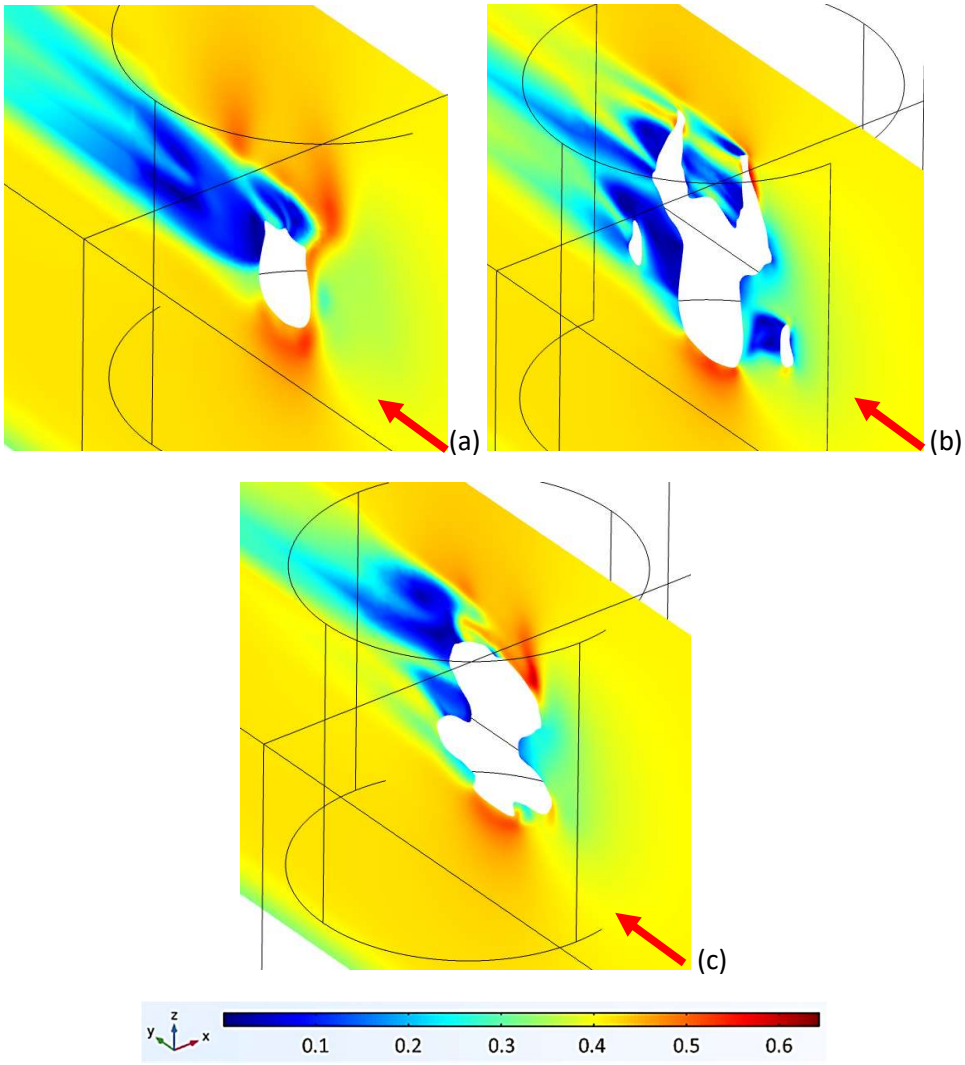

Figure 2.14: Flow field velocity (m/s) in yz-plane (vertical plane) around chicken. (a) chicken front breast section (x = -2.5 cm), (b) chicken mid-half/center section (x = 0 cm), and (c) chicken back section view (x = 2.5 cm)

Similarly, Figure 2.13 illustrates the flow velocity contour data surrounding the single carcass at varied heights in the horizontal plane, and Figure 2.14 shows the flow velocity contour data for the carcass vertical plane. As evident in examination of Figure 2.13(a), the flow dynamics resemble an inline dual cylinder series configuration presented by Kostic and Oka [23]. The front leg facing the oncoming channel flow incurs flow separation in the back half of the body and

shields the flow to the subsequent back leg. The front leg wake formation extends to the back leg and impacts the back leg wake formation to a certain extent. Additionally, the variable thickness of the carcass leg and irregular geometry induce a varied, merging flow to introduce a three-dimensional flow effect and produce an asymmetric wake. These flow phenomena can be seen in Figure 2.14(a).

Figures 2.13(c) and 2.14(a) display the flow velocity contour data for the carcass chest/wing section view in the xy-plane and the chicken mid-half/center section in the yz-plane, respectively. In these two figures, the noteworthy secondary flow impact of the carcass extensions (i.e. legs, wings) become apparent as these body features produce low-flow, recirculating regions downstream that affect the uniformity of the flow around the carcass. This phenomenon has major implications for the processing homogeneity such as heating, cooling, disinfection, and other relevant transport processes. A key nuance between the simple cylinder and complex carcass configurations that leads to the secondary flow complexity and wake formation variations is the multiple points of boundary layer formation and subsequent flow separation. These phenomena

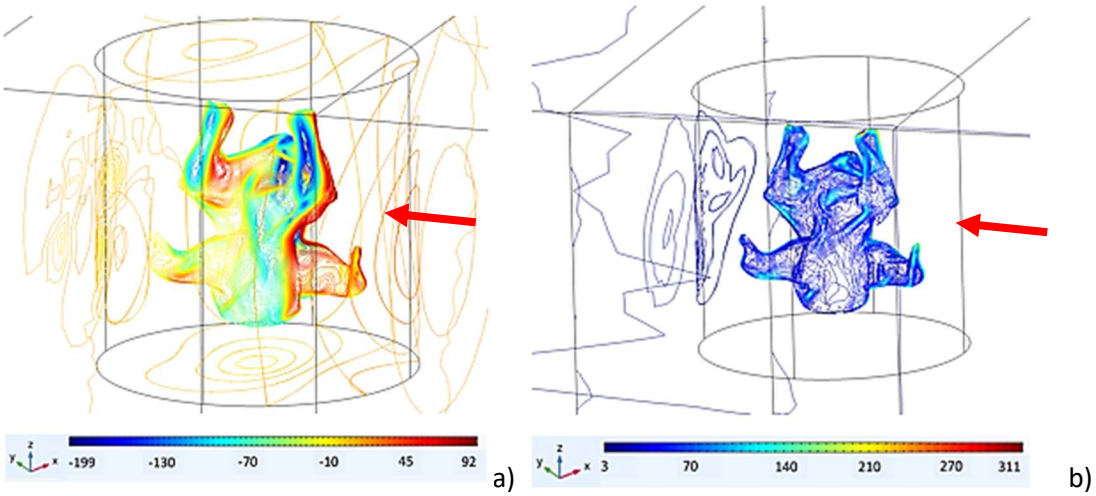

Figure 2.15: (a) Pressure field contours (Pa) (b) and Shear rate contours (s^{-1}) in test section

have a three-dimensional aspect to them and is evident in viewing planar data in Figures 2.12(a), 2.14(a), 2.14(b), and 2.14(c). The wakes from the multiple flow separation points coalesce further downstream into larger, more expansive wake regions that extend well beyond the domain test section.

Once again, the non-uniform flow exposure is evident in the pressure and shear rate surface contour plots displayed by Figure 2.15. This data shows the noticeable high/low pressure and shear rate regions developing at distinct, varied locations on the carcass surface. This further supports the stated notion that the carcass experiences non-uniform flow that can affect final product quality.

2.3.2 Numerical Simulation of In-line Carcass Series in Channel Flow

With industrial poultry processing involving multiple carcasses in an in-line series arrangement, it is important to focus on the key flow interactions between multiple carcasses in the channel flow. Correspondingly, the COMSOL® computational domain was modified to include a semblance of the industrial processing line by way of a finite in-line series of three and five carcasses. With a center-to-center spacing of 31.5 cm (12.4 in), numerical flow simulations were conducted for a series of three and five carcasses at the prescribed industrial flow condition (0.4 m/s). This shackle spacing was used in the flow studies as it is one shackle-to-shackle distance setting used in industrial processing and is the spacing used in the experimental carousel system developed for testing purposes as described in Section 3.5. Additionally, this shackle spacing was used to allow for flexibility in scaling the carcass size without needing to adjust the encapsulating domain size and mesh properties. For brevity, the detailed plane data for the flow field for an in-line series of five chickens will be presented only.

Figures 2.16 and 2.17 display the set of zoomed views for the horizontal (xy) and vertical (yz) planes of the velocity flow field around the series of five carcasses in the channel flow with the arrows indicating direction of flow. It is evident that flow stagnation points initially develop at the leading wing, body, and leg features, and this phenomenon extends to the carcasses downstream as well. However, the surrounding flow field for each carcass in series is not comparable to the isolated, single carcass configuration due to the interactions developing between the series of bluff bodies in the channel.

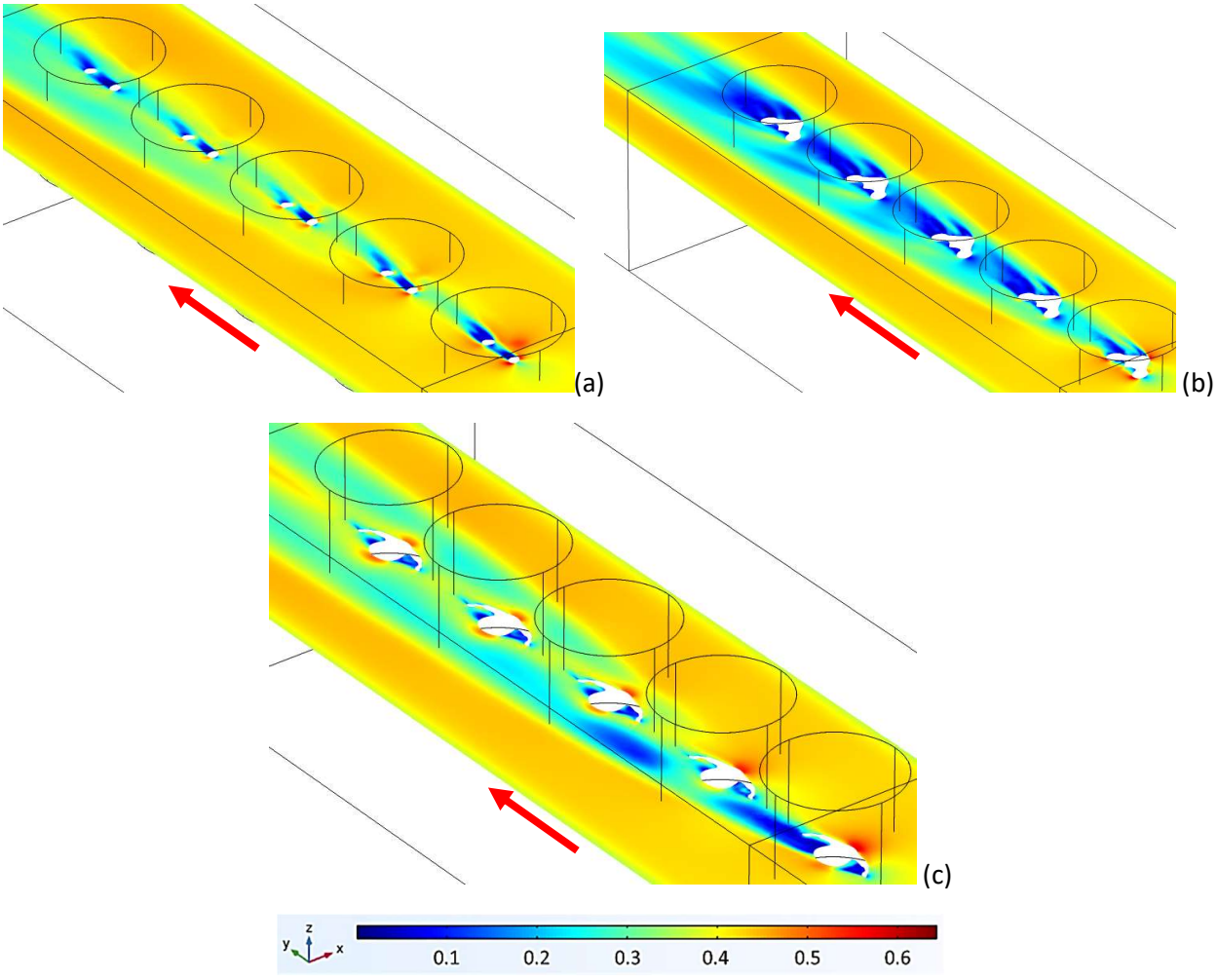

Figure 2.16: Flow field velocity (m/s) in xy-plane (horizontal plane) around series of five chickens. (a) chicken upper leg section (z = 145 cm), (b) chicken bottom/thigh section view (z = 125 cm), (c) chicken chest/wing section view (z = 50 cm)

In Figure 2.16, where the velocity contour data at various heights of the carcass can be examined, the downstream propagation of the upstream flow separation and wake formation occurring at the leading carcasses in the series is a noteworthy characteristic of this bluff body flow. As similarly gleaned in the single carcass simulation, the flow dynamics akin to a series of 10 unequally spaced cylinder can be examined from Figure 2.16(a), which shows the xy-section view of the series of carcass legs.

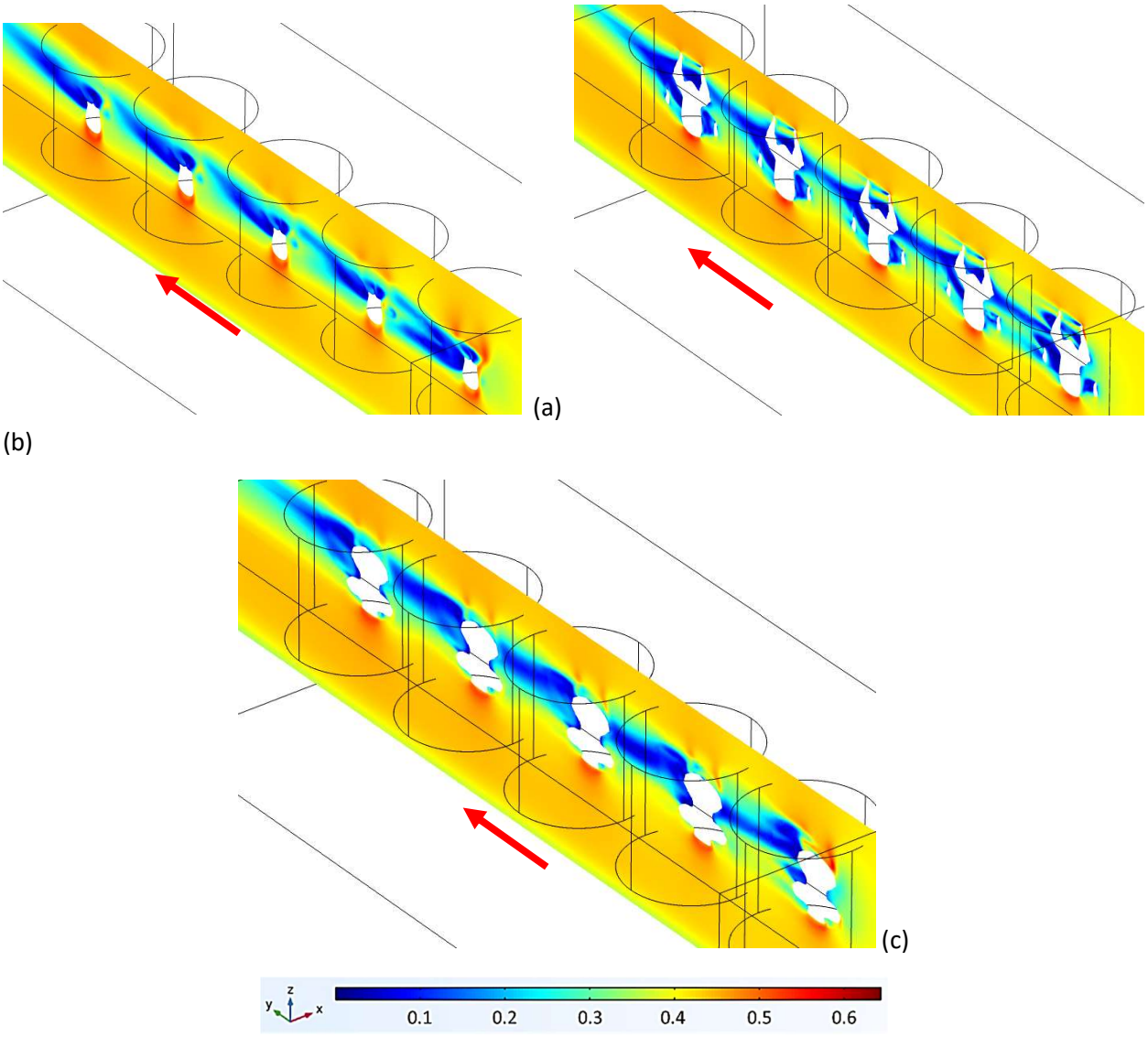

Figure 2.17: Flow field velocity (m/s) in yz-plane (vertical plane) around series of five chickens. (a) chicken front breast section (x = 2.5 cm), (b) chicken mid-half/center section (x = 0 cm), and (c) chicken back section view (x = -2.5 cm)

Tracking the bulk flow boundary layer development as flow progresses from the leading carcass to the trailing carcass, it is evident that the boundary layer and corresponding formation grows larger. The wake formation at the leading carcasses in series envelope successive downstream carcasses, and the leading carcasses shield flow for downstream carcasses, which furthers the non-uniform flow exposure narrative discussed in the single carcass simulation.

Figure 2.17 displays the velocity flow contour data for the vertical yz-plane, which gives insights on the three-dimensionality of the flow separation, wake formation, and recirculation regions. Multiple locations of flow separation and wake development are a result of multiple non-uniform geometric features and extensions from the carcass body. These formations coalesce and lead to the three-dimensional secondary flow effects. Additionally, in Figures 2.17(b) and 2.17(c), it can be seen that the wake of a preceding carcass extends to a subsequent carcass, once again supporting the notion of the flow shielding effect within the in-line series arrangement.

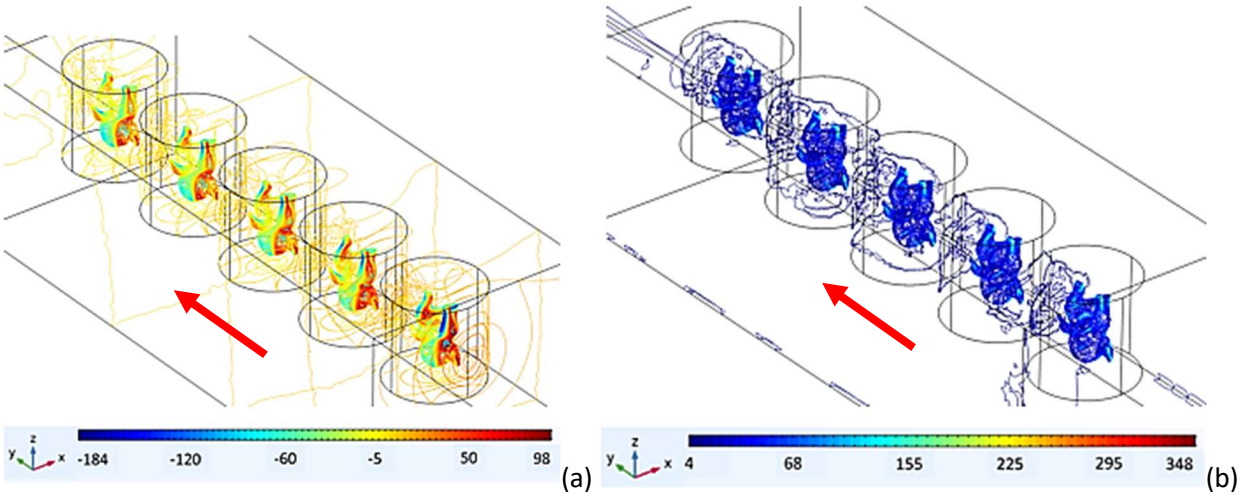

Figure 2.18: (a) Pressure field (Pa) contours and (b) shear rate (s^{-1}) contours in test section for series of five chickens

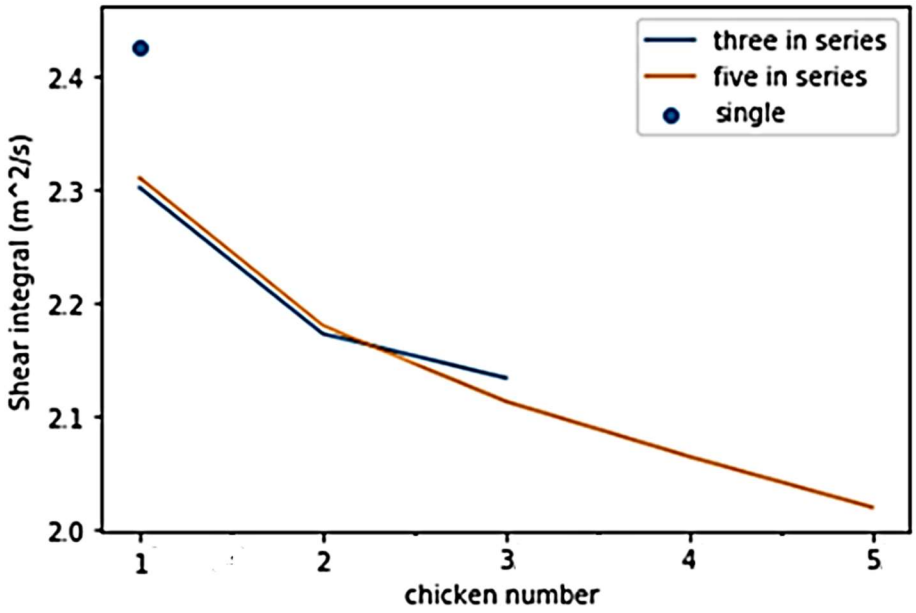

Figure 2.19: Integrated surface shear rate for numerical simulation of a single chicken, series of three chickens, and series of five chickens in channel flow

As previously stated in the single carcass flow simulation, there is apparent non-uniformity in the pressure distribution and surface shear for each carcass in series as can be seen in Figures 2.18(a) and 2.18(b). There are higher pressure and shear areas primarily on the front half of each carcass in the series. This has major implications on the poultry processing industry as inconsistency of the processing can lead to product quality issues. Figure 2.19 shows a comparison between the integrated surface shear rate for one, three, and five carcasses under the same industrial flow condition. The surface shear rate for the carcass is determined by the tangential, near-wall fluid velocity to the carcass surface divided by the distance between the near-wall fluid layer and the carcass surface. Multiplying surface shear rate by the fluid viscosity would result in surface shear stress. To determine the surface shear rate magnitude experienced by the carcass, the shear rate was numerically integrated on the carcass surface. This integrated surface shear rate indicates the strength of the fluid shear on the carcass boundary, which has direct implications on convective heat and mass transfer. Higher shear rates indicate higher convective heat/mass transfer

coefficients. In examining Figure 2.19, there is an apparent reduction in surface shear while proceeding from the leading carcass (chicken #1) to the trailing carcass (chicken #3 and #5 for the series of three and five carcasses, respectively). This further corresponds to the earlier point made about compounding wake formation as flow progresses in the channel and the flow shielding effect.

2.3.3 Conclusions

During industrial food processing and especially poultry chilling, one of the challenges processors face is deciphering the impact of industrial parameters (e.g., chiller medium/temperature, line speed, carcass shackle orientation) on maintaining final product and downstream process quality. Due to the complex geometry of the chicken carcass, it is very difficult to infer the corresponding flow field (as it pertains to in-line immersion chilling) from previously published references. Therefore, it was very important to simulate the industrial flow system to get an understanding of the flow dynamics involved in the chilling process and glean any potential issues and modifications that can be made in the process. The detailed flow simulations of industrial poultry chilling are reported in the prior sections and detail the initial simulations of highly three-dimensional flows encountered with a complex geometry suspended in series within a flow stream. It is preferable that this chilling process be performed under uniform exposure conditions, but the presented flow field data has revealed that this process is neither uniform nor consistent. Although the final product ultimately satisfies quality and safety standards, uneven exposure due to these flow variations can lead to process design inefficiencies. With the previous conclusions made, it is critical to design an alternative approach to the traditional in-line immersion chilling approach that will manipulate the flow dynamics experienced by the series of

carcasses on the poultry processing line to allow for enhanced relative motion between the carcass and chiller medium as well as provide more consistent, uniform chilling. A novel approach to favorably altering the flow dynamics during the in-line immersion chilling process is discussed in detail in the subsequent section.

3 THERMAL EXPERIMENTAL STUDY

3.1 INTRODUCTION/MOTIVATION OF STUDY

As mentioned in the review of poultry chilling, the primary reason for the poultry chilling step is to chill the carcass meat from 40 ºC to 4 ºC to help limit bacterial and microbial growth for food safety and quality standards. As previously noted, there are many industrial chilling methods selected based on end-market and facility operational preferences, such as air chilling, screw auger immersion chilling, spray chilling, and hybrid air/immersion chilling. While maintaining safety and quality standards and meeting customer demand is the primary focus of the facility, there is an important emphasis on streamlining facility operations, reducing input costs, and improving traceability of product within the facility. With regards to streamlining the facility operation, spatial footprint is a premium to plant operators so investigations into new technologies to reduce the space required for certain processes are underway. Additionally, energy can be thought of as an input raw material for poultry plant operators just as raw polymers would be for extrusion operations so reducing this input cost by way of implementing more energy-efficient equipment and/or processes is highly desirable for management and facility personnel. Recently, it has also been important for poultry plant operations to place an increased emphasis on traceability of product throughout the facility. With added traceability, defects in batches of product can be traced back more effectively so that problems such as contamination issues can be resolved without compromising many batches of final product.

To assess the effectiveness of various, standard poultry chilling methods, there have been extensive experimental studies conducted to determine chilling dwell times. Stadelman [24] gathered that most immersion chillers reduce breast muscle temperature from 40 ºC to 4 ºC in

about 30 to 50 minutes. Peric et al. [25] and Szentkuti et al. [26] were able to cool chickens from 35 ºC to about 5 ºC after 35 minutes by way of spraying the carcasses with chilled water (0 ºC). In an alternative method developed by Leistner et al. [27], they used a combination of a chilled water spray and subsequent air chilling stage. This hybrid approach required a 15 minute chilled water (10-12 ºC) spray to lower the breast temperature from 36 ºC to 18-20 ºC and a -40 ºC air chilling stage with an air velocity of 3.5 m/s. The apparent total chilling time for this hybrid approach was deemed comparable to full immersion chilling. As mentioned in the introductory section, an in-line approach to immersion chilling has been developed to take advantage of the convective heat transfer benefits of immersion chilling in a chilled water medium while also incorporating product traceability. It is apparent that there has been little-to-no previous work in studying in-line immersion chilling as studies regarding screw-auger and other batch-type immersion chillers are more prevalent. The present experimental study will focus on characterizing the incumbent in-line immersion chilling process and a novel immersion chilling process that introduces additional kinematics to the traditional process to increase convective heat transfer, improve chilling effectiveness, and reduce required chilling times.

Poultry chilling methods are partially governed by Newton's Law of Cooling, which specifies that heat leaving the carcass at the boundary is a product of the exposed carcass surface area, temperature difference between the carcass and the chiller medium, and the convective heat transfer coefficient. Convective theory suggests that the forced convective heat transfer coefficient is related to the local thickness of the boundary layer that develops at the carcass surface [28]. With the burgeoning boundary layer, the convective heat transfer is limited, and there is growing thermal resistance through the formed boundary layer. Since the heat transfer is less effective through the boundary layer, it is desirable to break up the boundary layer. In standard, in-line

immersive chilling, the series of carcasses are packed tightly and translating though a chilled water channel at a prescribed line speed. The nature of this process can be compared to an in-line series arrangement of cylinders, in which there are stagnation points that develop on the surface and lead to flow separation and corresponding wake formation. With the cylinders being arranged in series, the subsequent cylinders in the series face periodic, low velocity flow due to the preceding wake development. In addition, the trailing halves of the cylinders experience non-uniform, low flow velocities as compared to the leading sides.

Extending this to the translating carcass processing line, in the incumbent chilling method, boundary layer development, wake formation, and low velocity regions limit the convective heat transfer capability. Additionally, there will be non-uniform chilling due to the flow velocity variance between the leading and trailing halves of the carcass. With this under consideration, a novel in-line immersion chilling method was proposed and involves adding an additional vector of rotation/counter-rotation to the existing translating motion. This will aid in disrupting boundary layer formation, increasing the relative velocity between the chiller medium and the carcass surface, and uniformly exposing the carcass surface to the chiller medium flow. These factors will serve to increase the forced convective heat transfer coefficient, thereby increasing the convective heat transfer with all other conditions (i.e. carcass geometry, chiller medium fluid properties, carcass-chiller medium initial temperature difference) being equal. With a custom experimental design, novel in-line immersion chilling with induced rotational kinematics was assessed in relation to the industry-standard, in-line immersion chilling process via a series of thermal chilling experiments to measure carcass core temperature response. The following sections detail the experimental setup, methodology/rationale, and results in assessing the thermal benefits of the novel in-line immersion chilling approach for carcass chilling.

3.2 EXPERIMENTAL APPARATUS DEVELOPMENT – PROPELLER FLOW SYSTEM

As introduced in the prelude, the objective of the experimental study was to conduct a series of thermal measurement tests involving simulating the industrial poultry chilling process to compare the chilling effectiveness of the incumbent, in-line pure translation chilling to a varied set of shackle motion patterns involving a combination of translational and rotational kinematics. To do so, significant design and construction effort was undertaken to create an experimental apparatus to represent a finite segment of the in-line immersion chilling processing line.

3.2.1 Test Rig Design

To investigate various design parameters that were proposed to compare to the baseline industrial practice of pure translation of the carcasses through the chiller medium, a test rig was developed to simulate the relative fluid motion between the carcasses and chilled water that would be evident in the incumbent in-line scenario. The most feasible method of replicating this relative motion was to incorporate a finite, periodic element of the shackle line (five carcasses) that would be fixed in space while axial flow was imposed. Several designs were considered and evaluated thoroughly including, but not limited to, a pump inlet and a horizontal-axis propeller-driven flow design. The evaluations were done through two-dimensional COMSOL® Multiphysics flow analysis, as seen Figures 3.1 and 3.2, respectively. The main criteria included the ability to provide uniform flow within the testing section, which would be indicative of a smooth wall industrial channel containing the finite carcass array, and fit such within the geometrical constraints of the experiment area. As can be seen from the pump inlet design in Figure 3.1, it would be a challenge, given the space limitations, to generate a fully-developed, uniform flow within the test section due to the necessary volumetric flow rate, which would require a significant entrance length due to the

small pump inlet. With the propeller-driven flow design, the horizontal-axis propeller mount could be placed upstream from the testing section and would provide a more uniform flow throughout the width of the channel. The "secondary" channel could provide a path for recirculation so that the testing rig could be a compact, closed system.

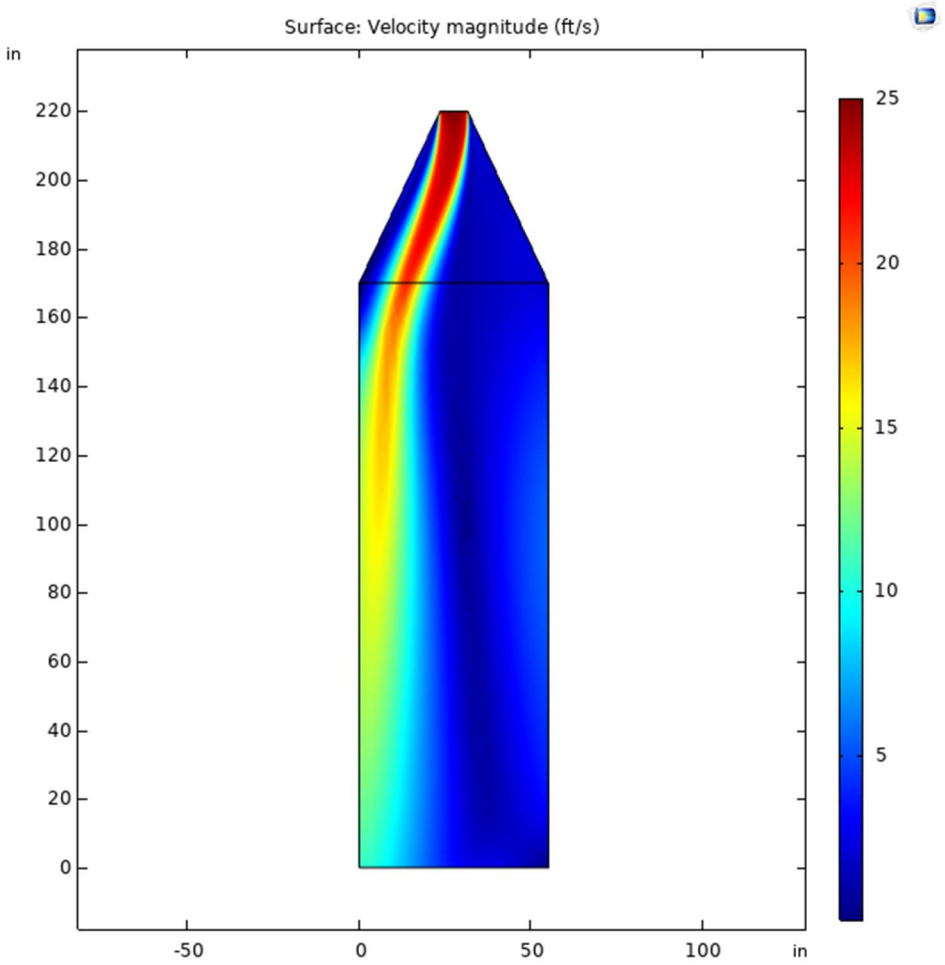

Figure 3.1: COMSOL® Flow Analysis of Pump Inlet Design

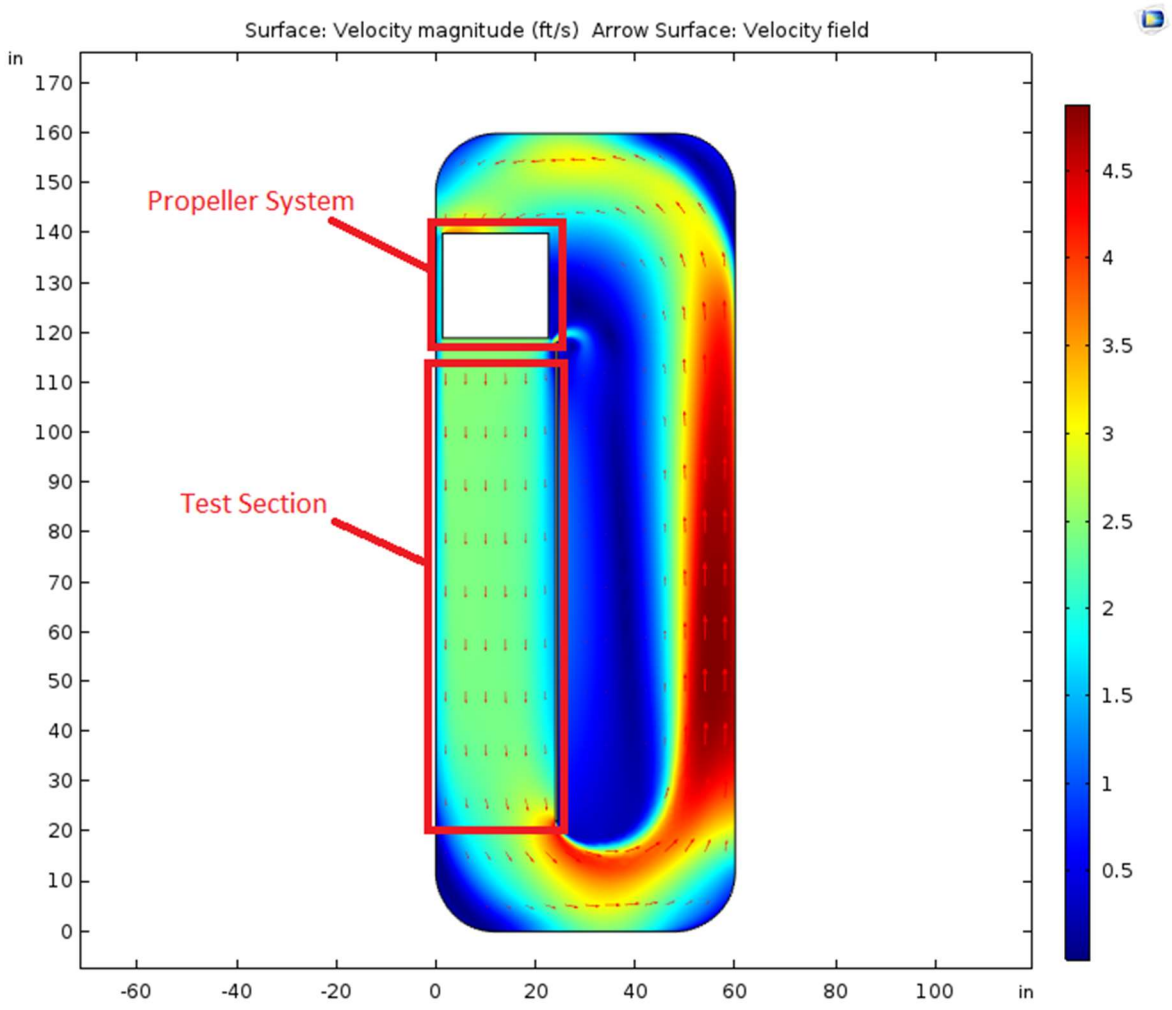

Figure 3.2: COMSOL® Flow Analysis of Propeller Flow Design

With this evaluation, the propeller-driven flow design was constructed as per the specifications detailed in Figure 3.3(a). The flow field interior was 160” (length) by 61” (width) by 24” (height) with a maximum fill capacity of approximately 1014 gallons. For testing purposes, the test rig was filled to an 18.5” height (781 gallons) to simulate an industrial setting. The shackle line was placed approximately 48” from the propeller shaft, which allows for sufficient distance for the flow to develop after the propeller system. The end of the shackle line was also sufficiently distanced from the downstream bend to mitigate an upstream effect.

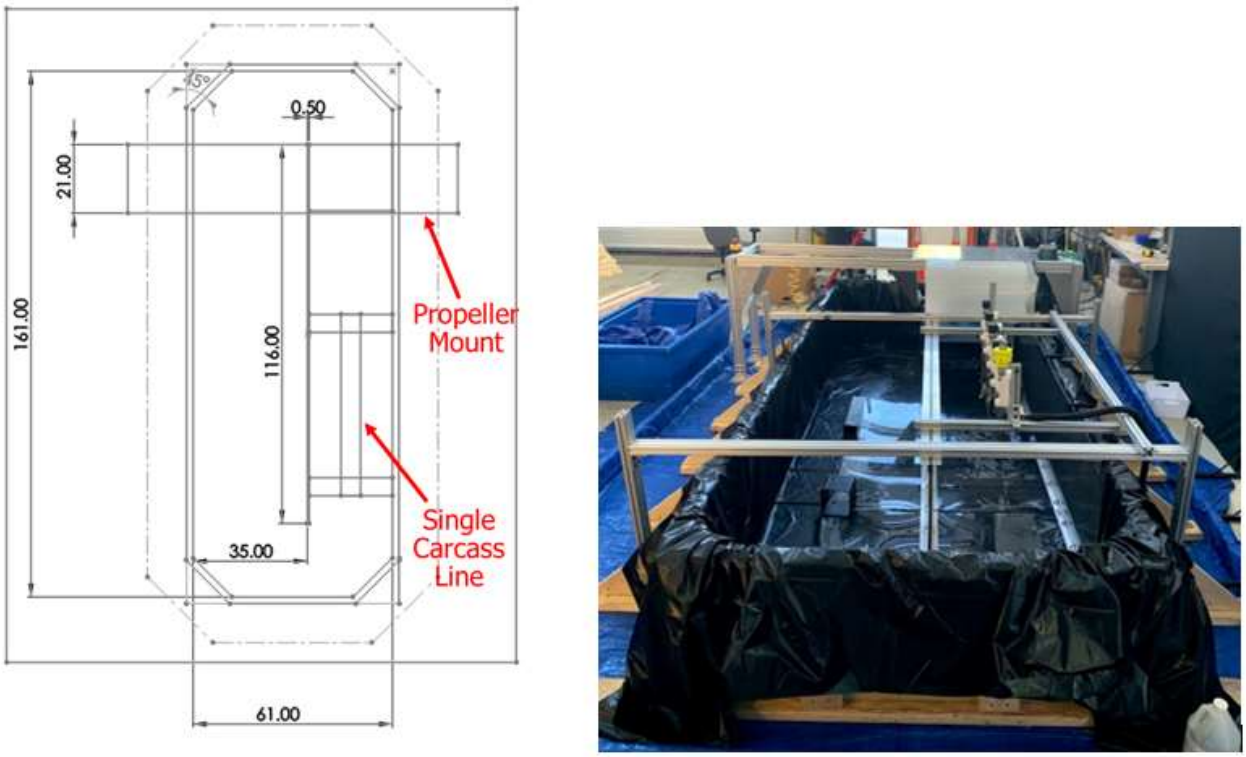

Figure 3.3(a): Propeller-Driven Flow Design Geometry (b) Full view of constructed test rig

The test rig was split into three major subsystems as shown in Figure 3.4: the modified propeller system, motorized shackle line within the smooth channel, and the flow velocity probe traverse system. The modified propeller system, displayed in Figure 3.4(a), is driven by a mounted 1 HP SEW EuroDrive motor, which is connected to a variable frequency drive to adjust the propeller rotational speed from 0 to 60 Hz. The modified propellers were constructed from stock aeration propellers with changes made to close the holes via the plastic sheet to provide more flow and the insertion of a PVC tube to provide a curvature akin to an airfoil to minimize water pickup as the propeller turns through the water. The smooth channel test section, displayed in Figure 3.4(b), was constructed with chemically-resistant PVC side walls and a polyethylene channel

Figure 3.4(a): Modified propeller system (b): Shackle line within the smooth channel (c): Flow velocity probe traverse system

bottom in order to have a smooth wall section to mitigate any concerns over secondary flow effects due to a rough wall. The dimensions of the test section channel include a 24" height, a 25.5" width, and a 116" length. The motorized shackle line, displayed in Figure 3.4(b), was placed within this smooth channel and was critical to the testing phase as it allowed for the shackles to be programmed with varied shackle rotational patterns as will be further detailed in subsequent sections. As depicted in Figure 3.4(c), a critical subsystem for measuring the velocity in channel

flow was developed and comprises of a JDC Electronic FLOWATCH® flow velocity probe and a traversable structure with a coordinate system. The coordinate point (0, 0, 25.5) in. is shown in Figure 1.5 as the positive x-coordinate runs down the shackle line direction, the positive y-coordinate runs from the indicated point to the middle channel wall, and the positive z-coordinate begins from the bottom of the channel moving up in height. As will be described in further detail in subsequent sections, this subsystem was utilized to characterize and calibrate the channel flow field at a propeller motor speed setting used in the experimental trials. This was important to do to reasonably simulate the flow dynamics occurring in the incumbent in-line immersion chilling process.

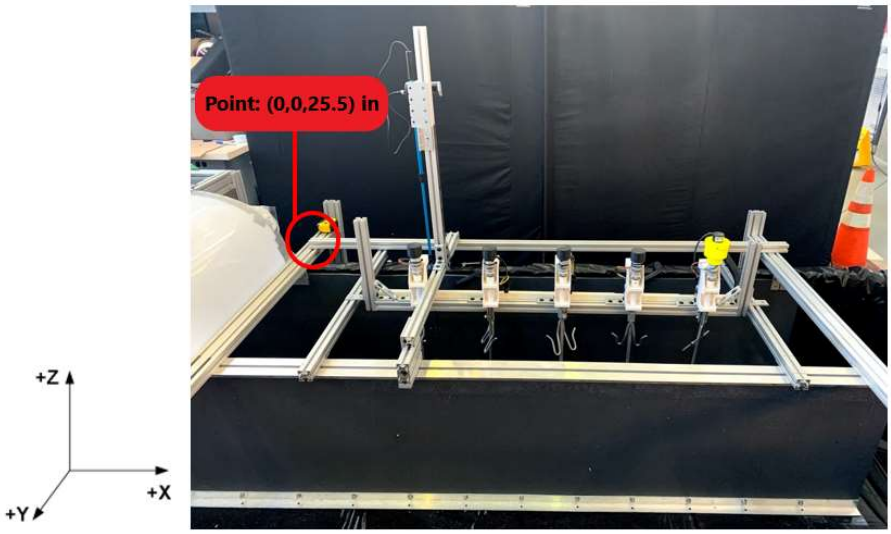

Figure 3.5: Flow velocity probe traverse system with 3D coordinate system

3.2.2 Experimental/Industrial Flow Field Theory

As briefly highlighted in the previous section, it was important to understand and match the flow dynamics (particularly the fluid relative velocity) surrounding the carcass between the industrial and experimental scenarios. . Because the experimental scenario aimed to mimic the carcass line translating through a passive medium (i.e., industrial reality) by way of inducing a

forced flow field around stationary carcasses (i.e., experimental set-up), there were nuances between the two scenarios that were subsequently addressed. Based on the industry-standard 140 birds per minute carcass line speed (equating to a 1.65 ft/s absolute line speed - given an 8.5" shackle-to-shackle centerline distance) and the hydraulic diameter of the channel flow (21.4 in.), this indicated a turbulent flow regime [29] with an associated Re of ~260,000 in both the actual and experimental setups. This flow regime nature benefitted the comparison between the actual and experimental scenarios as will be later discussed.

Because of the turbulent nature of the aggregate open channel, external flow over the carcass line, it was reasonable to assume that the fluid relative velocity profile along the x-axis is as shown in Figure 3.6. This industrial scenario is analogous to two symmetrical turbulent plane Couette flow scenarios with two stationary walls (channel walls) and two moving boundaries (carcass outer left/right boundaries) with a velocity, U_c, which is the target carcass line speed of 1.65 ft/s. Bech and Andersson [29] conducted numerical simulations for turbulent plane Couette flow in their work, and the behavior of the mean velocity corresponds well with the relative fluid velocity distribution below as a result of the carcass movement. Tillmark and Alfredsson [30] conducted experimental work on plane turbulent couette flow and have detailed comparable flow development behavior. They have indicated that the bulk mean velocity (as detailed in Figure 3.6 below) tends towards 50% of the moving wall's velocity. In this particular study, this equates to 0.83 ft/s.

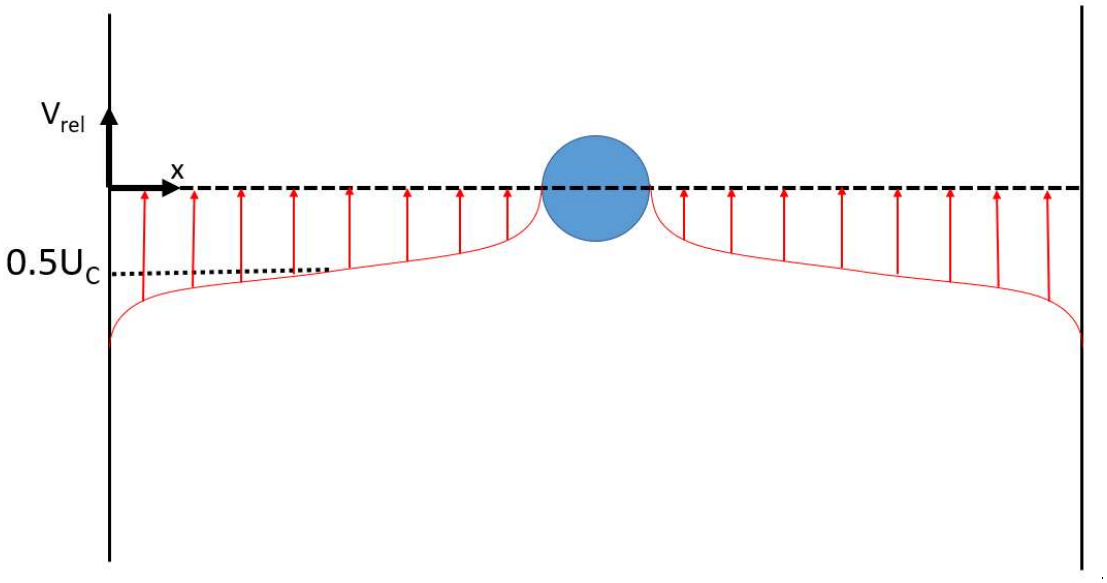

Figure 3.6: Flow Dynamics of Actual Industrial Scenario

However, as mentioned prior, the turbulent nature of the flow field did allow for the current experimental setup to be a reasonable approximation of the actual scenario with some subtle nuances, as seen in Figure 3.7. This flow profile was indicative of typical flow measurements taken in the plane aligned with the carcass as will be detailed in the following section. Because of the bluff body obstruction in the channel flow, there is a small displacement thickness that is apparent by the small slope in the fluid velocity profile from the carcass boundary to the near channel wall region. At the channel walls, there are small boundary layer regions (represented by δ) because of the no-slip condition. This is not represented in the actual industrial scenario, because the magnitude of the wall's relative velocity is highest in the actual flow scenario but is of zero magnitude in the experimental flow scenario. However, the experimental flow dynamics were relevant to simulating the actual industrial flow dynamics, because the bulk flow behavior corresponds well, with disparate behavior primarily just near the channel walls. These secondary flow effects at the wall were assumed to be negligible to the behavior of the bulk channel flow and are only comprised within the small boundary layers. This was a key claim as the fluid flow

phenomena close to the carcass was of more concern to the convective heat transfer that occurs between the carcass and chiller medium.

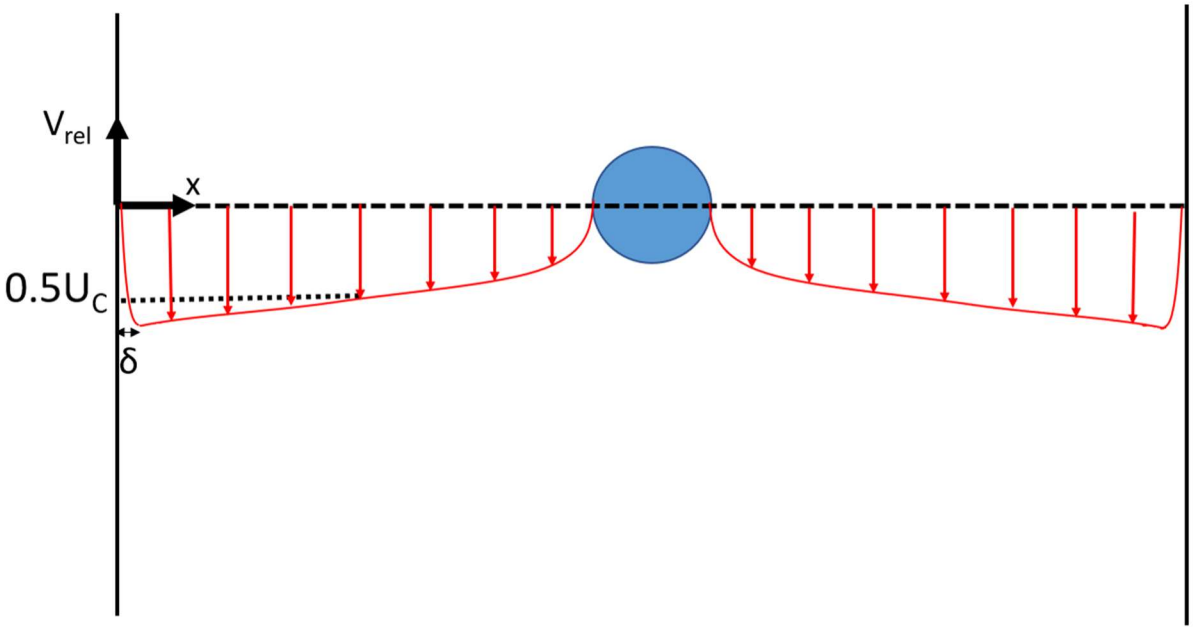

Figure 3.7: Flow Dynamics of Experimental Scenario

Given that the experimental and actual industrial flow scenarios were deemed comparable, the key experimental focus was to determine the propeller/motor system speed (Hz) setting that would, within reason, result in the 0.83 ft/s average flow velocity within the bulk plane flow between the leading carcass boundary and the channel wall boundary. The specific calibration process that follows this reasoning is next discussed in Section 3.2.3.

3.2.3 Experimental Flow Field Calibration

To calibrate the channel flow field to match the 0.83 ft/s average bulk flow velocity surrounding the carcass line, an iterative process was conducted consisting of tuning the propeller motor frequency while using the flow velocity probe system to take flow velocity measurements

at the corresponding propeller motor frequency. The motorized shackle line was arranged with five carcasses and placed within the test channel downstream of the propeller with a water level of 18.5”. Because the flow field was being calibrated to match the incumbent industrial flow scenario, there was no rotational motion pattern set by the motorized shackles, and the flowfield was intended to simulate a pure translation flow.

For a particular propeller motor frequency prescribed by the motor drive controller, the flow velocity probe was inserted at deliberate grid points into the channel flow within the mid-plane (yz-plane) of the leading carcass and average velocity over a sample period of 20 seconds for each point was gathered. The spatial grid for probe measurement is visually represented by Figure 3.8. The corresponding bulk flow velocity within the mid-plane on both sides of the carcass was calculated as an average of the gathered grid data on both sides of the carcass. The gathered table grid velocity data for two propeller settings is shown by Tables 3.1 and 3.2.

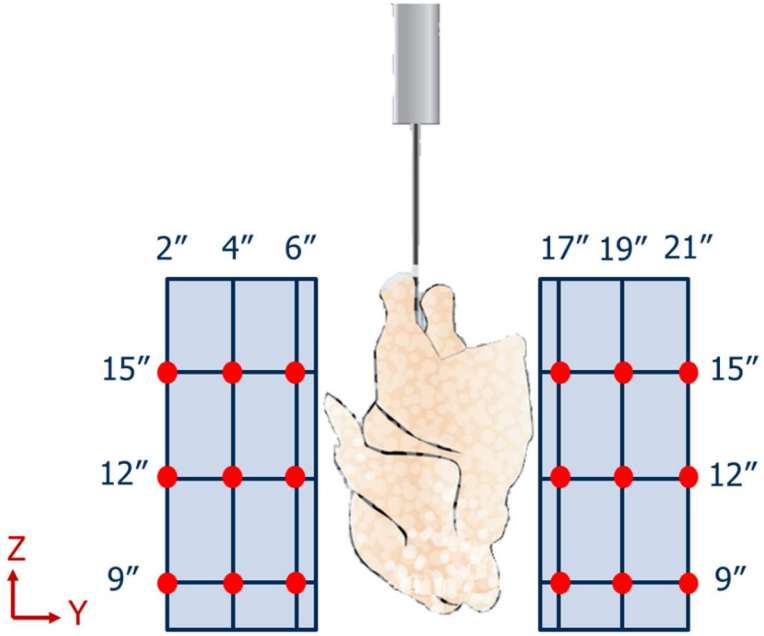

Figure 3.8: Visual Depiction of Mid-Plane Grid for Leading Carcass

Table 3.1: In-plane Carcass Flow Velocity Grid [fps] – First Carcass (60 Hz)

Z/Y	2"	4"	6"	17"	19"	21"
15"	1.8	1.7	1.5	1.4	1.4	1.3
12"	1.6	1.2	1.2	1.1	1.0	1.2
9"	1.3	1.0	0.8	0.7	0.6	1.0
Average:	1.3			1.1		

Table 3.2: In-plane Carcass Flow Velocity Grid [fps] – First Carcass (42 Hz)

Z/Y	2"	4"	6"	17"	19"	21"
15"	1.0	1.1	1.2	1.2	1.0	1.0
12"	0.8	0.9	0.9	0.8	0.8	0.9
9"	0.5	0.6	0.6	0.7	0.6	0.5
Average:	0.84			0.83		

As mentioned, the flow adjustment process was iterative, and the propeller motor frequency was gradually lowered from 60 Hz to 42 Hz, which resulted in the average bulk flow velocity desired on both sides of the carcass. This propeller setting (42 Hz) was used for all subsequent experimental trials as the simulated translation component of the carcass processing line.

3.3 IMMERSION CHILLING – CHILLED WATER THERMAL EXPERIMENTAL STUDY

The goal of this experimental study was to examine the thermal benefits of introducing superimposed rotational kinematics onto the traditional translation in-line immersion chilling process by way of a parametric sweep of various rotational shackle motion patterns. With this parametric study, key results and trends in the chilling effectiveness (i.e. temperature reduction, thermal time constant reduction) were analyzed and assessed. As previously highlighted, the flow testing apparatus, inclusive of the finite element of five shackles, simulated a scaled-down immersion chilling process. The subsequent sections detail the introduction of important

parameters that were used in the experimental analyses, the experimental testing methodology, and the organized progression of gathered results from the chilling tests.

3.3.1 Thermal Time Constant Justification/Formulation

Time constants are used in many mechanical and electrical systems as a transient response to a step input/change to the system. The time constant in these systems is the required time to reach 63.2% of the full response. Similarly, thermal time constants may be appropriate to characterize transient responses to changes in boundary conditions. For the purposes of this study, thermal time constants were used as it relates to convective cooling, explained by Newton's Law of Cooling, and transient heat conduction within the chicken carcass.

Generally, the temperature of a body will have spatial and temporal variance. However, lumped capacitance analysis (LCA) can be an effective simplification of transient heat transfer processes where the temperature of the body will only be a function of time rather than both time and space. The resulting transient temperature evolution as formulated by LCA is shown below by Equations 3.1-3.4, with the associated thermal time constant detailed as well.

$$\theta(t) = \theta_i * e^{\frac{-t}{\tau}} \quad (3.1)$$

$$\tau = \frac{\rho V C_p}{hA} \quad (3.2)$$

$$\{\theta(t) = T(t) - T_\infty\} \quad (3.3)$$

$$\{\theta_i = T_i - T_\infty\} \quad (3.4)$$

3.3.1.1 Analogous Thermal Circuit Setup

In association with the LCA, an analogous thermal circuit, akin to an electrical circuit, can be set up for the convective cooling of the chicken carcass. The analogous thermal circuit is

presented by Figure 3.9 below, where R_{therm} is the external convective resistance between the carcass surface and the chilled water medium, C_{therm} is the thermal capacitance of the carcass meat, and Θ_{cw} is the initial temperature difference between the chilled water medium and the carcass temperature.

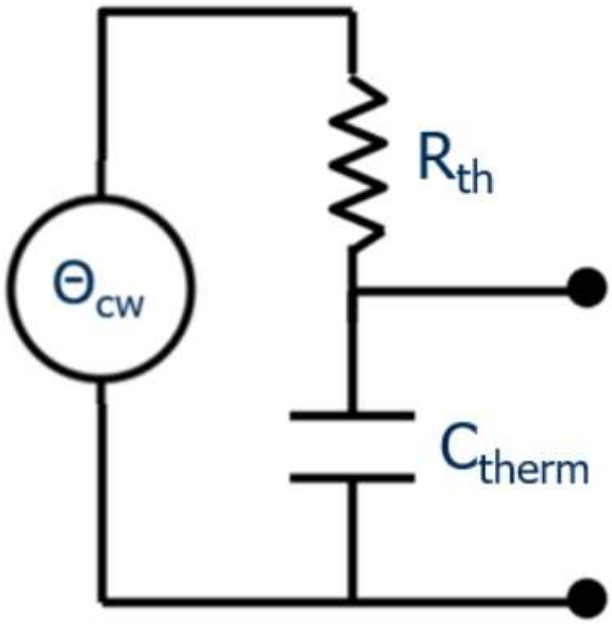

Figure 3.9: Analogous Thermal Equivalent Circuit for Carcass Transient Heat Transfer

This LCA idealization can only be used, however, if the Biot number, which is a ratio of internal conductive resistance to the external convective resistance, is less than or equal to 0.1. When evaluating the use of LCA in the convection cooling of chicken carcasses, it was apparent that LCA is not ideal for this application. From ASHRAE's reference data [31] on the thermal properties of foods, the thermal conductivity of the chicken breast meat was determined to be 0.52 W/m-K. Based upon an approximate characteristic length on the order of 1-1.75 inches (0.0254 – 0.0445 m) and a conservative range of forced convection heat transfer coefficients, the calculated Biot number for the chicken carcass was determined to be much greater than the 0.1 threshold. This indicates the importance of internal conductive resistance effects within the carcass meat.

Due to this, there will be noteworthy spatial temperature variance within the carcass meat in addition to the temporal temperature variance. To display this phenomenon further, a transient heat model was constructed in COMSOL® to simulate the carcass chilling process and track the core/deep muscle tissue (DMT) temperature with chilling time. With a chilling convective heat transfer coefficient of 2000 W/m^2-K (based on heat transfer correlations factoring in chilled water properties and relative fluid medium speed), a cut line temperature probe was inserted through the thickness of the carcass breast meat passing through the DMT location as shown in Figure 3.10 to measure the spatial and temporal variance of the carcass meat. This was done throughout a 60 minute chilling period. The temperature of the chilled water medium was set to be 8.5°C, as that was the average chilled water temperature used in thermal experiments described in Section 3.3.4, and the spatial temperature variance along the probed line for several time points is displayed by Figure 3.11.

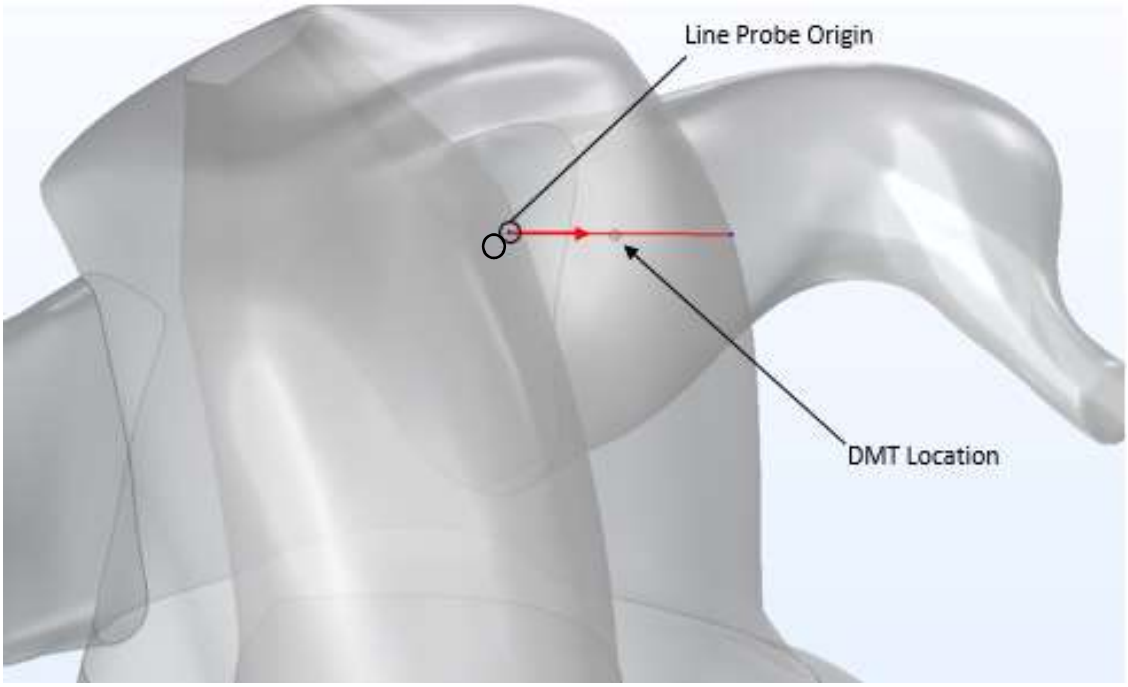

Figure 3.10: Carcass Geometry in COMSOL® with Temperature Line Probe Passing through DMT

With examination of Figure 3.11, it is apparent that after the chilling process begins, there is a temperature gradient that develops due to the chilling at the breast surface and interior cavity. The spatial variance is parabolic with a temperature maximum at the DMT location. As chilling time increases, the parabolic gradient starts to "flatten" as the temperature variation between the carcass meat temperature and chilled water temperature decreases leading to less heat convective heat transfer between the two domains. From the graph analysis, the notable spatial temperature variance can be attributed to the internal conductive resistance and thermal capacitance due to the carcass meat properties. This further supports the inapplicability of the LCA method of using thermal time constants. However, as can be seen in the following section, there was justification to use a thermal time constant approach for the poultry chilling process for experimental purposes.

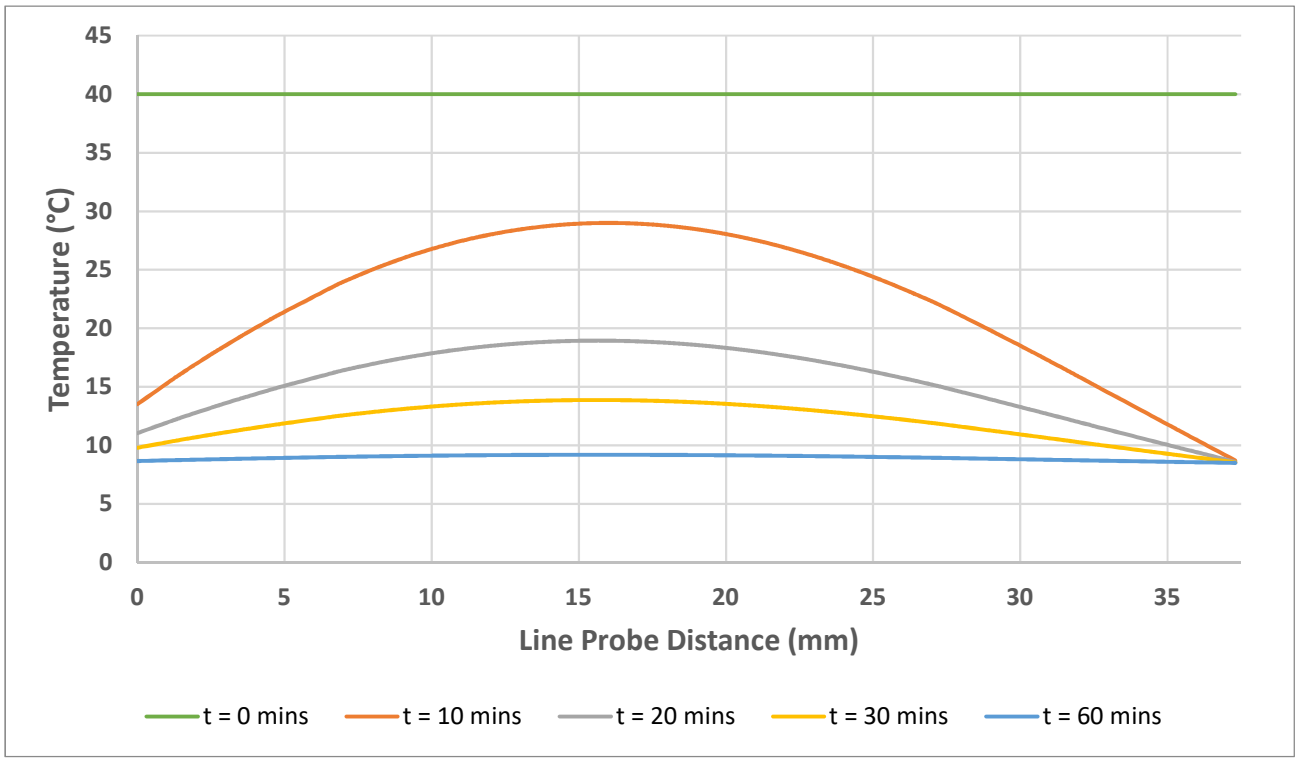

Figure 3.11: Spatial Temperature Variance along Line Probe through Carcass Breast Meat at Varied Chilling Time Points

3.3.1.2 COMSOL Analysis - Thermal Time Constant Justification

To validate the thermal time constant approach for the carcass chilling experimentation, a numerical investigation was done via COMSOL® Multiphysics software to simulate carcass core temperature evolution. To do so, the carcass geometry (identical as the one used in the computational section) was prescribed along with a convective boundary condition to simulate the immersion chilling process, and a range sweep of varied heat transfer coefficient values were selected based upon heat transfer coefficient correlations that factor in the typical translation speed of the carcass as well as the chilled water fluid properties. The range of heat transfer coefficient values varied from 500 – 2000 W/m^2-K. The carcass geometry was scaled to varied sizes as well in order to examine the impact of the internal conductive resistance as size is increased/decreased. Figure 3.12 details the carcass core temperature evolution from a starting temperature of 40 ºC

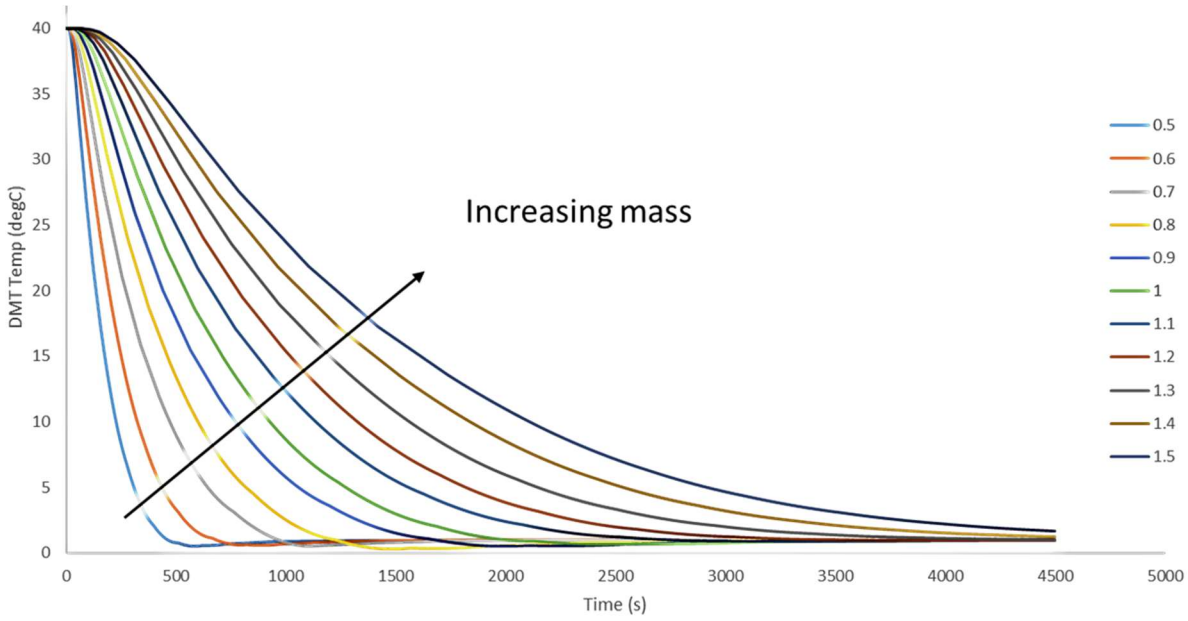

Figure 3.12: Deep Muscle Tissue (DMT)/Core Temperature Evolution for Varied Scale Factors at h = 1000 W/m^2-K

exposed to a 0 ºC chilled water medium with a convective heat transfer coefficient of 1000 W/m^2-K. As can be noticed in the temperature evolution for smaller scale carcasses, there seems to be temperature minima as the core temperature reaches 0 ºC. Physically, this should not occur, but this can be attributed to minor numerical fluctuations within the COMSOL® as it reaches the asymptotic limit. As evident in the beginning of the chilling process, there is a Fourier time delay due to the internal conductive resistance within the carcass breast meat. This is expected for a system that has noteworthy conductive resistance and/or capacitive effect. However, considering the typical scale factors of the carcasses used in the experiments ranging between 1.0-1.1, it was determined that the extent of the Fourier time delay at the beginning of the chilling process is very small compared to the typical total chilling time of the immersion chilling process, which as mentioned in prior sections can typically vary from 30 to 50 minutes. Therefore, the core temperature evolution can be modeled as an exponential decay process with an associated thermal time constant. When fitting the numerical data with exponential decay functions, all R^2 coefficients were greater than 0.8704 with the mean being 0.924 for all scale factors and standard deviation being 0.04.

With the LCA time constant approach, the time constant is analytically formulated based upon Equations 3.1 to 3.4, inclusive of a breakdown of the thermal time constant as a function of surface geometry and thermal properties. As indicated prior, traditional LCA does not apply for this particular carcass chilling problem, but rather the time constant can be semi-empirically formulated based upon a mathematical exponential fit approach. As previously mentioned, the core temperature evolution with time displays exponential decay behavior so the data can be fit accordingly, and the time constant can be determined. This further justified approximating the core temperature evolution as an exponential decay with an associated thermal time constant. This

thermal time constant approach was used as a metric for characterizing the chilling effectiveness of the various shackle motion patterns.

3.3.1.3 Experimental Determination of Chilling Thermal Time Constant

To determine the experimental thermal time constants associated with the chilling tests as described in Section 3.3.3.5, Equation 3.1 is rearranged to solve for τ as shown by Equations 3.5-3.7 below. Again, this takes into account the semi-empirical, mathematical approach to determining the time constant or rate of exponential decay for the core temperature evolution with time.

$$\tau = \frac{-t}{ln(\frac{\theta(t)}{\theta_i})} \quad (3.5)$$

$$\{\theta(t) = T(t) - T_{\infty,t}\} \quad (3.6)$$

$$\{\theta_i = T_i - T_{\infty,i}\} \quad (3.7)$$

Based on these set of equations, the chilling thermal time constant can be calculated using the chilling time (t), the starting temperature difference between the carcass core temperature and the chiller medium (Θ_i), and the ending temperature difference between the carcass core temperature and the chiller medium ($\Theta(t)$). There is a distinction in the $T_{\infty,t}$ and $T_{\infty,i}$ terms to account for the slight temperature increase in the chiller medium from the beginning of experimentation to the end. As an example, a sample thermal time constant calculation from collected experimental data is shown below for a 1.42 kg carcass undergoing '60 RPM Continuous

Rotation (1.5 Revolutions/Half Cycle)'[1] for a 12-minute chill time. The starting carcass core and chiller medium temperatures were 40.4 ºC and 8.3 ºC, respectively, and the ending carcass core and chiller medium temperatures were 20.4 ºC and 8.8 ºC, respectively.

$$\tau = \frac{-12\ mins.}{ln(\frac{20.4\ ºC - 8.8\ ºC}{40.4\ ºC - 8.3\ ºC})} = 11.8\ mins$$

3.3.2 Dimensionless Agitation Rigor – Testing Parameter Development

With the high number of possible rotational shackle motion patterns where angular velocity and/or angular displacement can be varied, a unique experimental parameter was formulated to equate various motion patterns tested to a simple, tangible value. To a certain extent, carcass agitation rigor can be tied to the convective heat transfer coefficient as increased agitation frequency and strength increases the shear and skin friction coefficient at the carcass surface, which correlates to an increase in Nusselt number and, correspondingly, the convective heat transfer coefficient. Agitation frequency is tied to the angular amplitude of carcass rotation in a particular clockwise or counterclockwise direction for a single cycle. As evident in boundary layer theory, disrupting the flow/thermal boundary layer growth will aid the convective heat transfer between the carcass and the chiller medium, so changing direction of rotation will aid in that process. Agitation strength corresponds to the angular velocity and the relative motion between the rotating carcass and the free-stream, translating motion of the chiller medium. With both agitation frequency and strength critical to convective heat transfer, an experimental parameter

[1] This motion pattern indicates a shackle angular velocity of 60 RPM completing 1.5 full rotations clock-wise/counter-clockwise (half-cycle) before preceding to reverse direction and complete 1.5 full rotations to complete a full cycle

that factors in both via carcass spin ratio and normalized angular displacement as sub-parameters was developed as shown below in the following expressions.

$$\text{Spin Ratio (SR)} = \frac{\text{Carcass Rotational Velocity}}{\text{Carcass Translational Velocity}} \qquad (3.8)$$

$$\text{Normalized Angular Displacement } (A_{dim}) = \frac{\text{Rotational Angular Displacement}}{360°} \qquad (3.9)$$

$$\text{Agitation Parameter (AgPar)} = \frac{SR}{A_{dim}} \qquad (3.10)$$

From a physical, practical standpoint, higher AgPar values relate to higher agitation rigor, and vice-versa. For perspective, using an average diameter of a carcass to convert shackle RPM to carcass rotational velocity, rotational patterns of '40 RPM Continuous Rotation (4 Rotations Per Half-Cycle)'[2] (Figure 3.13) and '40 RPM Half-Turn Churn (180º Rotation Per Half-Cycle)'[3] (Figure 3.14) would equate to AgPar values of 0.32 and 2.56. Due to the higher agitation frequency, the 'Half-Turn Churn' motion pattern has a higher AgPar value associated with it.

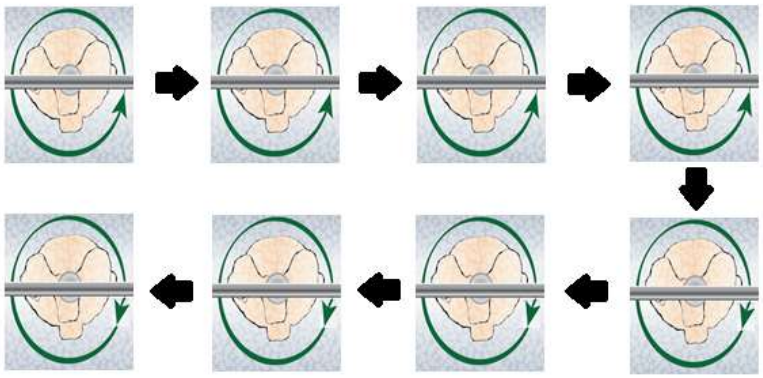

Figure 3.13: Progression of 40 RPM Continuous Rotation (4 Rotations Per Half-Cycle)

[2] This motion pattern indicates a shackle angular velocity of 40 RPM completing 4 full rotations clock-wise/counter-clockwise (half-cycle) before preceding to reverse direction and complete 4 full rotations to complete a full cycle

[3] This motion pattern indicates a shackle angular velocity of 40 RPM completing one half of a full rotation (180°) clock-wise/counter-clockwise (half-cycle) before preceding to reverse direction and rotate one half of a full rotation (180°) complete a full cycle

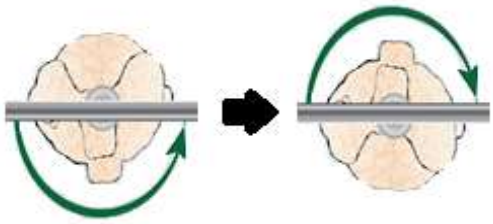

Figure 3.14: Progression of 40 RPM Half-Turn Churn (180º Rotation Per Half-Cycle)

3.3.3 Chilled Water Thermal Testing Experimental Techniques

As mentioned prior, the objective of the thermal experimental study was to effectively simulate the traditional and proposed, alternative in-line immersion chilling processes by way of the motorized propeller-driven flow contained within the open channel test rig as shown in Figure 3.15. To study the potential enhancement of the chilling process via alternative shackle kinematics, several experimental techniques and measurement procedures are employed within single day tests with a sample set of carcasses and will be described in detail in the subsequent sections.

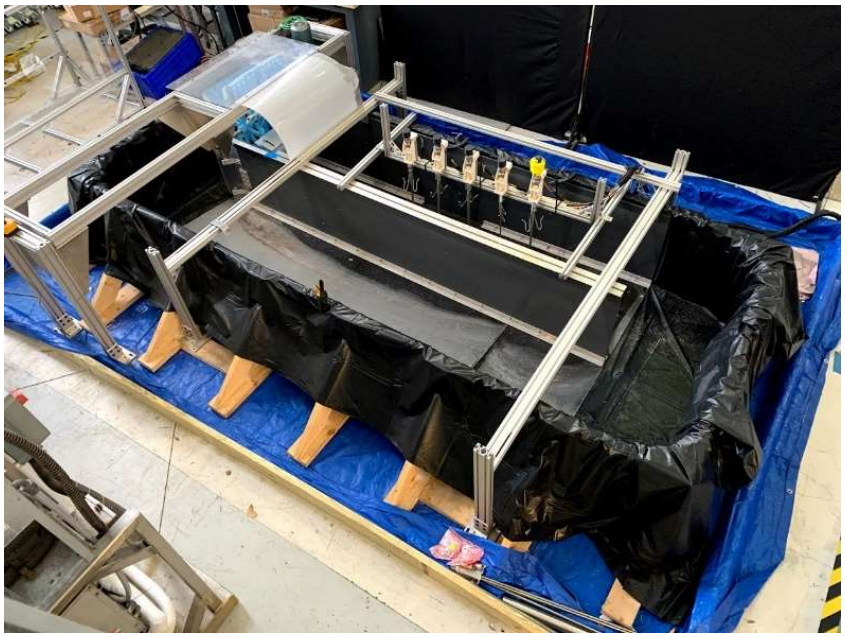

Figure 3.15: Open Channel Test Rig with Motorized Propeller System

3.3.3.1 Chiller Medium Preparation

To match representative industrial settings, the dimensions of the test rig channel's cross section were designed to be 24 inches (height) by 25.5 inches (width) with a water fill level of 18.5 inches. This corresponds to a total chilled water requirement of around 781 gallons. The test rig was filled primarily with a standard garden hose that outputs city water that varies seasonally from 11-12 ºC in the colder season to 20-22 ºC in the warmer season. The remaining volume came from ice taken from the Scotsman ice machine pictured in Figure 3.16 that is mixed into the water medium to achieve the desired chiller medium temperature. There is limited capacity in this ice machine, so ultimately the chiller medium temperature was set at 8.5 ºC in order to be attainable during all seasonal conditions. This chiller temperature still allowed for a significant temperature difference between the carcass core temperatures (40-42 ºC) and the chiller medium temperature for the chilling experimentation and evaluation of experimental thermal time constants.

Figure 3.16: Scotsman Ice Machine

An ice requirement calculation tool, shown in Figure 3.17, was created for the purpose of determining the mass of ice needed in conjunction with city water to reach a desired chiller medium

temperature based upon the total fill volume. This tool was used to justify the achievable chiller medium temperature of 8.5 ºC. The ice requirement governing equations (3.11-3.15) shown were based on an energy balance involving equating the sensible heat required to lower the chiller medium temperature a certain ΔT (q_4) to the combination of sensible heat in heating the ice from 0 ºF to 32 ºF (q_1), latent heat in melting the ice (q_2), and sensible heat in heating the melted ice from 32 ºF (0 ºC) to the final chiller medium temperature (q_3).

City Water Required Chilling Energy (q4)								
Volume of City Water:	610	gal		140910	in^3			
Mass of City Water:	5090.69	lbs						
Cp of Water:	1.00315	BTU/lb-F						
T1	75.2	F	24	C				
T2	32.9	F	0.5	C		**Blue cells are parameters**		
q4	216015	BTU				Heat Transfer Energy Balance		
Ice Heating Up - Stage 1 (q_1)						q4 = q1 + q2 + q3		
Mass of Ice:	1499.65	lbs				q4	216015	BTU
Cp of Ice:	0.5	BTU/lb-F						
T1	0	F				q1 + q2 + q3	216015	BTU
T2	32	F						
						Difference***:	0	
q1	23994.4	BTU						
						Density of Water:	8.344	lb/ft^3
Ice Melting (q_2)						Total Water Produced:	789.83	gal
Mass of Ice:	1499.65	lbs				Necessary Water Level (Before Adding Ice)	14.3	in
Latent heat of fusion for water:	143.54	BTU/lb				Water Level (After adding ice):	18.6	in
q_2	215259	BTU						
						***Under 'Data' tab, click on 'What-If Analysis' and select 'Goal Seek', then set cell 'I18' to '0' by changing cell		
Ice Heating Up - Stage 2 (q3)								
Mass of Ice Water:	1499.65	lbs						
Cp of Ice Water:	1.008	BTU/lb-F						
T1	0	F						
T2	0.5	F						
q3	755.822	BTU						

Figure 3.17: Ice Requirement Calculation Tool Display

$$q_4 = q_1 + q_2 + q_3 \quad (3.11)$$

$$q_4 = m_{water}\Delta T_1 \qquad \{\Delta T_1 = T_{i,citywater} - T_{f,mix}\} \quad (3.12)$$

$$q_1 = m_{ice} * (32\ °\text{F} - 0\ °\text{F}) \quad (3.13)$$

$$q_2 = m_{water} * L \quad \{L = Latent\ Heat\ of\ Melting\ Ice\} \qquad (3.14)$$

$$q_3 = m_{melted\ ice} * \Delta T_2 \qquad \{\Delta T_2 = T_{f,mix} - 32\ °\text{F}\} \qquad (3.15)$$

3.3.3.2 Temperature Probing Technique

ThermoWorks® ProNeedle™ thermometers (Figure 3.18) were used to track the core breast temperature of the sample carcasses before and after the chilling experiments. These water-resistant, wide temperature range probes (-40 to 300 ºC) have a response time of 3 seconds, a display resolution of 0.1ºC, and an accuracy of ±0.5 ºC. The probe length is 3 inches, and the desired depth to target the deep muscle core temperature is 1.75 inches as can be seen marked in Figure 3.18. This particular probe technique was adopted because there was no suitable embedded temperature logger that could be used to continually monitor the core temperature throughout the entire chilling experiment. Two major issues or requirements would need to be addressed by this potential logger, and a logger could not be found that passed these qualifications. First, the logger would need to be wireless so that wiring would not be tangled on the shackle or carcasses in the channel flow. Secondly, the probe would have to stay inserted and disallow any infiltration of water into the probed cavity, as that would potentially skew temperature results. This was determined to be difficult to overcome because the carcass breast meat and skin are inelastic, so the probed cavity does not naturally contract around the probe needle. Rather, the cavity would only seek to expand and allow water infiltration (especially with vigorous agitation) as the probe

needle moves around. For this reason, the specified ThermoWorks® logger was used pre- and post-chilling as it has been proven to be used in food temperature measurements. An example of how the carcass is probed for temperature during experimental trials is shown in Figure 3.19. To account for potential variations in bird geometry (i.e. asymmetry), the core breast temperature is taken for the right and left sides and an average is taken.

Figure 3.18: ThermoWorks® ProNeedle™ Temperature Logger with a 3-inch Probing Needle

Figure 3.19: Carcass with temperature probe in left and right breast

3.3.3.3 Carcass Heating Protocol

The sample of carcasses used in chilling experimentation were sourced in shipment boxes as commercially processed carcasses from a processing plant and stored in refrigerators once they arrived to the experimental site. Since they were held at a low temperature (~3 ºC) prior to testing, they needed to be heated to replicate typical pre-chilling core temperatures averaging 40 ºC for the first and second batches of testing on a testing day. In order to heat a batch of 10 carcasses for a typical testing day, a heating apparatus was constructed, as seen in Figure 3.20, with a 30-gallon vessel and two generic brand 1500W water heaters. It also comprises of a PLC water temperature control to regulate the on/off status of the water heaters, and the upper and lower bands of water temperature range are set at 111 ºF (43.9 ºC) and 110 ºF (43.3 ºC), respectively (i.e., small allowance for temperature deviation). For heating the cold carcasses, the water heating apparatus

Figure 3.20: Heating Apparatus with Heating Element Temperature Control

was filled to 75% capacity with tap hot water ranging from 40 ºC-42 ºC, and the sample set of carcasses was placed inside and heated for two hours. This heating time was determined as a result of a trial-and-error approach to achieve a typical average pre-chill core temperature between 40 ºC -42 ºC for the range of carcass sizes tested.

3.3.3.4 Motorized Shackle Line Development/Calibration

The main experimental tool used in the study was the finite motorized shackle line used to test various shackle rotational motion patterns. The motorized shackle line comprises of five evenly-spaced ServoCity® 12V 84 RPM HD planetary gear motors as seen in Figure 3.21, which are controlled by the BasicMicro® Motion Studio software program. The motor with a yellow cap contains an encoder that can be used to tie in a PID control. To couple the shackle to the motor, white 3D printed hubs were constructed that contained nylon bearings for reduced friction when the shackles are rotating. The BasicMicro® Motion Studio software was downloaded to a lab computer and can be connected to the shackle line via a USB cable. The motor electronics and wiring were contained within a transportable station shown in Figure 3.22.

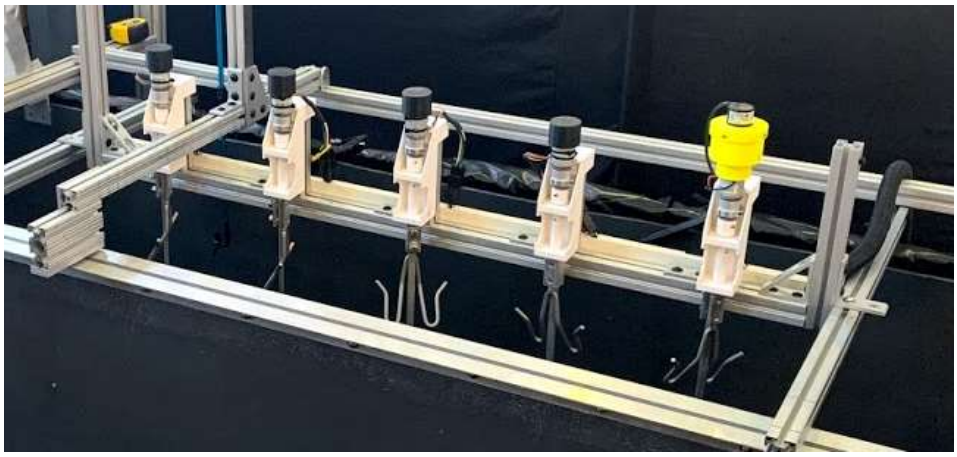

Figure 3.21: Motorized Shackle Line Assembly

Figure 3.22: Motor Electronics and Wiring Storage

With the BasicMicro® Motion Studio software, various shackle rotation patterns can be configured with the use of BasicMicro's specific coding logic, which is very similar to the BASIC language. To start the process of running a specific shackle rotational pattern, the software is opened and connected to the motor line unit, displayed as 'MCP 2x60A'. General settings are set, and the correct max/min voltage and current settings are imposed. A key step is to set the motor signal to 'Quadrature,' because the code specifies motor motion through quadrature pulses per second (QPPS). This QPPS value corresponds to a certain motor RPM. After this, the motor line velocity PID constants were tuned by pressing a 'Tune M1' button in the software. This was done on each experiment day because there may be slight variations in the motor responses from day-to-day. After all of the settings are configured, the specific motor motion code for controlling the rotating shackle apparatus is opened in the MCL Editor, which is used to access, write, and execute MCL Basic scripts. Once the code is compiled and sent to run, the motorized shackle line can be operated during the chilling experiments. Periodically, the motor QPPS values, which correspond to the motor angular velocity, were tuned to make sure they are in compliance with the desired

RPM for the experiment. This was done by using the Extech® Tachometer Counter (Figure 3.23) and placing reflective strips on the side of the shackle assembly (Figure 3.24) for measurement. If measured deviations from the desired RPM occur, the script is adjusted accordingly. For brevity, examples of a continuous, single-directional shackle rotation and alternating, churning shackle rotation code can be seen in Appendix A.

Figure 3.23: Extech Tachometer Counter

Figure 3.24: Rotating Shackle with Reflective Tape for Calibration

3.3.3.5 Experiment Day Testing Protocol

On the day of the chilling experiment, the process starts by labeling the set of 10 carcasses according to their tag number, shackle position (#1 through #5), and batch color (yellow or gray).

The green tags (Figure 3.25), which had a number labeled, were wrapped around the carcass leg and used as back-up labeling in the event of an accidental re-arrangement in the shackle line order; or if the rare event occurred wherein two or more carcasses fell off the shackles while in the flow field. There would have been a need to be re-hang them in the correct shackle positions. The cold carcasses were placed in thin plastic bags that were wrapped tightly and sealed with a yellow or gray zip tie (Figure 3.25) to distinguish batch 1 (yellow) from batch 2 (gray), which both contained a set of five carcasses. The shackle position of #1 through #5 was noted on the zip tie as well. Once the carcasses were bagged and labeled, the water heater was filled with hot tap water and configured for water heating maintenance as described in Section 3.3.3.3. The bagged carcasses were immersed in the water heater for two hours. As the heating process was underway, the flow test rig was filled to the 18.5 inch water level as specified in Section 3.3.3.1, while the necessary ice quantity was added to achieve a chiller medium temperature of 8.5 ºC. Additionally, the motor controller for the propeller-motor system was set to the correct Hz setting (42 Hz), which corresponded to the desired channel flow speed to simulate the translation of the processing line.

Figure 3.25: Yellow/Gray Zip Ties and Leg Tags for Carcass Labeling

After this water fill and the two-hour heating process was complete, the first batch of five carcasses (yellow zip ties) was taken from the water heater and placed in the staging area. First, the masses of the carcasses were measured and recorded. Then, the left and right side core breast

temperatures were probed to a 1.75 inch depth with the temperature logger as specified in Section 3.3.3.2. These left and right core temperatures were logged and were ultimately averaged in the reported results. Typically, the pre-chill core temperatures varied between 39 ºC and 42 ºC, which closely matched the industrial pre-chill temperature. After the masses and temperatures of the five carcasses were recorded, they were hung on the motorized shackle line on their corresponding shackle position and placed within the test rig channel. Then, the BasicMicro Motion Studio software was used to start the motion code script for the particular rotation pattern under scope. After the selected 12-minute chilling exposure time was complete, the shackle line was moved from the test rig to the staging area for the post-chill measurement phase. For the post-chill measurement process, left and right side core temperatures were measured and recorded first to minimize any time lag in measurement from the preceding chilling stage, and then the masses were measured. As done previously, the carcass set was bagged and labeled once again and placed in the water heater for the second test. Then, the second batch of five carcasses (gray zip tie) was taken out, and the same steps for the first chilling stage were taken for this batch. During the second heating phase, a minimal amount of ice was added to the chiller medium due to a slight increase in temperature from the beginning of the first series of tests to the start of the second series of tests, and this was done after the second heating process was completed. No water is removed to compensate for the additional ice as the water level increase due to the second ice addition is minimal. Once the two-hour heating time for the first batch of carcasses was complete, the same, preceding steps were taken for the first and second batches of carcasses. Once all testing was complete, the carcasses were stored in a freezer for eventual disposal, the test rig was drained via sump pump, and the experiment area was sanitized thoroughly.

3.3.4 Chilled Water Thermal Testing Experimental Results

The results reported in this section follow a progression of confirmation and exploratory experimental trials. The focus was to assess the thermal chilling enhancement by way of superimposing additional, alternative rotational kinematics to the traditional pure translation immersion chilling process in industry. For the following chilling experiments, the dwell time was set to be 12 minutes (except for the 16.5 minute dwell time for the Thermal Time Constant Approach Validation test detailed in Section 3.3.4.4), and the experimental testing protocol corresponds to the measurement techniques and protocols described in Section 3.3.3 Chilled Water Thermal Testing Experimental Techniques. The first section (3.3.4.1) details the testing to confirm that there is no significant thermal hysteresis affecting the material properties of the carcass breast meat from repeated heating/chilling cycles within an experiment test day. Following this confirmation, Section 3.3.4.2 details the first experimental test conducted, comparing the 'Pure Translation' process to '40 RPM Full Turn Churn' to investigate how superimposed shackle rotation can aid convective cooling among a common sample of 10 carcasses. With promising results gathered from this initial test, a series of chilling experiments were conducted across a range of shackle motion patterns for batches of carcass samples to investigate trends in varying shackle agitation frequency and angular velocity. Due to the variance in carcass mass encountered during testing, the thermal results are categorized into distinct mass ranges of 1.4-1.6 kg, 1.6-1.8 kg, and 1.8-2.0 kg. Lastly, to confirm the validity of the thermal time constant approach experimentally, Section 3.3.4.4 details the experimental tests involving 16.5-minute chilling dwell times to compare to the previously tested 12-minute chilling dwell time to ensure no significant variance in thermal time constant results.

3.3.4.1 Chilled Water Thermal Testing – Thermal Hysteresis Effect

For this set of chilling tests, the intended objective was to confirm the absence of significant thermal hysteresis in the effective thermal properties (i.e. thermal conductivity, thermal heat capacitance) of the carcass meat. In this phenomenon, thermal properties can be affected by the preceding thermal history of the object material of interest. The study of this phenomenon in food has precedence as indicated by Wesolowski et al. [32] in their determination if hysteresis occurs in ground meat during thermal cycles via measurement of ultrasonic wave velocity. The reason this set of tests was conducted was to provide basis for cycling a sample of carcasses through two different heating/chilling cycles for one experiment day without having to account for thermal hysteresis affecting the carcass meat thermal properties between Test 1 and Test 2.

To confirm the absence of significant thermal hysteresis, one experiment set involving cycling a sample of five carcasses through the heating and subsequent '40 RPM Full Turn Churn'[4] chilling processes twice in one day was analyzed to highlight any variations between the carcass chilling thermal time constants associated with both test cycles (Test 1 and Test 2). The chilled water medium temperatures for this trial were 8.05 ºC for Test 1 and 8.2 ºC for Test 2, and the details for the carcass sample set (i.e. test pre-chill/post-chill core temperatures, carcass mass, test thermal time constants) are shown in Table 3.3. As conducted in a similar manner, an additional experiment set involving cycling a sample of five carcasses through the heating and subsequent 'Pure Translation' chilling processes twice in one day was examined for any significant chilling response variations from Test 1 to Test 2. For the 'Pure Translation' data set, the chilled water medium temperatures were 8.15 ºC and 8.40 ºC for Test 1 and Test 2, respectively, and the details for the carcass sample set are shown in Table 3.4.

[4] This motion pattern indicates a shackle angular velocity of 40 RPM completing 1 full rotation clock-wise/counter-clockwise (half-cycle) before preceding to reverse direction and complete 1 full rotation to complete a full cycle

When one examines the thermal time constant variance (absolute percent difference) between Tests 1 and 2 within the '40 RPM Full Turn Churn' and 'Pure Translation' data sets, it is apparent that there is minimal variance between Test 1 and Test 2 thermal time constants as indicated by the majority of absolute percent differences being less than 5%. These results suggest reasonable repeatability of thermal results in conducting two identical heating/chilling cycles for the same carcass set without having to account for significant changes in thermal properties due to the carcass's thermal history.

Table 3.3: 40 RPM Full Turn Churn Thermal Hysteresis Results

Bird Number	Test 1 Pre-Chill Temp. (ºC)	Test 1 Post-Chill Temp. (ºC)	Test 2 Pre-Chill Temp. (ºC)	Test 2 Post-Chill Temp. (ºC)	Mass (kg)	Test 1 Time Const. (mins.)	Test 2 Time Const. (mins.)	Time Const. Abs. % Diff.
Y1 - 88	42.7	24	41.8	23.4	1.49	14.7	14.4	1.76%
Y2 - 19	42.2	23.7	42.5	24.5	1.45	14.6	15.4	5.40%
Y3 - 17	42	24.4	42.1	24.7	1.60	15.5	15.9	2.04%
Y4 - 2	42.7	25.9	42	26.5	1.52	17.1	18.5	8.39%
Y5 - 15	43	25.9	41.5	25.1	1.47	16.9	16.8	0.55%

Table 3.4: Pure Translation Thermal Hysteresis Results

Bird Number	Test 1 Pre-Chill Temp. (ºC)	Test 1 Post-Chill Temp. (ºC)	Test 2 Pre-Chill Temp. (ºC)	Test 2 Post-Chill Temp. (ºC)	Mass (kg)	Test 1 Time Constant (mins.)	Test 2 Time Constant (mins.)	Time Const. Abs. % Diff.
Y1 - 11	42.5	28.6	41.8	28	1.47	22.3	21.8	2.06%
Y2 - 35	42.7	28.7	41	27.6	1.40	22.3	22.0	1.30%
Y3 - 56	43.1	31.8	42.4	31.2	1.84	29.4	29.0	1.46%
Y4 - 5	42	29.3	41.2	28.5	1.66	24.5	23.7	3.32%
Y5 - 12	43.4	30.3	42	29.3	1.57	24.8	24.5	1.51%

3.3.4.2 40 RPM Full Turn Churn – Pure Translation Baseline Comparison

In this experiment, a sample set of 10 carcasses, split into sets of five carcasses mentioned in the experimental protocol described in Section 3.3.3.5, was cycled through heating/cooling stages via the '40 RPM Full Turn Churn' motion condition (Test 1) and industry baseline 'Pure Translation' motion condition (Test 2). The chiller medium temperatures for the two tests were comparable at 7.95 ºC and 8.10 ºC for Tests 1 and 2, respectively. Additionally, the average carcass core temperatures were nearly identical as well at 42.62 ºC and 42.49 ºC for Tests 1 and 2, respectively. Both chilling tests comprised of 12-minute chilling times, and pre- and post-chill core temperatures, as well as carcass mass measurements, were recorded. The key derived results are displayed in Table 3.5.

Table 3.5: Thermal Results for 40 RPM Full Turn Churn (Test 1)-Pure Translation (Test 2) Chilling Comparison

Bird Number	Mass (kg)	Test 1 Pre-Chill Temp. (ºC)	Test 1 Post-Chill Temp. (ºC)	Test 2 Pre-Chill Temp. (ºC)	Test 2 Post-Chill Temp. (ºC)	Test 1 Time Constant (mins.)	Test 2 Time Constant (mins.)	Time Const. Abs. % Diff.
Y1 - 12	1.46	42.3	22.8	41.7	25.7	13.8	17.8	29.71%
Y2 - 1	1.56	41.6	22.5	42.5	25.7	13.7	17.2	25.44%
Y3 - 82	1.49	42.7	24	42.6	26.5	14.9	18.4	23.07%
Y4 - 3	1.45	42.2	23.7	43.1	27.2	14.8	19.0	28.48%
Y5 - 89	1.60	42	24.4	42	26.8	15.8	19.4	22.48%
G1 - 4	1.36	43.2	23.7	43.1	26.7	14.3	18.3	27.55%
G2 - 20	1.57	43.2	23.1	42.9	26.2	13.7	17.7	29.27%
G3 - 78	1.52	42.7	25.9	42.3	26.7	17.4	18.9	8.87%
G4 - 33	1.47	43	25.9	42.7	27.6	17.2	20.1	16.94%
G5 - 19	1.66	43.3	28.4	42	30.4	20.9	27.2	30.20%

From examination of individual carcass data from Table 3.5, there is an apparent chilling enhancement due to the addition of the '40 RPM Full Turn Churn' shackle motion kinematics

superimposed onto the 'Pure Translation' process. This can be seen when looking at the reduction of thermal time constants from Test 2 ('Pure Translation') to Test 1 ('40 RPM Full Turn Churn') ranging from 8.87% to 30.20%. The results from this initial test further promoted the notion that significant convective heat transfer enhancements can be implemented by way of introducing additional shackle agitation and rotational kinematics.

3.3.4.3 Parametric Sweep of 40 & 60 RPM Motion Patterns

With promising thermal enhancement results seen from the '40 RPM Full Turn Churn-Pure Translation' comparison for a common set of carcasses, a series of chilling experiments were conducted for a number of programmed shackle motion patterns involving shackle angular velocities of 40 RPM and 60 RPM. Among these two tested shackle RPMs, there was variance in the agitation frequency or shift from clockwise to counterclockwise rotational direction. For example, the '40 RPM Continuous Rotation (3 Mins./Half Cycle)' shackle motion pattern indicates a shackle angular velocity of 40 RPM that rotates in a clockwise or counterclockwise direction for 3 minutes before switching rotational direction. Similarly, the '60 RPM Three-Quarter Turn Churn' shackle motion pattern indicates a shackle angular velocity of 60 RPM that rotates with an angular displacement of 270º in a clockwise or counterclockwise direction before flipping rotational direction. A series of one-day chilling experiment days involving sets of 10 carcasses within a chiller medium spanning a narrow temperature range of 8.3ºC - 8.7ºC, and pre-chill carcass core temperatures typically ranging from 39-43 ºC, were performed to compile this extensive data set for varied shackle motion patterns.

Presenting the "raw" thermal results, Figures 3.26 and 3.27 as follow show the core temperature drop versus carcass mass and chilling thermal time constant (Section 3.3.1.3 discusses the calculation of thermal time constants) versus carcass mass relationships, respectively, for the

sampled carcasses that went through the varied shackle motion patterns. Each individual point on the scatterplot represents the thermal response for an individual carcass under the specified shackle motion pattern as indicated in the chart legend. As indicated by both Figures 3.26 and 3.27, higher carcass masses tend to have smaller core temperature drops and higher associated thermal time

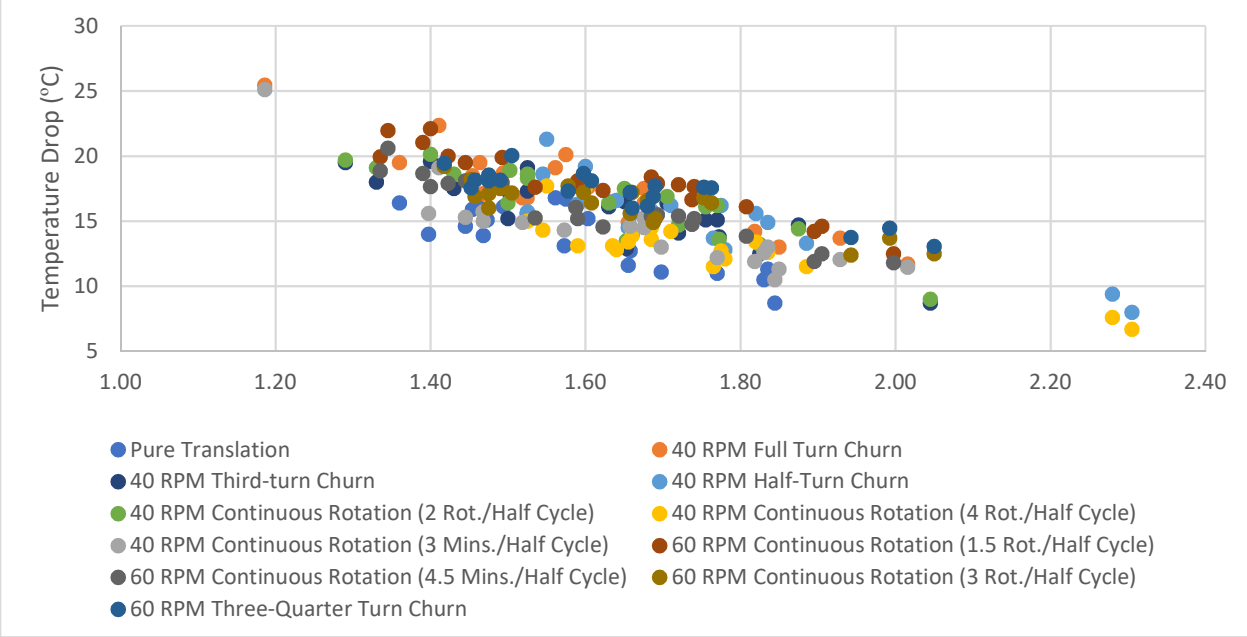

Figure 3.26: Chilling Experiments Raw Thermal Results - Core Temperature Drop vs. Carcass Mass

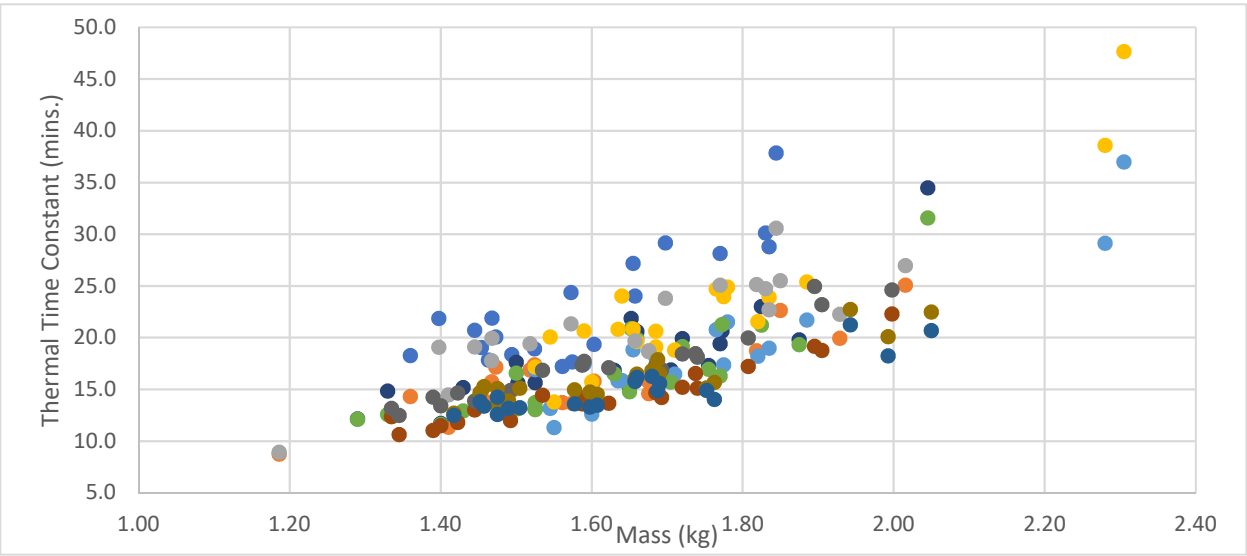

Figure 3.27: Chilling Experiments Raw Thermal Results – Chilling Thermal Time Constant vs. Carcass Mass

constants. This indicates a strong impact of carcass mass on the chilling rates irrespective of the nature of the shackle motion pattern, which can be attributed to the noteworthy internal conductive thermal resistance within the carcass meat and the thermal heat capacitance that is compounded with larger mass.

With this extensive set of scattered data, Excel pivot tables were used to consolidate this data and present it in a more meaningful way to distinguish trends amongst the varied shackle motion patterns with respect to chilling effectiveness. Because of the large variance in carcass mass experienced in the chilling experiments, the thermal data results were aggregated into three targeted mass categories: 1.4-1.6 kg, 1.6-1.8 kg, and 1.8-2.0 kg for ease of examining trends. Among these three target mass categories, for a particular shackle motion pattern, chilling thermal results such as pre-chill/post-chill core temperatures, thermal time constants, and carcass masses were reported as averages within the specified range. For brevity, the aggregated results for '40 RPM Third-turn Churn' are shown in Table 3.6 below, however; the aggregated table results for the remaining motion patterns are included in Appendix A.

Table 3.6: Aggregated Thermal Results for 40 RPM Third-turn Churn Shackle Motion Pattern

Mass Category	Number of Carcasses	Average Mass (kg)	Average of Pre-Chill Temp. (ºC)	Average of Post-Chill Temp. (ºC)	Average of Time Constant (mins.)	Average of ΔT (ºC)	Max of Time Constant (mins.)	Min of Time Constant (mins.)	StdDev of Time Constant (mins.)
1.2-1.4	2	1.31	41.45	22.70	13.50	18.75	14.85	12.16	1.91
1.4-1.6	6	1.48	41.33	23.70	14.83	17.63	17.63	11.73	2.08
1.6-1.8	9	1.70	41.27	26.38	18.74	14.89	21.87	15.15	2.25
1.8-2	2	1.85	41.70	28.10	21.40	13.60	23.03	19.78	2.29
>2	1	2.05	40.60	31.90	34.50	8.70	34.50	34.50	-

As mentioned, the thermal results for the '40 RPM Third-turn Churn' motion pattern are aggregated and averaged within the mass categories detailed. The targeted mass categories of

interest to the present study are shaded in light green in preceding Table 3.6. For these three targeted mass categories, the number of carcasses falling in the particular mass category is noteworthy to the sample breadth. Therefore, a green highlight suggests a strong sample breadth of at least five carcasses, a yellow highlight suggests a satisfactory sample breadth of three or four carcasses, and a red highlight suggests a weak sample breadth of less than or equal to two carcasses. These conditional statements stated prior only apply for the targeted mass categories (1.4-1.6 kg, 1.6-1.8 kg, and 1.8-2.0 kg). Essentially, this conditional statement suggests a need for more data to be gathered in the future for the red highlight (weak sample breadth), and to some extent, the yellow highlight (satisfactory sample breadth).. As can be noticed, within each mass category, there is notable variance as indicated by the standard deviation. This partly can be attributed to sampling/measurement error, but also can be pointed to the impact of mass on the thermal time constant as stated before. Even with these mass categories, the thermal responses from carcass mass variance within these ranges has noteworthy variance, but the mass categories are important for summarizing and presenting the findings from experimentation.

Using this aggregated thermal data for the tested shackle motion patterns, the table data was further summarized visually by replacing the shackle motion pattern identification with its corresponding scalar Agitation Parameter (AgPar) value. This conversion process is described in detail in Section 3.3.2 and is useful for this study in providing a common metric for comparing thermal data results amongst the tested shackle motion patterns within a certain RPM. Using this methodology, the entire chilling experiment data set can be presented by way of Figures 3.28, 3.29, and 3.30 as follows.

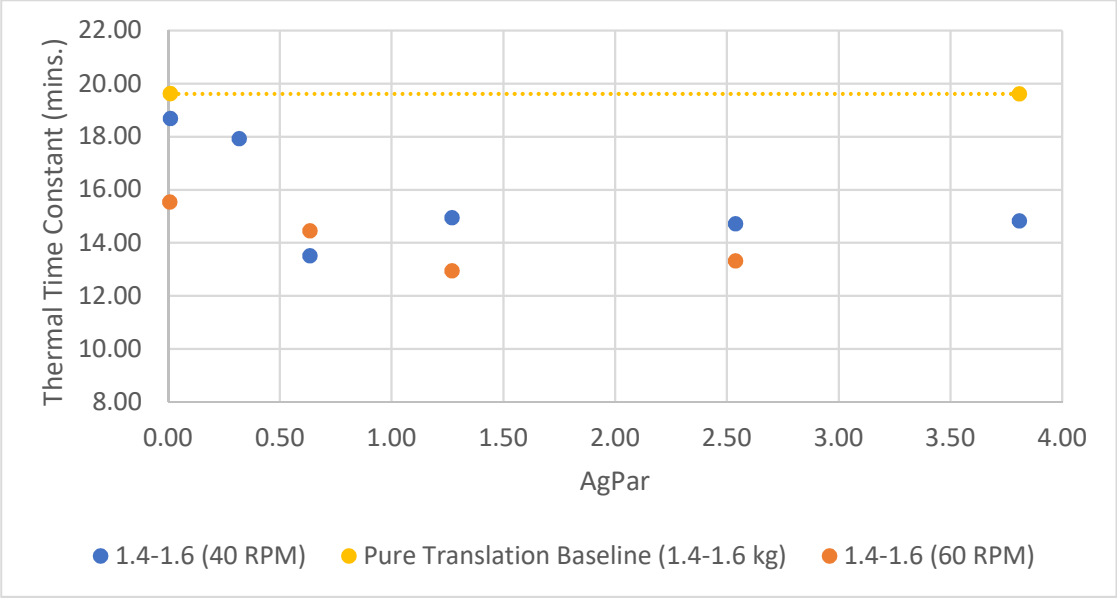

Figure 3.28: Chilling Thermal Time Constant vs. Agitation Parameter (AgPar) Relationship for 1.4-1.6 kg

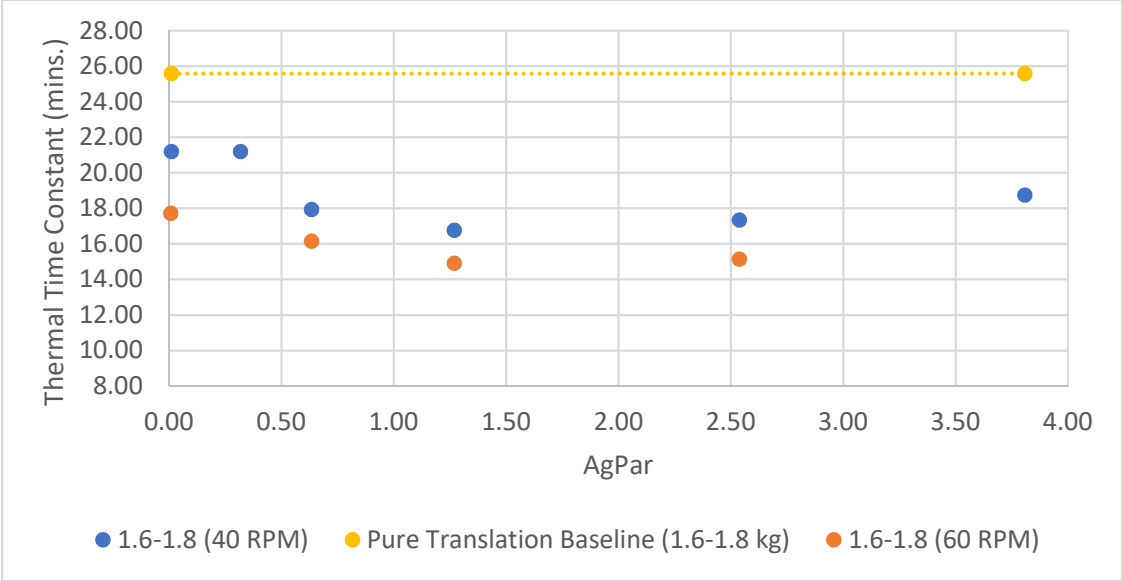

Figure 3.29: Chilling Thermal Time Constant vs. Agitation Parameter (AgPar) Relationship for 1.6-1.8 kg

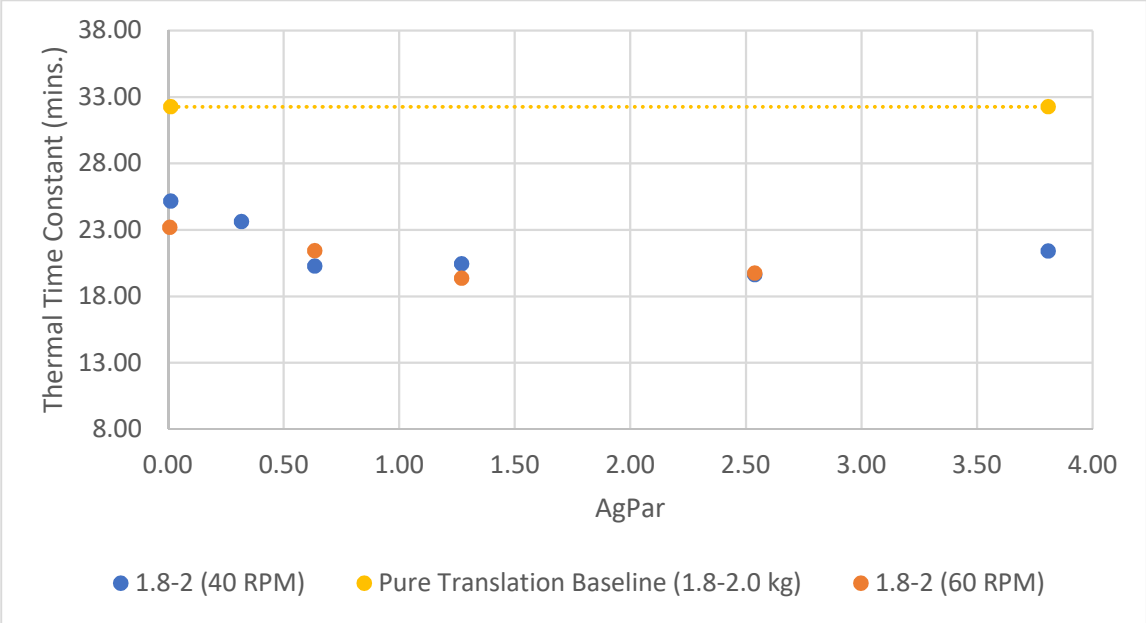

Figure 3.30: Chilling Thermal Time Constant vs. Agitation Parameter (AgPar) Relationship for 1.8-2.0 kg

Figures 3.28, 3.29, and 3.30 display the relationship between the shackle motion Agitation Parameter (AgPar) and average chilling thermal time constant for the 1.4-1.6 kg, 1.6-1.8 kg, and 1.8-2.0 kg carcass mass categories, respectively. In each of the figures for the three mass categories, the dashed yellow line represents the average thermal time constant for the Pure Translation Baseline shackle motion pattern. The blue and orange data points represent the six 40 RPM and four 60 RPM shackle motion patterns, respectively, with their associated AgPar values and average thermal time constants for that particular mass category. Due to a limited testing time frame, more rotational patterns were not tested in the 60 RPM range, but this will be completed in the future. In the 1.4-1.6 kg carcass mass category, the '60 RPM Continuous Rotation (1.5 Rot./Half Cycle)' shackle motion pattern (AgPar = 1.27) proves to be most effective chilling pattern with a thermal time constant of 12.94 minutes as compared to the industry 'Pure Translation' baseline of 19.62 minutes, presenting a 34.05% chilling improvement. In the 1.6-1.8

kg carcass mass category, the '60 RPM Continuous Rotation (1.5 Rot./Half Cycle)' shackle motion pattern (AgPar = 1.27) again proves to be most effective chilling pattern with a thermal time constant of 14.91 minutes as compared to the industry 'Pure Translation' baseline of 25.58 minutes, presenting a 41.71% chilling improvement. Lastly, in the 1.8-2.0 kg carcass mass category, the '60 RPM Continuous Rotation (1.5 Rot./Half Cycle)' shackle motion pattern (AgPar = 1.27) once again proves to be most effective chilling pattern with a thermal time constant of 19.37 minutes as compared to the industry 'Pure Translation' baseline of 32.26 minutes, presenting a 39.96% chilling improvement.

From examination of the trends, it is clear that the 40 RPM and 60 RPM shackle motion patterns improve convective heat transfer rates and chilling effectiveness as indicated by the reduction in chilling thermal time constants. With regards to the impact of AgPar on thermal time constant, there seems to be an initial decrease in thermal time constant as AgPar is increased, but it seems there is a "leveling off" or plateau effect that occurs after an AgPar of 1 or greater. It is theorized this occurs, because, initially, as shackle rotational agitation is increased, increased convective heat transfer and chilling rates occur. However, at some point, increased agitation does not correspond to increased chilling effectiveness and lower carcass core temperatures, because it is possible that the heat transfer is limited by the internal conductive resistance and the thermal heat capacitance of the carcass meat. This hypothesis will be validated in further heat transfer computational studies. This possible phenomenon can also be further emphasized by the marginal reduction, or lack thereof in the 1.8-2.0 kg mass category, in thermal constant going from 40 RPM to 60 RPM shackle motion patterns. However, more sample data needs to be gathered in future trials for the 1.8-2.0 kg mass category as the number of carcasses in this aggregate data was considered to be low. It is also theorized that the "leveling off" in the average thermal time

constants associated with further increases in AgPar seen within the 40 RPM and 60 RPM shackle motion patterns is due to the reasoning that small, limited angular displacement ranges do not allow for the carcass angular momentum to sufficiently build before switching rotational direction. From this, there seems to be an optimal periodic angular displacement for the shackle motion pattern.

3.3.4.4 Thermal Time Constant Approach Validation

With the chilling thermal time constant approach used as a key metric for the characterization of the carcass cooling process, it was deemed important to experimentally validate the approach in conjunction with the theoretical/computational rationale and validation specified in Section 3.3.1. To do so, a series of chilling tests for four varied shackle motion patterns as detailed in Table 3.7 below were conducted at a longer, non-standard 16.5-minute exposure time to gather aggregate carcass thermal response data for the three target mass categories as done similarly for the series of 12-minute chilling tests. The longer 16.5-minute chilling time was decided based upon previous resultant thermal time constant data gathered from the 12-minute series of chilling tests. Due to inherent carcass mass variation, which corresponds to a sizeable range of chilling thermal time constants, the longer chilling time results from a compromise between the upper bound of low mass range (1.4-1.6 kg) thermal time constants (~1.2*τ) and lower bound of high mass range (1.8-2.0 kg) thermal time constants (~0.8*τ). This bound was deliberately specified in determining the 16.5-minute chilling time, because a reasonable chilling time needed to be chosen that would not overextend smaller carcasses into the asymptotic region of the chilling exponential decay. At the same time, the chilling time should not be too small for the larger carcasses to only allow for measuring the initial rapid chilling region of the exponential decay. These two extremes would make experimental time constant measures more difficult.

With the previous statements considered, Table 3.7 displays the comparison of the aggregate thermal time constant data between the 12-minute and 16.5-minute chilling exposure times for the four shackle motion patterns tested. Generally, there is good agreement between the results from the two exposure times with all contrasts below 6.9%, and the average percentage difference being 4.04%. Withstanding the small differences that could be attributed to inherent experimental error, this experimental corroboration of the measure of thermal time constants as a performance metric was proven to be successful.

Table 3.7: Chilling Thermal Time Constant Approach Validation

Testing Condition	Mass Range (kg)	Thermal Time Constant (12 minute chilling exposure)	Thermal Time Constant (16.5 minute chilling exposure)	% Difference
40 RPM Continuous Rotation (3 Mins./Half Cycle)	1.4-1.6	18.68	18.24	2.4%
	1.6-1.8	21.20	21.14	0.3%
	1.8-2.0	25.17	26.11	3.8%
40 RPM Half Turn Churn	1.4-1.6	14.72	14.87	1.1%
	1.6-1.8	17.33	18.13	4.6%
	1.8-2.0	19.64	20.88	6.3%
60 RPM Continuous Rotation(4.5 Mins./Half Cycle)	1.4-1.6	15.54	16.50	6.2%
	1.6-1.8	17.72	18.28	3.1%
	1.8-2.0	23.20	22.11	4.9%
60 RPM Three-Quarter Turn Churn	1.4-1.6	13.32	13.77	3.4%
	1.6-1.8	15.14	15.97	5.5%
	1.8-2.0	19.75	18.48	6.9%

3.4 THEORETICAL/PERFECT CONVECTION CHILLING LIMIT INVESTIGATION

With the results gathered from the chilling tests involving various rotational patterns and the impact on the chilling effectiveness, it was deemed important to understand the theoretical/"perfect" convection chilling limit as a measure to gauge how far the experimentally-gathered results are from this limit and determine if there is still room for design space exploration

for new rotational patterns. Another objective of this investigation was to glean any insights on why there may be a "leveling off" effect on thermal time constants as agitation parameter is increased beyond a certain value as mentioned in prior sections. To gain insight on carcass chilling with "perfect" convection, a transient heat model was constructed with COMSOL® Multiphysics with the carcass geometry as shown in Figure 3.31 with the initial temperature of the carcass domain set to be 40 °C and the core/Deep Muscle Tissue (DMT) location identified based upon previous convection simulations to determine the minimum/maximum temperature location within the breast meat.

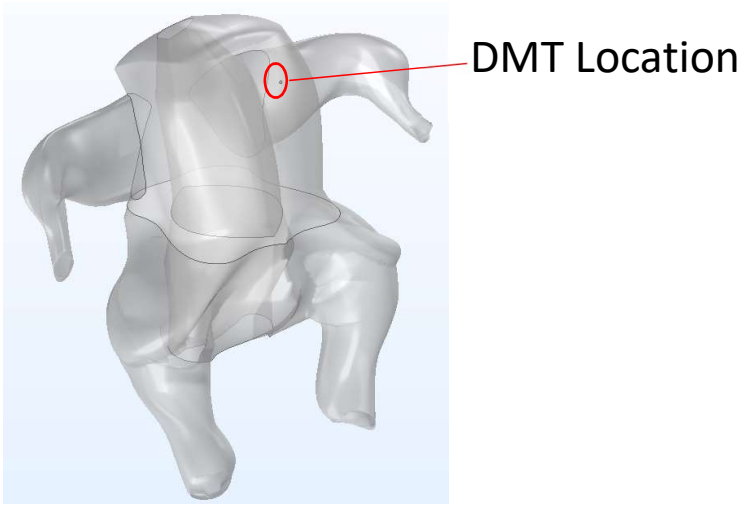

Figure 3.31: Carcass geometry with Deep Muscle Tissue (DMT) location

Theoretically, in a "perfect" convection scenario, there is no convective heat transfer resistance as convective heat transfer coefficient (h) tends to ∞ W/m^2-K and convective thermal resistance (R_{conv}) tends to 0 K/W. With these stated points, this reduces the heat transfer problem to a classic conduction heat transfer situation with an initial carcass domain temperature and a specified surface/boundary temperature condition set at time t = 0 seconds. Since previous chilling experiments involved a chilled water temperature on average of 8.5 °C, within the COMSOL® heat transfer model, the carcass boundary was specified to be set to the chiller medium temperature

of 8.5 °C at time t = 0 seconds. The transient heat transfer simulation was run for 3600 seconds (60 minutes) with 1 second time steps and DMT temperature evolution for this "perfect" convection scenario was monitored for scaled carcasses of 1.50 kg, 1.69 kg, and 1.88 kg masses. These mass values were determined as an average mass value amongst all rotational/translation motion patterns tested in the thermal experimental study chilling experiments within the three specified mass categories (1.4-1.6 kg, 1.6-1.8 kg, and 1.8-2.0 kg).

With the DMT temperature evolution data gathered for the three carcass masses, the data was fit with the best exponential decay fit that allowed to determine the associated chilling thermal time constant for the "perfect" convection scenario. This methodology is very well supported by the basis of using thermal time constants to describe the carcass chilling process in Section 3.3.1.2. As a step of due diligence, there were two methods of exponential decay curve fitting that were used to determine the thermal time constant and ultimately averaged to determine the "perfect" convection time constant. As an example, methodology for determining the 1.69 kg carcass "perfect" convection time constant will be described as follows. Describing the first method, Figure 3.32 displays the simulation data for the DMT temperature evolution for a 1.69 kg carcass with an associated exponential decay curve fit. As can be seen, there is an apparent Fourier time delay due to the internal conductive resistance and capacitive effects of the carcass meat, but the exponential decay fit is a strong fit with the data with an R^2 fit value of 0.99098. With this method, the fitted thermal constant was determined to be 12.2 minutes for a "perfect" convection scenario.

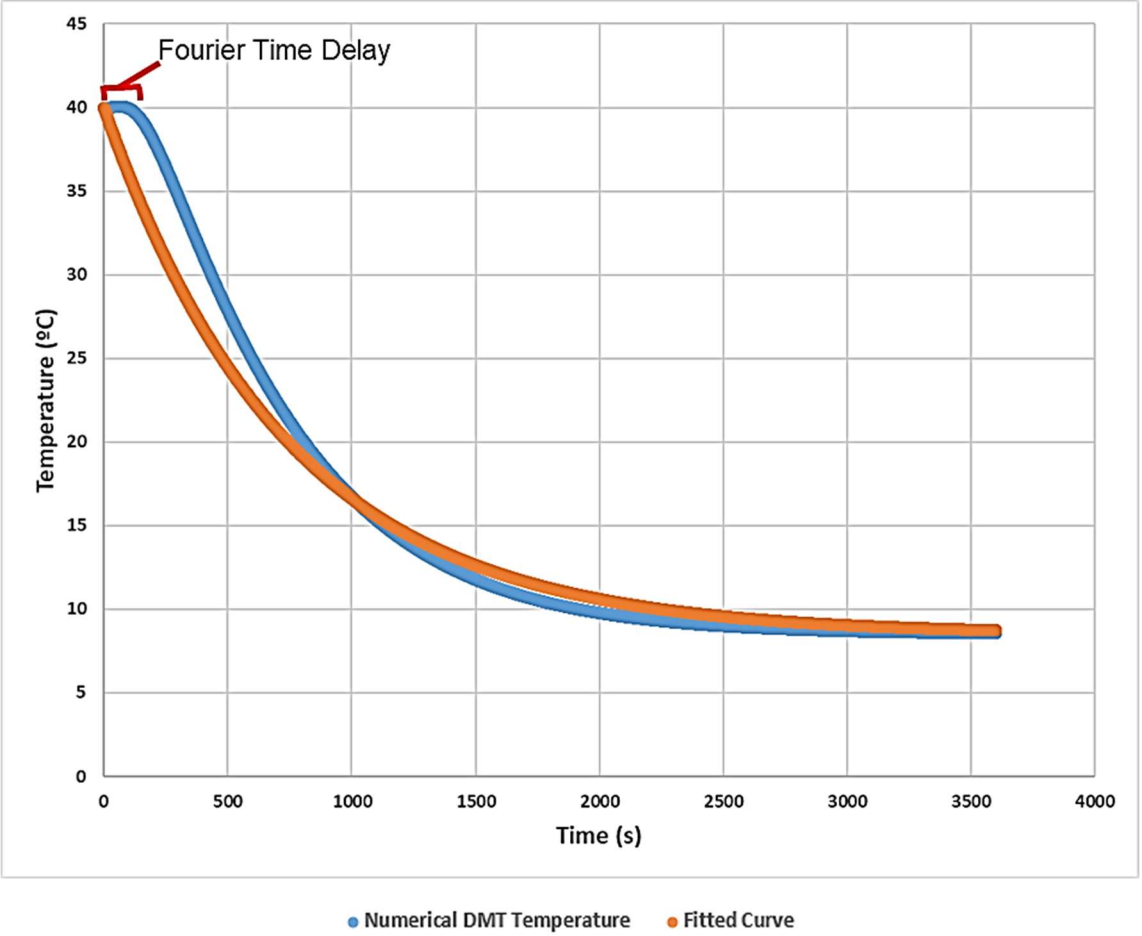

Figure 3.32: Deep Muscle Tissue (DMT) temperature evolution data and exponential decay curve fit for 1.69 kg carcass

To alleviate concerns over the slight misalignment of the two temperature curves due to the slight Fourier time delay, an additional method was used to determine an "adjusted" time constant. Figure 3.33 displays the adjusted simulation data for the DMT temperature evolution for a 1.69 kg carcass with an associated exponential decay curve fit. In this display of data, the DMT temperature curve is shifted to remove the initial Fourier time delay of 1.4 minutes and start the chilling process when the DMT temperature starts to decrease. Fitting this adjusted temperature evolution with an exponential decay curve fit, the R^2 fit value is higher at 0.996826, and the fitted time constant is 11 minutes. Accounting for the initial Fourier time delay of 1.4 minutes, this addition results in an adjusted thermal time constant value of 12.4 minutes, which is comparable

to the 12.2 minutes from the first method described. Averaging both methods' time constants results in a 12.3 minute value for the 1.69 kg carcass.

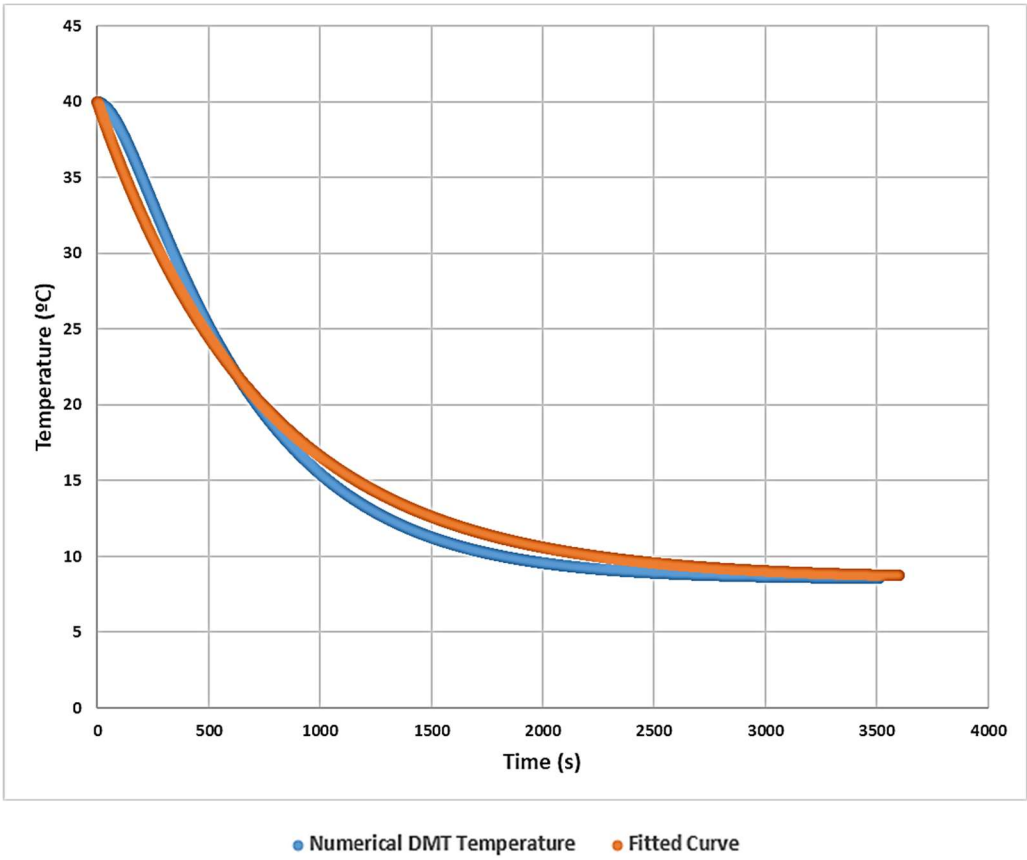

Figure 3.33: Adjusted Deep Muscle Tissue (DMT) temperature evolution data and exponential decay curve fit for 1.69 kg carcass

Using this methodology for the 1.50 kg and 1.88 kg carcasses, the theoretical/"perfect" convection thermal time constants for the chilling process were determined to be 11.25 minutes and 13.31 minutes, respectively. To visually depict the limits in association with prior data, the "perfect" convection limit line was plotted on the prior agitation parameter-thermal time constant relationship graphs for the three distinct mass categories as indicated by the gray dashed lines in Figures 3.34, 3.35, and 3.36. As can be seen in the charts, there is still potential for design space exploration for further reductions in chilling time constants to get closer to the theoretical chilling limits. Currently, given the current experimental setup and hardware, it may not be possible to

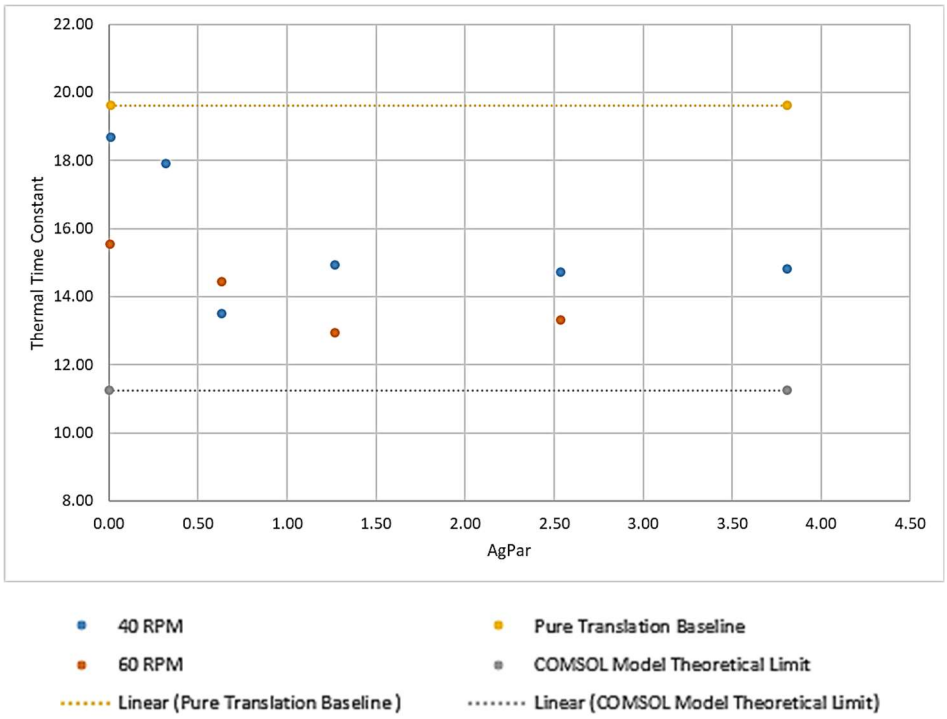

Figure 3.34: Chilling Thermal Time Constant vs. Agitation Parameter Relationship for 1.4-1.6 kg (w/ Theoretical Limit)

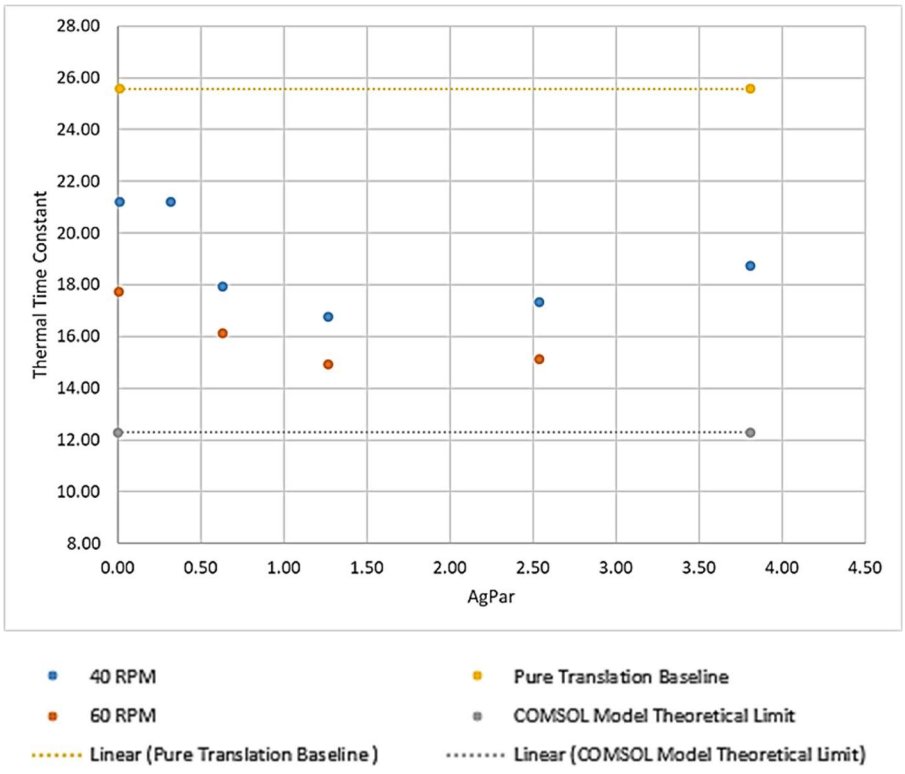

Figure 3.35 Chilling Thermal Time Constant vs. Agitation Parameter Relationship for 1.6-1.8 kg (w/ Theoretical Limit)

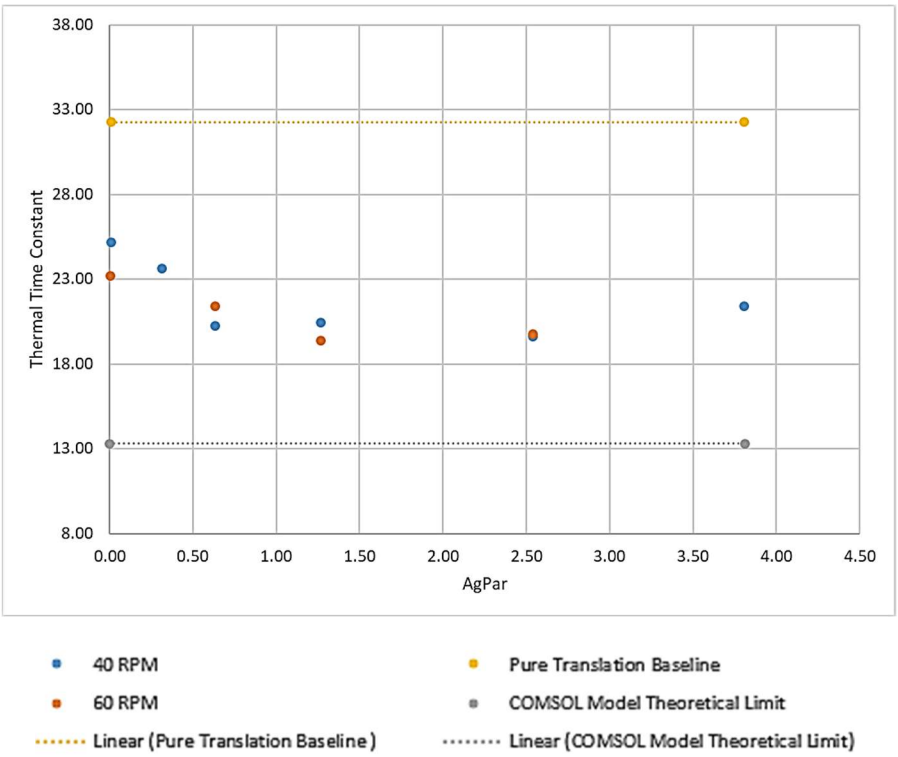

Figure 3.36: Chilling Thermal Time Constant vs. Agitation Parameter Relationship for 1.8-2.0 kg (w/ Theoretical Limit)

make significant advancements to the chilling limit, but this provides a good reference point for future testing and exploration.

3.5 ROTATING SHACKLE SYSTEM PROOF-OF-CONCEPT DEVELOPMENT

While the experimental setup involving the propeller-driven flow test rig with finite motorized shackle line was good for exploring the design space for improving convective heat transfer and chilling rates, industry stakeholders are increasingly interested in practical tech transfer to their industrial facilities. They are interested in how they can implement a system of a rotating shackle processing line in their facility, and the previous experimental test rig does not relay this to them. In reality, it is not practical for the poultry processing facilities to have each shackle on the line be powered with motor electronics to allow for rotational patterns. Therefore, significant emphasis was focused upon a practical shackle carousel system with induced passive-

mechanical shackle rotation indicative of motion patterns tested in the previous propeller-driven flow setup.

3.5.1 System Geometry/Specifications

3.5.1.1 Carousel Test Rig Subsystem

Figure 3.37 below displays the entire shackle carousel system. The carousel track is 280.12 inches (~23.3 ft) in total length with two straight track lengths of 111 inches and two half-circle bends with diameters of 18.5 inches each. The test rig capacity was modified to hold a maximum capacity of 593.8 gallons with a width of 36 inches, length of 161 inches, and a height of 24 inches. The test rig was modified in this manner to accommodate the standard, industrial 18.5-inch diameter pulleys and allow for the shackle line to be moving within the center of the channel at all times. The shackle carousel line is driven by the same 1 HP SEW EuroDrive motor and motor VFD controller used in the propeller-driven setup in conjunction with a timing belt that is coupled

Figure 3.37: Rotating Shackle Carousel System – Complete View

to the driver pulley. The driver pulley has notches where the shackle trolleys (linked by Grade 30 chain and spaced 12 inches apart) fall into place and are transported around the carousel track.

With the motor VFD control, the carousel line speed can be varied up to 3.3 ft/s. Based upon typical industrial processing speeds of 130-140 birds per minute (which translates to a high end speed of 2.17-2.33 ft./s), there is more than enough motor power to drive the system. Additionally, as of now, there are five active trolleys with shackles hanging as seen in Figure 3.38, but in the future, the plan is to have 23-24 active trolleys with shackles to complete the entire loop to promote an "infinite series" line effect where there is no start or end to this system.

Figure 3.38: Finite element of carousel shackle line

3.5.1.2 Modified Rotational Shackle Subsystem

In lieu of the motorized shackle that is programmed to rotate in a certain manner, a mechanical rotational shackle assembly, displayed in Figure 3.39, was designed and constructed for this proof-of-concept system. The modified assembly adds rotational shackle kinematics to the traditional translational shackle motion by way of the pinion gear. In this assembly, the pinion gear can be varied in size depending on the desired shackle RPM for a fixed line speed. The diameter of the pinion gear in the current proof-of-concept is 6.5 inches, which corresponds to shackle RPMs of 76.5-82.2 RPM based upon industrial translation line speeds of 2.17-2.33 ft./s. As

mentioned, the relationship between shackle angular velocity and translational velocity is fixed due to the pinion gear sizing, but it can be varied with replacement of a smaller/larger gear. Another key feature of the rotational shackle assembly is the stabilizing rod that extends beyond the shackle. This is necessary for this system to keep the carcass center of mass in line with the shackle center axis as it rotates back and forth. Without this rod, the carcass's rotational inertia may take it off the central shackle axis and can cause the carcass to fall off the shackle.

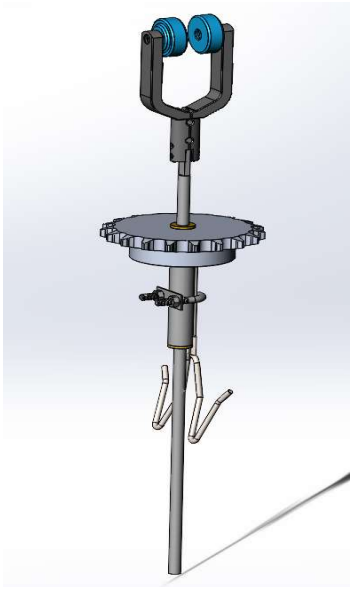

Figure 3.39: Rotational Shackle Assembly

3.5.1.3 Rotational Guidance Track System

To complete the passive-mechanical rotating shackle system, a guidance track system consisting of four 7-foot straight aluminum u-channels (i.e., two for each flow channel "straightway") with 127 holes each are arranged in the plane of the rotating pinion gear to serve as a track for the prescribed rotation. The drilled holes along the length of the u-channel allowed for a robust, custom track to be configured with the bolts and pins as can be seen in Figures 3.40 and 3.41. In a previous iteration of the track construction, a standard bike chain, as can be seen in Figure 3.42, was used to pair with the pinion gear. However, alignment issues were prevalent in

this iteration as any slight tilt due to the shackle motion or drag due to the carcass moving in water would cause the system to jam and not rotate in the desired manner. To address this issue, the robust u-channel track has a greater channel height to accommodate slight pinion tilts, and this method allows for the rotational method and length of rotation to be varied as the operator desires.

If churning patterns are desired, then the pins within the u-channels can be configured to have alternating segments of pins and no pins. With the same rationale, continuous rotation can be achieved by arranging one u-channel side with all pins while having no pins on the other u-channel side. As can be seen in Figure 3.41, the u-channel is lined with blue strips of ultra-high molecular-weight polyethylene for the areas where there are no pins to allow for proper gear meshing on the opposite side where there are pins. Without the low-friction padding as a backing, the pinion gear will attempt to "push out" when it encounters a sequence of pins. With this rotational shackle assembly coupled with the rotational guidance track system, industrial processers can implement this hardware within their current processing lines to take advantage of the enhanced heat transfer/

Figure 3.40: Robust U-Channel Pin Track with Pinion Gear Meshing

Figure 3.41: Complete View of U-Channel Pin Track

Figure 3.42: Bike Chain Rotational Track

chilling benefits with this passive-mechanical system. Beyond the necessary motor power to run the chilling processing line for the traditional in-line pure translation process, this rotational shackle-track system will require additional power due to the frictional losses and additional load

that it puts on the drive motor. However, in comparison to the traditional screw-auger chilling approach which is the dominant chilling method in the United States, this new system can replace the water agitation due to compressed air lines feeding into the tank. Compressed air lines require significant electrical energy consumption that may considerably exceed the electrical power demand of the drive motor for the rotational shackle-track system proposed. With this passive-mechanical system, the facility energy expenditures could be significantly be reduced by bypassing the use of compressed air in favor of a potentially slight additional demand on the drive motor.

4 CONCLUSIONS/FUTURE WORK

Considering the complex carcass geometry and the industrial flow, it was important to understand the complex flow dynamics involved in the poultry chilling process using COMSOL® Multiphysics and note any potential areas of improvement within the process. The detailed flow simulations of industrial poultry chilling are reported and detail the initial simulations of highly three-dimensional flows encountering the complex carcass geometry within the channel flow. Preferably, this chilling process should be performed under uniform exposure conditions, but the presented flow field data has shown that this process is non-uniform and inconsistent, which can lead to process design inefficiencies. With the stated conclusions, it was deemed critical to design an alternative approach to the traditional in-line immersion chilling approach that would manipulate the flow dynamics experienced by the series of carcasses on the poultry processing line to allow for enhanced relative motion between the carcass and chiller medium as well as provide more consistent, uniform chilling. Therefore, a novel approach to favorably alter the flow dynamics during the in-line immersion chilling process was developed and tested.

Using the experimental setup to simulate the industrial chilling line with added rotational kinematics, it was clear from examining the experimental trends that the 40 RPM and 60 RPM shackle motion patterns improve convective heat transfer rates and chilling effectiveness as indicated by the reduction in chilling thermal time constants. There also seemed to be an initial decrease in thermal time constant as AgPar is increased with a shallow minimum or plateau effect that occurs after around an AgPar of 1 or greater. This is theorized to occur, because, initially, as shackle rotational agitation is increased, increased convective heat transfer coefficients and chilling rates result. However, at some point, increased agitation does not correspond to increased chilling effectiveness and lower carcass core temperatures, because it is possible that the heat transfer is capped by the internal conductive resistance and the thermal heat capacitance of the carcass meat, and increased agitation and higher heat transfer coefficients do not yield significantly increased chilling rates and lower core temperatures. It is also theorized that limited angular displacement sweeps do not allow for the carcass angular momentum to build before altering direction so this leads to the "leveling off" in the average thermal time constants associated with further increases in AgPar seen within the 40 RPM and 60 RPM shackle motion patterns. From the gathered data, there seems to be an optimal periodic angular displacement for the shackle motion patterns tested. These hypotheses will be validated in future heat transfer experimental and computational studies.

Additionally, to gauge the upper limits of carcass chilling rates for future design exploration, in future studies, COMSOL® Multiphysics was used with varied carcass masses (1.50 kg, 1.69 kg, and 1.88 kg) with an imposed step change of the carcass boundary temperature to the chiller medium temperature at t = 0 seconds. With this method, the upper limit of carcass chilling was examined as there was no convective resistance, and the heat transfer between the carcass and

the chiller medium was only limited by the internal conductive resistance and thermal heat capacitance of the carcass meat. The results indicate there is still room for improvement for the previously tested motion patterns and the design space for rotational patterns can be further explored. Future computational studies will also involve design exploration of varied carcass rotational patterns and the impact of these patterns on the complex flow dynamics surrounding the carcass line. This study step will engage the rotating domain capsule surrounding the carcass geometry to induce rotation as specified. In future computational endeavors, a combined conjugate heat transfer and fluid dynamics model can be constructed to tie both of these physics involved in carcass chilling to study the impacts of varied inline rotational/translation motion patterns.

With regards to further experimentation, Liquid Ice Technologies has provided the group with an ice slurry generation unit as shown in Figure 4.1. With this slurry unit, the goal is to operate and run thermal chilling tests using the new carousel experimental setup with ice slurry as it is a superior heat sink when compared to chilled water. Additionally, the carousel setup will be used to gather additional thermal chilling sample data for previously tested patterns using the propeller-driven flow setup as well as examine data variations between the two experimental setups. Many poultry processors use much larger birds than used in the presented study so the group will work with industrial partners to acquire larger carcasses to be used in thermal chilling tests with the carousel setup. The goal will be to see if favorable impacts to the carcass chilling rate can be seen with larger carcasses, which can have significant relevance to many poultry processing facilities.

Figure 4.1: Liquid Ice Technologies Ice Slurry Unit

APPENDIX A

A.1 BasicMicro® Motion Studio Example Experimental Codes

A.1.1 60 RPM Continuous Rotation (4.5 Mins./Half Cycle) Sample Code

```
'This code will spin the motors for 4.5 minutes in one direction at 60 RPM before reversing direction


'Initialize Variables
Clear

pause 10000
puts 0,["Starting motors in 10 seconds",13]

Main
vel1 VAR Slong
vel1 = 412299
vel2 VAR Slong
vel2 = -412299
acc1 VAR Slong 'Limiting acceleration and deceleration value
acc1 = 0
n VAR Word
n=1

'Motor 1 Variables
MOTORVELKP(0) = TOINT(0.0)         'Control Rise
MOTORVELKI(0) = TOINT(0.0)        'Control Offset
MOTORVELKD(0) = TOINT(0.0)           'Unnecessary
MOTORVELQPPS(0) = 650000    'Approx fastest encoder will tick at
                            'In Quadrature Pulses Per Second
'Motor 2 Variables
MOTORVELKP(1) = TOINT(0.0)         'Control Rise
MOTORVELKI(1) = TOINT(0.0)        'Control Offset
MOTORVELKD(1) = TOINT(0.0)           'Unnecessary
MOTORVELQPPS(1) = 650000    'Approx fastest encoder will tick at
                            'In Quadrature Pulses Per Second

'Begin Actuating Motors
pause 5000 'Gives 5 seconds to start up terminal window

value2 VAR long

For value2 = 1 to 1

'Period 1 (4.5 minutes)
speed2 vel1,acc1,vel1,acc1
Gosub DataGet[MOTORSPEED(0),MOTORSPEED(1),MOTORCURRENT(0),MOTORCURRENT(1),MOTORENCSPEED(0),MOTORENCSPEED
(1),MOTORENCSPEEDS(0),MOTORENCSPEEDS(1),MOTORTARGETSPEED(0),MOTORTARGETSPEED(1),MOTORPWM(0),MOTORPWM(1),n]
power2 0,0,0,0

pause 75

'Period 2 (4.5 minutes)
speed2 vel2,acc1,vel2,acc1
Gosub DataGet[MOTORSPEED(0),MOTORSPEED(1),MOTORCURRENT(0),MOTORCURRENT(1),MOTORENCSPEED(0),MOTORENCSPEED
(1),MOTORENCSPEEDS(0),MOTORENCSPEEDS(1),MOTORTARGETSPEED(0),MOTORTARGETSPEED(1),MOTORPWM(0),MOTORPWM(1),n]
power2 0,0,0,0
```

```
'Period 3 (3 minutes)
speed2 vel1,acc1,vel1,acc1
Gosub DataGet2[MOTORSPEED(0),MOTORSPEED(1),MOTORCURRENT(0),MOTORCURRENT(1),MOTORENCSPEED(0),MOTORENCSPEED
(1),MOTORENCSPEEDS(0),MOTORENCSPEEDS(1),MOTORTARGETSPEED(0),MOTORTARGETSPEED(1),MOTORPWM(0),MOTORPWM(1),n]
power2 0,0,0,0

Next

power2 0,0,0,0

end

'Data Acquistion Function
DataGet[MOTORSPEED(0),MOTORSPEED(1),MOTORCURRENT(0),MOTORCURRENT(1),MOTORENCSPEED(0),MOTORENCSPEED
(1),MOTORENCSPEEDS(0),MOTORENCSPEEDS(1),MOTORTARGETSPEED(0),MOTORTARGETSPEED(1),MOTORPWM(0),MOTORPWM(1),n]

value VAR long

For value= 1 to 540

'Print
puts 0, ["n: ",dec n, " ","MVel: ",sdec MOTORSPEED(0), " ",sdec MOTORSPEED(1), " ","MCurr: ",sdec
MOTORCURRENT(0), " ",sdec MOTORCURRENT(1), " ","EncSpd: ",sdec MOTORENCSPEED(0), " ",sdec MOTORENCSPEED(1),
" ","AvgEncSpeeds(1secavg): ",sdec MOTORENCSPEEDS(0), " ",sdec MOTORENCSPEEDS(1), " ","TargetSpd: ",sdec
MOTORTARGETSPEED(0), " ",sdec MOTORTARGETSPEED(1), " ","PWMSet: ",sdec MOTORPWM(0), " ",sdec MOTORPWM(1),
13]

'Count up one tick
n=n+1
'Sampling Time in ms
pause 500
next
return n

'Data Acquistion Function
DataGet2[MOTORSPEED(0),MOTORSPEED(1),MOTORCURRENT(0),MOTORCURRENT(1),MOTORENCSPEED(0),MOTORENCSPEED
(1),MOTORENCSPEEDS(0),MOTORENCSPEEDS(1),MOTORTARGETSPEED(0),MOTORTARGETSPEED(1),MOTORPWM(0),MOTORPWM(1),n]

value3 VAR long

For value3= 1 to 360

'Print
puts 0, ["n: ",dec n, " ","MVel: ",sdec MOTORSPEED(0), " ",sdec MOTORSPEED(1), " ","MCurr: ",sdec
MOTORCURRENT(0), " ",sdec MOTORCURRENT(1), " ","EncSpd: ",sdec MOTORENCSPEED(0), " ",sdec MOTORENCSPEED(1),
" ","AvgEncSpeeds(1secavg): ",sdec MOTORENCSPEEDS(0), " ",sdec MOTORENCSPEEDS(1), " ","TargetSpd: ",sdec
MOTORTARGETSPEED(0), " ",sdec MOTORTARGETSPEED(1), " ","PWMSet: ",sdec MOTORPWM(0), " ",sdec MOTORPWM(1),
13]

'Count up one tick
n=n+1
'Sampling Time in ms
pause 500
next
return n

end
```

A.1.2 60 RPM Half-Turn Churn Sample Code

```
'This code will spin the motors for back and forth in a half-turn (180deg) churning manner with continuous
duty for 12 minutes

Clear

pause 10000
puts 0,["Starting motors in 10 seconds",13]

Main
vel1 VAR Slong
vel1 = 412299
vel2 VAR Slong
vel2 = -412299
acc1 VAR Slong 'Limiting acceleration and deceleration value
acc1 = 0
n VAR Word
n=1

'Motor 1 Variables
MOTORVELKP(0) = TOINT(0.0)         'Control Rise
MOTORVELKI(0) = TOINT(0.0)        'Control Offset
MOTORVELKD(0) = TOINT(0.0)           'Unnecessary
MOTORVELQPPS(0) = 650000    'Approx fastest encoder will tick at
                            'In Quadrature Pulses Per Second
'Motor 2 Variables
MOTORVELKP(1) = TOINT(0.0)         'Control Rise
MOTORVELKI(1) = TOINT(0.0)        'Control Offset
MOTORVELKD(1) = TOINT(0.0)           'Unnecessary
MOTORVELQPPS(1) = 650000    'Approx fastest encoder will tick at
                            'In Quadrature Pulses Per Second

'Begin Actuating Motors
pause 5000 'Gives 5 seconds to start up terminal window

value2 VAR long

For value2= 1 to 675
'Period 1

pause 75

speed2 vel1,acc1,vel2,acc1
Gosub DataGet[MOTORSPEED(0),MOTORSPEED(1),MOTORCURRENT(0),MOTORCURRENT(1),MOTORENCSPEED(0),MOTORENCSPEED
(1),MOTORENCSPEEDS(0),MOTORENCSPEEDS(1),MOTORTARGETSPEED(0),MOTORTARGETSPEED(1),MOTORPWM(0),MOTORPWM(1),n]
power2 0,0,0,0

pause 75

'Period 2
speed2 vel2,acc1,vel1,acc1
Gosub DataGet[MOTORSPEED(0),MOTORSPEED(1),MOTORCURRENT(0),MOTORCURRENT(1),MOTORENCSPEED(0),MOTORENCSPEED
(1),MOTORENCSPEEDS(0),MOTORENCSPEEDS(1),MOTORTARGETSPEED(0),MOTORTARGETSPEED(1),MOTORPWM(0),MOTORPWM(1),n]
power2 0,0,0,0
```

```
power2 0,0,0,0

end

'Data Acquistion Function
DataGet[MOTORSPEED(0),MOTORSPEED(1),MOTORCURRENT(0),MOTORCURRENT(1),MOTORENCSPEED(0),MOTORENCSPEED
(1),MOTORENCSPEEDS(0),MOTORENCSPEEDS(1),MOTORTARGETSPEED(0),MOTORTARGETSPEED(1),MOTORPWM(0),MOTORPWM(1),n]
value VAR long
For value= 1 to 10

'Print
puts 0, ["n: ",dec n, " ","MVel: ",sdec MOTORSPEED(0), " ",sdec MOTORSPEED(1), " ","MCurr: ",sdec
MOTORCURRENT(0), " ",sdec MOTORCURRENT(1), " ","EncSpd: ",sdec MOTORENCSPEED(0), " ",sdec MOTORENCSPEED(1), "
","AvgEncSpeeds(1secavg): ",sdec MOTORENCSPEEDS(0), " ",sdec MOTORENCSPEEDS(1), " ","TargetSpd: ",sdec
MOTORTARGETSPEED(0), " ",sdec MOTORTARGETSPEED(1), " ","PWMSet: ",sdec MOTORPWM(0), " ",sdec MOTORPWM(1), 13]

'Count up one tick
n=n+1
'Sampling Time in ms
pause 45
next
return n

end
```

A.2 Aggregated Thermal Experimentation Data for Shackle Motion Patterns

A.2.1 Pure Translation – 12 Minutes

Mass Category	Number of Carcasses	Average Mass (kg)	Average of Pre-Chill Temp. (ºC)	Average of Post-Chill Temp. (ºC)	Average of Time Constant (mins.)	Average of ΔT (ºC)	Max of Time Constant (mins.)	Min of Time Constant (mins.)	StdDev of Time Constant (mins.)
1.2-1.4	2	1.38	42.90	27.70	20.06	15.20	21.86	18.27	2.54
1.4-1.6	10	1.50	42.64	27.26	19.62	15.38	24.38	17.24	2.22
1.6-1.8	5	1.68	42.10	29.78	25.58	12.32	29.18	19.36	3.98
1.8-2	3	1.84	42.53	32.37	32.26	10.17	37.85	28.78	4.89

A.2.2 40 RPM Full-Turn Churn – 12 Minutes

Mass Category	Number of Carcasses	Average Mass (kg)	Average of Pre-Chill Temp. (ºC)	Average of Post-Chill Temp. (ºC)	Average of Time Constant (mins.)	Average of ΔT (ºC)	Max of Time Constant (mins.)	Min of Time Constant (mins.)	StdDev of Time Constant (mins.)

<1.2	1	1.19	43.20	17.75	8.76	25.45	8.76	8.76	-
1.2-1.4	1	1.36	43.20	23.70	14.32	19.50	14.32	14.32	-
1.4-1.6	10	1.49	42.49	23.89	14.94	18.61	17.38	11.34	1.91
1.6-1.8	4	1.65	41.48	24.88	16.76	16.60	20.89	14.59	2.81
1.8-2	3	1.87	40.17	26.53	20.44	13.63	22.63	18.75	1.99
>2	1	2.02	40.50	28.80	25.10	11.70	25.10	25.10	-

A.2.3 40 RPM Continuous Rotation (3 Mins./Half Cycle) – 12 Minutes

Mass Category	Number of Carcasses	Average Mass (kg)	Average of Pre-Chill Temp. (ºC)	Average of Post-Chill Temp. (ºC)	Average of Time Constant (mins.)	Average of ΔT (ºC)	Max of Time Constant (mins.)	Min of Time Constant (mins.)	StdDev of Time Constant (mins.)
<1.2	1	1.19	43.20	18.10	8.93	25.10	8.93	8.93	-
1.2-1.4	1	1.40	42.60	27.00	19.09	15.60	19.09	19.09	-
1.4-1.6	6	1.48	42.27	26.55	18.68	15.72	21.33	14.47	2.36
1.6-1.8	5	1.70	41.36	27.45	21.20	13.91	25.08	18.65	3.03
1.8-2	6	1.85	40.80	28.91	25.17	11.89	30.59	22.28	2.97
>2	1	2.02	41.70	30.25	26.97	11.45	26.97	26.97	-

A.2.4 40 RPM Continuous Rotation (4 Rot./Half Cycle) – 12 Minutes

Mass Category	Number of Carcasses	Average Mass (kg)	Average of Pre-Chill Temp. (ºC)	Average of Post-Chill Temp. (ºC)	Average of Time Constant (mins.)	Average of ΔT (ºC)	Max of Time Constant (mins.)	Min of Time Constant (mins.)	StdDev of Time Constant (mins.)
1.4-1.6	4	1.55	40.70	25.68	17.92	15.03	20.66	13.80	3.14
1.6-1.8	11	1.69	41.32	27.74	21.20	13.58	24.89	15.73	2.91
1.8-2	3	1.85	41.17	28.67	23.62	12.50	25.40	21.56	1.93
>2	2	2.29	40.15	33.00	43.14	7.15	47.67	38.62	6.40

A.2.5 40 RPM Half-Turn Churn

Mass Category	Number of Carcasses	Average Mass (kg)	Average of Pre-Chill Temp. (ºC)	Average of Post-Chill Temp. (ºC)	Average of Time Constant (mins.)	Average of ΔT (ºC)	Max of Time Constant (mins.)	Min of Time Constant (mins.)	StdDev of Time Constant (mins.)
1.4-1.6	4	1.55	41.43	23.45	14.72	17.98	17.46	11.31	2.97
1.6-1.8	11	1.69	40.91	25.29	17.33	15.62	21.53	12.61	2.47
1.8-2	3	1.85	42.23	27.63	19.64	14.60	21.70	18.21	1.83
>2	2	2.29	39.85	31.15	33.07	8.70	37.01	29.13	5.57

A.2.6 40 RPM Continuous Rotation (2 Rot./Half Cycle)

Mass Category	Number of Carcasses	Average Mass (kg)	Average of Pre-Chill Temp. (ºC)	Average of Post-Chill Temp. (ºC)	Average of Time Constant (mins.)	Average of ΔT (ºC)	Max of Time Constant (mins.)	Min of Time Constant (mins.)	StdDev of Time Constant (mins.)
1.2-1.4	2	1.31	40.95	21.55	12.35	19.40	12.58	12.11	0.34
1.4-1.6	6	1.48	41.12	22.63	13.51	18.49	16.59	11.62	1.66
1.6-1.8	9	1.70	41.61	26.14	17.94	15.47	21.27	14.80	2.38
1.8-2	2	1.85	41.15	27.35	20.27	13.80	21.21	19.33	1.33
>2	1	2.05	39.40	30.40	31.58	9.00	31.58	31.58	-

A.2.7 60 RPM Continuous Rotation (1.5 Rot./Half Cycle)

Mass Category	Number of Carcasses	Average Mass (kg)	Average of Pre-Chill Temp. (ºC)	Average of Post-Chill Temp. (ºC)	Average of Time Constant (mins.)	Average of ΔT (ºC)	Max of Time Constant (mins.)	Min of Time Constant (mins.)	StdDev of Time Constant (mins.)
1.2-1.4	3	1.36	41.12	20.13	11.34	20.98	12.36	10.64	0.90
1.4-1.6	7	1.50	41.04	21.76	12.94	19.27	14.44	11.50	1.19
1.6-1.8	6	1.70	41.43	23.81	14.91	17.63	16.56	13.66	1.00
1.8-2	4	1.90	40.48	26.13	19.37	14.35	22.30	17.24	2.12

A.2.8 60 RPM Continuous Rotation (4.5 Mins./Half Cycle)

Mass Category	Number of Carcasses	Average Mass (kg)	Average of Pre-Chill Temp. (ºC)	Average of Post-Chill Temp. (ºC)	Average of Time Constant (mins.)	Average of ΔT (ºC)	Max of Time Constant (mins.)	Min of Time Constant (mins.)	StdDev of Time Constant (mins.)
1.2-1.4	3	1.36	41.70	22.33	13.31	19.37	14.25	12.51	0.88
1.4-1.6	7	1.50	40.26	23.39	15.54	16.87	17.71	13.41	1.74
1.6-1.8	6	1.70	39.66	24.53	17.72	15.13	18.47	16.92	0.69
1.8-2	4	1.90	40.11	27.60	23.20	12.51	24.97	19.99	2.27

A.2.9 60 RPM Continuous Rotation (3 Rot./Half Cycle)

Mass Category	Number of Carcasses	Average Mass (kg)	Average of Pre-Chill Temp. (ºC)	Average of Post-Chill Temp. (ºC)	Average of Time Constant (mins.)	Average of ΔT (ºC)	Max of Time Constant (mins.)	Min of Time Constant (mins.)	StdDev of Time Constant (mins.)
1.4-1.6	9	1.49	40.46	23.02	14.45	17.44	15.28	12.72	0.87
1.6-1.8	8	1.69	40.31	24.18	16.15	16.14	17.88	14.55	1.04
1.8-2	2	1.97	40.25	27.20	21.42	13.05	22.72	20.12	1.84
>2	1	2.05	40.60	28.10	22.48	12.50	22.48	22.48	-

A.2.10 60 RPM Three-Quarters-Turn Churn

Mass Category	Number of Carcasses	Average Mass (kg)	Average of Pre-Chill Temp. (ºC)	Average of Post-Chill Temp. (ºC)	Average of Time Constant (mins.)	Average of ΔT (ºC)	Max of Time Constant (mins.)	Min of Time Constant (mins.)	StdDev of Time Constant (mins.)
1.4-1.6	9	1.49	40.54	22.10	13.32	18.44	14.25	12.51	0.55
1.6-1.8	8	1.69	40.89	23.74	15.14	17.15	16.27	13.48	1.00
1.8-2	2	1.97	40.75	26.65	19.75	14.10	21.24	18.26	2.11
>2	1	2.05	39.55	26.50	20.70	13.05	20.70	20.70	-

References

[1] P. N. Canning, A. Charles, S. Huang, K. R. Polenske and A. Waters, Energy Use in the U.S. Food System, 2010.

[2] S. Barbut, The Science of Poultry and Meat Processing, 2015.

[3] N. C. Council, "Statistics & research: How Broilers Are Marketed," 2006.

[4] P. PAPINAHO, D. FLETCHER and R. I. T. A. H., "Relationship of breast fillet deboning time to shear force, pH, cooking loss and color in broilers stunned by high electrical current," *Agricultural and food science,* vol. 5, 2008.

[5] M. F. Pool, D. De Fremery, A. A. Campbell and A. A. Klose, "Poultry tenderness II. Influence of processing on tenderness of chicken," *J Food Technol.,* 1959.

[6] C. James, C. Vincent, T. I. de Andrade Lima and S. J. James, "The primary chilling of poultry carcasses—a review," *International journal of refrigeration,* vol. 29, p. 847–862, 2006.

[7] P. L. DAWSON, D. M. JANKY, M. G. DUKES, L. D. THOMPSON and S. A. WOODWARD, "Effect of Post-Mortem Boning Time During Simulated Commercial Processing on the Tenderness of Broiler Breast Meat," *Poultry science,* vol. 66, p. 1331–1333, 1987.

[8] J. W. Dodge and W. J. Stadelman, "Post mortem aging of poultry and its effect on the tenderness of breast muscle," *Food Technol,* 1959.

[9] L. O. N. G. and J. WALLACE, "The velocity field of the turbulent very near wake of a circular cylinder," *Experiments in fluids,* vol. 20, p. 441–453, 1996.

[10] T. Zhou, Y. Zhou, M. W. Yiu and L. P. Chua, "Three-dimensional vorticity in a turbulent cylinder wake," *Experiments in fluids,* vol. 37, p. 616–616, 2004.

[11] F. Scarano and C. Poelma, "Three-dimensional vorticity patterns of cylinder wakes," *Experiments in fluids,* vol. 47, p. 69–83, 2009.

[12] D. A. Lyn, S. Einav, W. Rodi and J.-H. Park, "A laser-Doppler velocimetry study of ensemble-averaged characteristics of the turbulent near wake of a square cylinder," *Journal of fluid mechanics,* vol. 304, p. 285–319, 1995.

[13] Y. Bao, Q. Wu and D. Zhou, "Numerical investigation of flow around an inline square cylinder array with different spacing ratios," *Computers & fluids,* vol. 55, p. 118–131, 2012.

[14] S. U. Islam, W. S. Abbasi and Z. C. Ying, "Transitions in the unsteady wakes and aerodynamic characteristics of the flow past three square cylinders aligned inline," *Aerospace science and technology,* vol. 50, p. 96–111, 2016.

[15] C. Liang, G. Papadakis and X. Luo, "Effect of tube spacing on the vortex shedding characteristics of laminar flow past an inline tube array: A numerical study," *Computers & fluids,* vol. 38, p. 950–964, 2009.

[16] A. A. Hetz, M. N. Dhaubhadel and D. P. Telionis, "Vortex shedding over five in-line cylinders cylinders," *Journal of fluids and structures,* vol. 5, p. 243–257, 1991.

[17] C. M. Sewatkar, R. Patel, A. Sharma and A. Agrawal, "Flow around six in-line square cylinders," *Journal of fluid mechanics,* vol. 710, p. 195–233, 2012.

[18] U. Goldberg and D. Apsley, "A wall-distance-free low Re k — ϵ turbulence model," *Computer methods in applied mechanics and engineering,* vol. 145, p. 227–238, 1997.

[19] W. P. Jones and B. E. Launder, "The prediction of laminarization with a two-equation model of turbulence," *International journal of heat and mass transfer,* vol. 15, p. 301–314, 1972.

[20] B. E. Launder and B. I. Sharma, "Application of the energy-dissipation model of turbulence to the calculation of flow near a spinning disc," *Letters in heat and mass transfer,* vol. 1, p. 131–137, 1974.

[21] C. K. G. Lam and K. Bremhorst, "A Modified Form of the k-ε Model for Predicting Wall Turbulence," *Journal of fluids engineering,* vol. 103, p. 456–460, 1981.

[22] W. Rodi and N. N. Mansour, "Low Reynolds number k—ε modelling with the aid of direct simulation data," *Journal of fluid mechanics,* vol. 250, p. 509–529, 1993.

[23] P. J. Roache, "Perspective: A Method for Uniform Reporting of Grid Refinement Studies," *Journal of fluids engineering,* vol. 116, p. 405–413, 1994.

[24] P. J. Roache, "QUANTIFICATION OF UNCERTAINTY IN COMPUTATIONAL FLUID DYNAMICS," *Annual review of fluid mechanics,* vol. 29, p. 123–160, 1997.

[25] Ž. G. Kostić and S. N. Oka, "Fluid flow and heat transfer with two cylinders in cross flow," *International Journal of Heat and Mass Transfer,* vol. 15, pp. 279-299, 1972.

[26] W. J. Stadelman, "How shall I cool my birds?," *Broiler Industry,* vol. 24, pp. 39,40, 1961.

[27] M. Peric, E. Rossmanith and L. Leistner, "Verbesserung der mikrobiologischen Qualitat vonSchluchthaknchen durch die Spriih-Kuhlung (Improving the microbiological quality of chickens by spray chilling)," *Die Fleischwirtschaft,* vol. 51, pp. 574-577, 1971.

[28] L. Szentkuti, G. Pavlus and L. Leistner, "Entwicklung eines hygienisch einwandfreien und wirtschaftlich tragbaren Spriih-Kiihlverfahrens fiirSchlachtgeflttgel (Development of a hygienic andeconomical spray-chilling method for poultry)," *DieFleischwirtschaft,* vol. 49, p. 1639, 1969.

[29] L. Leistner, E. Rossmanith and W. Woltersdorf, "Rationalisierung des Spriih-Kuhlverfahrens furSchlachthahnchen (Rationalizing the spray methodof chilling poultry)," *Die Fleischwirtschaft,* vol. 52, pp. 362-364, 1972.

[30] A. Bejan, Convection Heat Transfer, 4. Aufl. ed., Somerset: Wiley, 2013.

[31] M. Sano and K. Tamai, "A universal transition to turbulence in channel flow," *Nature physics,* vol. 12, p. 249–253, 2016.

[32] B. E. C. H. KNUT H and H. I. ANDERSSON, "Turbulent plane Couette flow subject to strong system rotation," *Journal of fluid mechanics,* vol. 347, p. 289–314, 1997.

[33] N. Tillmark and P. H. Alfredsson, "Turbulence in plane Couette flow," *Applied Scientific Research,* vol. 51, p. 237–241, 1993.

[34] R. American Society of Heating and A.-C. Engineers, "2006 Ashrae handbook : refrigeration (Inch-pound)," *ASHRAE,* 2006.

[35] A. Wesolowski, J. J. Sienkiewicz, K. A. Skibniewska, D. Luczycka and D. Choszcz, "Hysteresis of ultrasound velocity in pork lard and water during a thermal cycle," *Journal of food engineering,* vol. 190, p. 48–53, 2016.